VOL.107 NO.ST12. DEC. 1981

JOURNAL OF THE STRUCTURAL DIVISION

PROCEEDINGS OF
THE AMERICAN SOCIETY
OF CIVIL ENGINEERS

VOL.107 NO.ST12. DEC. 1981

JOURNAL OF THE STRUCTURAL DIVISION

PROCEEDINGS OF
THE AMERICAN SOCIETY
OF CIVIL ENGINEERS

Copyright© 1981 by
American Society
of Civil Engineers
All Rights Reserved
ISSN 0044-8001

John E. Bower, Editor
U.S. Steel Corporation

AMERICAN SOCIETY OF CIVIL ENGINEERS

BOARD OF DIRECTION

President
James R. Sims

Past President
Irvan F. Mendenhall

President Elect
John H. Wiedeman

Vice Presidents
Lyman R. Gillis
Albert A. Grant
Paul A. Kuhn
William H. Taylor

Directors
Martin G. Abegg
L. G. Byrd
Frederick W. DeWitt
Larry J. Feeser
John A. Focht, Jr.
Sergio Gonzalez-Karg
Kenneth D. Hansen
Ronald C. Hirschfield
Louis M. Laushey
Leon D. Luck
Arthur R. McDaniel
Robert L. Morris
Paul R. Munger
William R. Neuman
Leonard S. Oberman
John D. Parkhurst
Celestino R. Pennoni
Robert B. Rhode
Gerald E. Speitel
Lawrence E. Wilson, Jr.
Richard W. Woodruff

EXECUTIVE OFFICERS

Eugene Zwoyer, *Executive Director*
Julie E. Gibouleau, *Assistant to the Executive Director*
Louis L. Meier, *Washington Counsel/Assistant Secretary*
William H. Wisely, *Executive Director Emeritus*
Michael N. Salgo, *Treasurer*
Elmer B. Isaak, *Assistant Treasurer*

STAFF DIRECTORS

Donald A. Buzzell, *Managing Director for Education and Professional Affairs*
Robert A. Crist, Jr., *Managing Director for Publications and Technical Affairs*
Alexandra Bellow, *Director, Human Resources*
Joseph A. DeFiglia, *Director, Management Information Services*
David Dresia, *Director, Publications Production and Marketing*
Barker D. Herr, *Director, Membership*
Richard A. Jeffers, *Controller*
Carl E. Nelson, *Director, Field Services*
Don P. Reynolds, *Director, Policy, Planning and Public Affairs*
Bruce Rickerson, *Director, Legislative Services*
Albert W. Turchick, *Director, Technical Services*
George K. Wadlin, *Director, Education Services*
R. Lawrence Whipple, *Director, Engineering Management Services*

COMMITTEE ON PUBLICATIONS

William R. Neumann, *Chairman*
Martin G. Abegg
John A. Focht, Jr.
Ronald C. Hirschfield
Paul R. Munger
Lawrence E. Wilson, Jr.

STRUCTURAL DIVISION

Executive Committee
Ronald G. Domer, *Chairman*
Roland L. Sharpe, *Vice Chairman*
John E. Bower
R. Richard Avent, *Secretary*
Joseph H. Appleton, *Management Group B Contact Member*
Sherman A. Nelson, *Management Group B Contact Member*
Donald McDonald

Publications Committee
John E. Bower, ***Chairman, Editor and Exec. Comm. Contact Member***
Mihran S. Agbabian
Subhash Anand
David Darwin
John T. DeWolf
Douglas Foutch
Ovadia E. Lev
Le-Wu Lu
Bruce E. Lyons
Walter Podolny
Emil Simiu
John F. Stolz
James T. P. Yao

PUBLICATIONS SERVICES DEPARTMENT

David Dresia, *Director, Publications Production and Marketing*

Technical and Professional Publications

Richard R. Torrens, *Manager*
Chuck Wahrhaftig, *Chief Copy Editor*
Corinne Bernstein, *Copy Editor*
Linda Ellington, *Copy Editor*
Walter Friedman, *Copy Editor*
Richard C. Scheblein, *Draftsman*

Information Services

Melanie G. Edwards, *Editor*

PERMISSION TO PHOTOCOPY JOURNAL PAPERS

Permission to photocopy for personal or internal reference beyond the limits in Sections 107 and 108 of the U.S. Copyright Law is granted by the American Society of Civil Engineers for libraries and other users registered with the Copyright Clearance Center, 21 Congress Street, Salem, Mass. 01970, provided the appropriate fee is paid to the CCC for all articles bearing the CCC code. Requests for special permission or bulk copying should be addressed to the Manager of Technical and Professional Publications, American Society of Civil Engineers.

CONTENTS

Post-Buckling Analysis of Guyed Towers
by Alexander Chajes and David Ling 2313

Nonlinear Dynamic Analysis by Modal Superposition
by Louis F. Geschwindner, Jr. 2325

Optimization with Frequency Constraint
by William R. Spillers, Sohan Singh, and Robert Levy 2337

Strength of Old Wood Joists
by Ross M. Lanius, Jr., Robert Tichy, and William M. Bulleit 2349

Dynamic Collapse of Frames under Wind Disturbances
by Kiyotaka Morisako, Shuzo Ishida, Tsuneyoshi Nakamura, and Hatsuo Ishizaki 2365

Buckling of Reinforced Concrete Shells
by Endre Dulácska 2381

Shear Reinforcement for Concrete Slabs
by Walter H. Dilger and Amin Ghali 2403

The Journal of the Structural Division (ISSN 0044-8001) is published monthly by the American Society of Civil Engineers. Publications office is at 345 East 47th Street, New York, N.Y. 10017. Address all ASCE correspondence to the Editorial and General Offices at 345 East 47th Street, New York, N.Y. 10017. Allow six weeks for change of address to become effective. Subscription price to members is $22.50. Nonmember subscriptions available; prices obtainable on request. Second-class postage paid at New York, N.Y. and at additional mailing offices. ST.

POSTMASTER: Send address changes to American Society of Civil Engineers, 345 East 47th Street, New York, NY 10017.

The Society is not responsible for any statement made or opinion expressed in its publications.

Point Loads on Composite Deck-Reinforced Slabs
by Charles W. Roeder 2421

TECHNICAL NOTES

Proc. Paper 16690

Optimum Design of Three-Span I-Beams
by Abul K. Azad 2433

Aeroelastic Stability of Suspension Bridges
by Augustin Petre and Ramiro Sofronie 2437

Reinforced Concrete Beams in Pure Torsion
by Himat T. Solanki 2443

DISCUSSION

Proc. Paper 16686

Seismic Design Input for Secondary Systems, by Mahendra P. Singh (Feb., 1980. Prior Discussion: Dec., 1980).
closure 2453

Design of Counterstressed Cable Structures, by Dennis Clark (Nov., 1980).
errata 2454

Research Needs in Stability of Metal Structures,* by Reidar Bjorhovde (Dec., 1980).
by Peter F. Adams 2454
by Joachim Lindner and Narayanan Subramanian 2455

Proposed Specifications for Steel Box Girder Bridges,* by Roman Wolchuk (Dec., 1980).
by Charles Seim and Steve Thoman 2457

Edge Stiffeners for Thin-Walled Members,* by Thomas P. Desmond, Teoman Pekoz, and George Winter (Feb., 1981).
by Srinivasan Sridharan 2459

*Discussion period closed for this paper. Any other discussion received during this discussion period will be published in subsequent Journals.

16754 POST-BUCKLING ANALYSIS OF GUYED TOWERS

KEY WORDS: **Buckling;** Cables; **Guy wires; Horizontal loads;** Poles; Stability; Structural engineering; **Towers; Vertical loads**

ABSTRACT: The post-buckling behavior of short towers, supported by a single set of guy wires is investigated. Using the principle of stationary potential energy, a set of non-linear algebraic equations are obtained for both fixed and hinged-base towers. The equations are solved numerically for several actual systems. The results of the investigation include the shape of the post-buckling curves for towers subjected to vertical loads, the effect of cable pretension on the post-buckling behavior and the effect of horizontal forces on the capacity of the towers to supprot vertical loads.

REFERENCE: Chajes, Alexander (Assoc. Prof. of Civ. Engrg., Univ. of Massachusetts, Amherst, Mass. 01003), and Ling, David, "Post-Buckling Analysis of Guyed Towers," *Journal of the Structural Division,* ASCE, Vol. 107, No. ST12, **Proc. Paper 16754,** December, 1981, pp. 2313-2323

16768 NONLINEAR DYNAMIC ANALYSIS BY MODAL SUPERPOSITION

KEY WORDS: Analysis; **Approximation method; Cables; Dynamic response;** Dynamics; **Structural engineering;** Superposition (mathematics); Vibration

ABSTRACT: A modified modal superposition method is developed and used to evaluate the nonlinear dynamic response of a cable network composed of a linkage of straight members with lumped masses. The method is compared with Newmark's B method for accuracy and the time interval requirements for stability. To show the usefulness of the method a number of parameter studies are presented using the cable network as an example.

REFERENCE: Geschwindner, Louis F., Jr. (Asst. Prof. of Architectural Engrg., Pennsylvania State Univ., University Park, Pa.), "Nonlinear Dynamic Analysis by Modal Superposition," *Journal of the Structural Division,* ASCE, Vol. 107, No. ST12, **Proc. Paper 16768,** December, 1981, pp. 2325-2336

16771 OPTIMIZATION WITH FREQUENCY CONSTRAINT

KEY WORDS: **Algorithms; Allowable stress;** Eigenvalues; Frequency stabilizers; **Mathematical programming;** Optimization; Vibration analysis

ABSTRACT: The use of allowable stress algorithms for a simple structural optimization problem with a single frequency constraint and a constant mass matrix is discussed. The mathematical properties of the eigenvalue problem are reviewed. An Allowable stress algorithm is stated and its properties discussed. Two simple examples are presented. The primary concern of this paper lies in placing allowable stress-type algorithms within the mathematical programming literature.

REFERENCE: Spillers, William R. (Prof., Dept. of Civ. Engrg., Rensselaer Polytechnic Inst., Troy, N.Y. 12181), Singh, Sohan, and Levy, Robert, "Optimization with Frequency Constraint," *Journal of the Structural Division,* ASCE, Vol. 107, No. ST12, **Proc. Paper 16771,** December, 1981

16767 STRENGTH OF OLD WOOD JOISTS

KEY WORDS: Buildings; **Joists; Nondestructive tests;** Reinforcement (structures); Statistical analysis; **Strength of materials;** Stress waves; **Structural engineering; Timber construction;** Visual inspection

ABSTRACT: Two nondestructive techniques are used to evaluate the strength of wood joists in an existing structure. The traditional visual grading and longitudinal stress wave approaches are employed, with the latter technique providing better insight into the strength of the floor system. Further refinements of the stress wave method are suggested.

REFERENCE: Lanius, Ross M., Jr. (Assoc. Prof., Dept. of Civ. and Environmental Engrg., Univ. of New Haven, W. Haven, Conn.), Tichy, Robert, and Bulleit, William M., "Strength of Old Wood Joists," *Journal of the Structural Division,* ASCE, Vol. 107, No. ST12, **Proc. Paper 16767**, December, 1981, pp. 2349-2363

16770 COLLAPSE OF FRAMES UNDER WIND DISTURBANCES

KEY WORDS: Collapse; **Dynamics;** Frame design; Framed structures; **Frames;** Load factors; **Numerical analysis;** Parametric equations; **Safety; Strain hardening; Wind loads**

ABSTRACT: A parametric numerical analysis is conducted on strain-hardening multi-story frames subjected to wind disturbances generated by amplifying a recorded fluctuating wind pressure. The effect of spreading and diminishing of the strain-hardening regions has been taken into account in the one dimensional finite element formulation employed here. The dynamic behavior including in particular the dynamic collapse behavior is extensively examined and the details are presented for the first time. The effect of a fluctuating wind disturbance on a frame may be represented by the required overall plastic strength, the therefore measured by a multiplier (load factor) of the basic design wind loads. There exists a critical frame which just exhibits the dynamic collaps behavior under a wind disturbance. The corresponding critical value of the multiplier has been called the dynamic collapse gust load factor. The factor provides a rational basis for a practical safety factor and is therefore recommended for a more rational method of wind resistant design of ductile structures.

REFERENCE: Morisako, Kiyotaka (Asst., Dept. of Architecture, Kyoto Tech. Univ., Kyoto, Japan), Ishida, Shuzo, Nakamura, Tsuneyoshi, and Ishizaki, Hatsuo, "Dynamic Collapse of Frames Under Wind Disturbances," *Journal of the Structural Division,* ASCE, Vol. 107, No. ST12, **Proc. Paper 16770**, December, 1981, pp. 2365-2380

16753 BUCKLING OF REINFORCED CONCRETE SHELLS

KEY WORDS: **Buckling; Concrete (reinforced);** Domes (structural); Engineering mechanics; Loads (forces); Plastic properties; **Shells (structural forms);** Stability

ABSTRACT: The special phenomena of reinforced concrete shell buckling is described on the basis of the latest results of research. The method presented takes into consideration the special properties of the reinforced concrete including, plasticity, creep, and quantity of reinforcement. Snap-through critical loads calculated by the described method are compared to the results of model tests and to the loads and critical loads of erected domes. The shell buckling stiffness was seen to be composed of two parts; the bending and the axial stiffness of the reinforced concrete cross section. The critical load is reduced by the plasticity and the imperfections. The critical load of the reinforced concrete shells decreases by the craks of concrete and increases by the reinforcement.

REFERENCE: Dulacska, Endre (Struct. Lead. Engr., Planning Office, BUVATI of Budapest, HUNGARY), "Buckling of Reinforced Concrete Shells," *Journal of the Structural Division,* ASCE, Vol. 107, No. ST12, **Proc. Paper 16753**, December, 1981, pp. 2381-2401

16752 SHEAR REINFORCEMENT FOR CONCRETE SLABS

KEY WORDS: Columns (supports); Connections; Cracking (fracturing); Deformation; **Ductility;** Economics; **Flat concrete plates;** Flexural strength; **Reinforced concretes;** Shear properties; **Shear strength (concrete)**

ABSTRACT: A review of the different types of shear reinforcement for concrete flate plates is presented and the difficulties encountered when these are used in practice are reviewed. Practical shear reinforcement should efficienty increase the shear strength and ductility of the slab-column connection, and should be easy to fabricate and install. New Type of shear reinforcement which satisfies these requirements is presented. An individual reinforcing element is in the form of vertical bars with mechanical anchorages at the two ends. The size and shape of the anchors are examined as well as the arrangement of the shear elements around the column. From the results of 40 full-size tests, rules for the design of the new type of shear reinforcement are given in the form of suggested revisions to the current codes.

REFERENCE: Dilger, Walter H. (Prof. of Civ. Engrg., The Univ. of Calgary, Calgary, Alberta, Canada, T2N 1N4), and Ghali, Amin, "Shear Reinforcement for Concrete Slabs," *Journal of the Structural Division,* ASCE, Vol. 107, No. ST12, **Proc. Paper 16752**, December, 1981, pp. 2403-2420

16769 COMPOSITE DECK-REINFORCED SLABS

KEY WORDS: **Composite structures; Concrete (reinforced); Floors;** Load limits; Shear strength (concrete); **Slabs;** Structural engineering

ABSTRACT: The behavior of composite deck-reinforced floor systems under concentrated loads is described. Laboratory experiments show that these floor systems may have a considerably larger capacity to support concentrated loads than indicated by existing design techniques. There are two sources of this additional strength. First, continuity of the slab and slip restraint of stud shear connectors increase the shear bond capacity. Further benefit is obtained through the distribution of the load effects over the weak direction of the one way slab. The utilization of these benefits may produce significant economics in the design of floors to resist concentrated loads.

REFERENCE: Roeder, Charles W. (Assoc. Prof., Dept. of Civ. Engrg., Univ. of Washington, Seattle, Wash. 98195), "Point Loads on Composite Deck-Reinforced Slabs," *Journal of the Structural Division,* ASCE, Vol. 107, No. ST12, **Proc. Paper 16769**, December, 1981, pp. 2421-2429

U.S. Customary-SI Conversion Factors

In accordance with the October, 1970 action of the ASCE Board of Direction, which stated that all publications of the Society should list all measurements in both U.S. Customary and SI (International System) units, the following list contains conversion factors to enable readers to compute the SI unit values of measurements. A complete guide to the SI system and its use has been published by the American Society for Testing and Materials. Copies of this publication (ASTM E-380) can be purchased from ASCE at a price of $3.00 each; orders must be prepaid.

All authors of *Journal* papers are being asked to prepare their papers in this dual-unit format. To provide preliminary assistance to authors, the following list of conversion factors and guides are recommended by the ASCE Committee on Metrication.

To convert	To	Multiply by
inches (in.)	millimeters (mm)	25.4
feet (ft)	meters (m)	0.305
yards (yd)	meters (m)	0.914
miles (miles)	kilometers (km)	1.61
square inches (sq in.)	square millimeters (mm^2)	645
square feet (sq ft)	square meters (m^2)	0.093
square yards (sq yd)	square meters (m^2)	0.836
square miles (sq miles)	square kilometers (km^2)	2.59
acres (acre)	hectares (ha)	0.405
cubic inches (cu in.)	cubic millimeters (mm^3)	16,400
cubic feet (cu ft)	cubic meters (m^3)	0.028
cubic yards (cu yd)	cubic meters (m^3)	0.765
pounds (lb) mass	kilograms (kg)	0.453
tons (ton) mass	kilograms (kg)	907
pound force (lbf)	newtons (N)	4.45
kilogram force (kgf)	newtons (N)	9.81
pounds per square foot (psf)	pascals (Pa)	47.9
pounds per square inch (psi)	kilopascals (kPa)	6.89
U.S. gallons (gal)	liters (L)	3.79
acre-feet (acre-ft)	cubic meters (m^3)	1,233

POST-BUCKLING ANALYSIS OF GUYED TOWERS

By Alexander Chajes,[1] M. ASCE and David Ling[2]

INTRODUCTION

Cable-guyed towers can be subdivided into two categories: (1) Very tall towers supported by several sets of guy wires; and (2) relatively short towers supported by a single set of cables. The tall towers, which are used primarily as radio and television antennas, and for which wind and gravity are the primary loads, have been studied extensively and significant information about their behavior is available in the literature (3,4,6). By comparison, short towers, which are used frequently today to support wind turbines and offshore platforms and are consequently subjected to large concentrated vertical and horizontal loads at their tops, have not yet been fully investigated.

A previous paper (1) presented the results of a linear stability analysis, whose aim was to obtain the critical loads of axially compressed short towers supported by a single set of guy wires. It is the purpose of this paper to extend the results of that investigation by describing the elastic post-buckling behavior of short towers. It is by now a well-known fact that the elastic collapse load of an actual imperfect structure can be less than, equal to, or greater than the critical load, depending on the post-buckling characteristics of the system. As a consequence, a knowledge of those characteristics is essential for predicting the collapse load.

The nonlinearities considered in the finite deflection analysis described here include axial shortening of the mast due to bending and axial stress, and changes in slope and length of the cables. The cables are, however, assumed to remain straight at all times, i.e., cable sag is neglected. Based on a more precise investigation, which accounts for the actual shape of the cables, it has been concluded that cable sag is relatively unimportant for short towers (5).

Using the theorem of stationary potential energy, the governing equations are obtained in closed form and then solved by numerical analysis.

Since the behavior of a guyed tower depends on the support conditions at the base of the mast, the relative stiffness of mast and cables, the initial slope of the cables, and the pretension in the cables, the effect of each of these

[1]Assoc. Prof. of Civ. Engrg., Univ. of Massachusetts, Amherst, Mass. 01003.
[2]Grad. Student in Civ. Engrg., Univ. of Massachusetts, Amherst, Mass. 01003.

Note.—Discussion open until May 1, 1982. To extend the closing date one month, a written request must be filed with the Manager of Technical and Professional Publications, ASCE. Manuscript was submitted for review for possible publication on December 22, 1980. This paper is part of the Journal of the Structural Division, Proceedings of the American Society of Civil Engineers, ©ASCE, Vol. 107, No. ST12, December, 1981. ISSN 0044-8001/81/0012-2313/$01.00.

factors is investigated. In addition, systems with four cables, 90° apart, and systems with three cables, 120° apart, are considered.

Derivation of Equations

Consider the guyed tower depicted in Fig. 1(*a*). The mast has length, L; moment of inertia, I; cross-sectional area, A; and modulus of elasticity, E. Each cable has an initial length, S, and makes an initial angle, α, with the horizontal. They have a cross-sectional area, A_c, and modulus of elasticity, E_c. The loading consists of a vertical load, P, and a horizontal load, H, applied

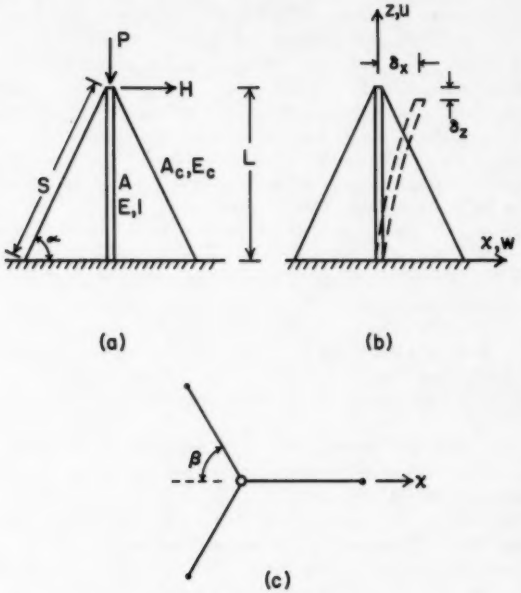

FIG. 1.—Guyed Tower

at the top of the tower. In addition, the cables may be subjected to an initial tension, T, which induces an axial compression, C, in the mast.

To obtain the differential equations and boundary conditions of the system, the principle of stationary potential energy is utilized. The total potential energy is

$$\Pi = U_M + U_c + \Omega \quad \ldots\ldots\ldots\ldots\ldots\ldots\ldots\ldots\ldots\ldots\ldots\ldots\ldots\ldots (1)$$

in which U_M = the strain energy in the mast; U_c = the strain energy in the cables; and Ω = the potential of the external loads. Only the increase in energy beyond that existing due to cable pretension is considered.

The strain in the mast due to bending and axial deformation is

$$\epsilon = u' + \frac{1}{2}(w')^2 - zw'' \quad \ldots\ldots\ldots\ldots\ldots\ldots\ldots\ldots\ldots\ldots\ldots\ldots (2)$$

in which u and w = the displacements in the z and x directions, as indicated in Fig. 1(*b*); and $'$ = differentiation with respect to z. In view of Eq. 2, the strain energy in the mast is given by

$$U_M = \int_o^L \left\{ \frac{EA}{2}\left[u' + \frac{1}{2}(w')^2\right]^2 + \frac{EI}{2}(w'')^2 \right.$$

$$\left. - C\left[u' + \frac{1}{2}(w')^2\right)\right]\right\} dz \quad \ldots\ldots\ldots\ldots\ldots\ldots\ldots\ldots\ldots\ldots\ldots\ldots (3)$$

The strain energy in the cables is

$$U_c = \sum_{i=1}^{n}\left(\frac{1}{2}K\Delta_i^2 + T\Delta_i\right) \quad \ldots\ldots\ldots\ldots\ldots\ldots\ldots\ldots\ldots\ldots\ldots\ldots (4)$$

in which $K = A_c E_c / S$ = the stiffness of each cable; Δ_i = the elongation of any cable; and n = the number of cables.

The cable elongation Δ_i is given by

$$\Delta_i = \sqrt{S^2 + 2D\cos\beta_i\delta_x + 2L\delta_z + \delta_x^2 + \delta_z^2} - S \quad \ldots\ldots\ldots\ldots\ldots\ldots\ldots\ldots (5)$$

in which $D = S\cos\alpha$; β_i = the angle between the plane containing any cable and the x-z plane as shown in Fig. 1(*c*); and δ_x and δ_z = the horizontal and vertical displacements of the top of the pole as indicated in Fig. 1(*b*).

The potential energy of the external loads is

$$\Omega = P\delta_z - H\delta_x \quad \ldots\ldots\ldots\ldots\ldots\ldots\ldots\ldots\ldots\ldots\ldots\ldots\ldots\ldots\ldots\ldots (6)$$

It should be noted that P is assumed positive when acting down.

Combining the expressions in Eqs. 3, 4, and 6 gives the total potential energy

$$\Pi = P\delta_z - H\delta_x + \int_o^L \left\{ \frac{EA}{2}\left[u' + \frac{1}{2}(w')^2\right]^2 + \frac{EI}{2}(w'')^2 \right.$$

$$\left. - C\left[u' + \frac{1}{2}(w')^2\right]\right\} dz + \sum_{i=1}^{n}\left(\frac{1}{2}K\Delta_i^2 + T\Delta_i\right) \quad \ldots\ldots\ldots\ldots\ldots\ldots\ldots\ldots (7)$$

The requirement that this expression has a stationary value leads to the differential equations

$$\frac{d}{dz}\left[u' + \frac{1}{2}(w')^2\right] = 0 \quad \ldots\ldots\ldots\ldots\ldots\ldots\ldots\ldots\ldots\ldots\ldots\ldots\ldots\ldots\ldots\ldots (8)$$

$$EIw^{iv} - \backslash EA\,\frac{d}{dz}\left\{w'\left[u' + \frac{1}{2}(w')^2\right]\right\} + Cw'' \quad \ldots\ldots\ldots\ldots\ldots\ldots\ldots\ldots\ldots\ldots (9)$$

and to the boundary conditions

$$P + \sum_i \frac{L + \delta_z}{\Delta_i + S}(K\Delta_i + T) + EA\left[u' + \frac{1}{2}(w')^2\right]_L - C = 0 \quad \ldots\ldots\ldots\ldots (10)$$

$$-H + \sum_i \frac{D \cos \beta_i + \delta_x}{\Delta_i + S} (K\Delta_i + T)$$

$$+ w' \left\{ EA \left[u' + \frac{1}{2} (w')^2 \right]_L - C \right\} - EI\, w'''_L = 0 \quad \ldots\ldots\ldots\ldots (11)$$

in which the notation $[\ ]_L$ denotes that the function is evaluated at $z = L$.

Eqs. 10 and 11 are conditions of equilibrium for forces in the vertical and lateral direction, respectively, at the top of the mast. In addition to these boundary conditions, $w_o = u_o = 0$, and either $w''_o = 0$ for a hinged base, or $w'_o = 0$ for a fixed base.

In the form presented above, Eqs. 8 and 9 are nonlinear and coupled in u and w. However, following a procedure outlined in Ref. 2, it is possible to simplify the equations considerably. Integrating Eq. 8 gives

$$u' + \frac{1}{2} (w')^2 = \text{constant} \quad \ldots\ldots\ldots\ldots\ldots\ldots\ldots\ldots (12)$$

and from Eq. 10, the axial strain at the top of the mast at $z = L$ is

$$\left[u' + \frac{1}{2} (w')^2 \right]_L = \frac{1}{EA} \left[-P - \sum_i \frac{L + \delta_z}{\Delta_i + S} (K\Delta_i + T) + C \right] \quad \ldots\ldots (13)$$

In view of Eq. 12, the axial strain is constant along the entire length of the mast. Thus, Eq. 13 is valid not only at $z = L$ but for all values of z.

Substitution of Eq. 13 into Eq. 9 gives

$$EI\, w^{iv} + \left[P + \sum_i \frac{L + \delta_z}{\Delta_i + S} (K\Delta_i + T) \right] w'' = 0; \quad \text{or} \quad w^{iv} + \mu^2 w'' = 0 \qquad (14)$$

$$\text{in which} \quad \mu^2 = \frac{1}{EI} \left[P + \sum_i \frac{L + \delta_z}{\Delta_i + S} (K\Delta_i + T) \right] \quad \ldots\ldots\ldots\ldots (15)$$

Eq. 9 has thus been reduced from a nonlinear equation in u and w, to a linear equation with constant coefficients involving only w.

Making use of Eq. 13, it is also possible to remove u from Eq. 11. Combining Eqs. 13 and 15 leads to

$$u' + \frac{1}{2} (w')^2 = \frac{1}{EA} (-EI\mu^2 + C) \quad \ldots\ldots\ldots\ldots\ldots\ldots (16)$$

and substitution of Eq. 16 in Eq. 11 gives

$$-H + \sum_i \frac{D \cos \beta_i + \delta_x}{\Delta_i + S} (K\Delta_i + T) - \mu^2 EI\, w'_L - EI\, w'''_L = 0 \quad \ldots\ldots\ldots (17)$$

A third equation, containing only the variable w, is obtained by solving Eq. 16 for u' and integrating the resulting expression. Thus

$$\int_o^L u'\, dz = \int_o^L \left[\frac{1}{EA} (C - EI\mu^2) - \frac{1}{2} w'^2 \right] dz \quad \ldots\ldots\ldots\ldots\ldots (18)$$

and since $\delta_z = \int_o^L u'\, dz$, one obtains

$$dz = \frac{L}{EA}(C - EI\mu^2) - \frac{1}{2}\int_o^L w'^2\,dz \quad \ldots\ldots\ldots\ldots\ldots\ldots \quad (18a)$$

The final step consists of solving Eq. 14 and substituting the result into Eqs. 17 and 18. The solution of Eq. 14 is

$$w = A_1 \sin \mu z + A_2 \cos \mu z + A_3 z + A_4 \quad \ldots\ldots\ldots\ldots\ldots\ldots \quad (19)$$

Making use of the appropriate boundary conditions for either a hinged or a fixed base tower, the constants in Eq. 19 can be evaluated, and the resulting expression and its derivatives substituted into Eqs. 17 and 18. This leads to two sets of nonlinear algebraic equations in δ_x and δ_z whose solutions give the load-deflection characteristics of the towers.

Fixed Base.—If the base of the mast is fixed, the final equations are

$$-H + \sum_i \frac{D\cos\beta_i + \delta_x}{\Delta_i + S}(K\Delta_i + T) + \frac{\mu^3 EI\,\delta_x}{\tan \mu L - \mu L} = 0 \quad \ldots\ldots\ldots \quad (20)$$

$$\delta z = \left(\frac{nT\sin\alpha}{EA} - \mu^2 r^2\right) L - \frac{\mu^2 L\,\delta_x^2}{4(\tan \mu L - \mu L)^2}\left(3 - \frac{3\tan \mu L}{\mu L} + \tan^2 \mu L\right) \quad \ldots\ldots\ldots\ldots\ldots \quad (21)$$

in which $r^2 = I/A$.

Hinged Base.—If the base is hinged, there exists two possible modes of deformation. The mast can either rotate as a rigid body about its base, or it can bend like a hinged-hinged column, in addition to rotating. The former of these two modes occurs only when the stiffness of the cable system is small compared to that of the mast. Since this will rarely be the case for an actual tower, only the bending mode will be considered. The equations governing this mode are

$$-H + \sum_i \frac{D\cos\beta_i + \delta_x}{\Delta_i + S}(K\Delta_i + T) - \frac{\pi^2 EI\,\delta_x}{L^3} = 0 \quad \ldots\ldots\ldots\ldots \quad (22)$$

$$P + \sum_i \frac{L + \delta_z}{\Delta_i + S}(K\Delta_i + T) - \frac{\pi^2 EI}{L^2} = 0 \quad \ldots\ldots\ldots\ldots\ldots\ldots \quad (23)$$

Solution of Equations

Using the Newton-Raphson iteration method, numerical solutions of the coupled nonlinear equations in δ_x and δ_z, derived in the previous section, have been obtained. Although the natural procedure in dealing with equations of this type is to vary the applied load and solve for δ_x and δ_z, it is necessary, in order to obtain convergence in the vicinity of the maximum load, to vary δ_x and solve for the corresponding load and δ_z. If, during any iteration cycle, the force in a cable becomes negative, indicating the cable to be slack, the term corresponding to that cable is dropped from the solution. All solutions have been carried out for a tower 100 ft (30.5 m) high, with a 6.625 in. (168.3 mm)

diam pipe mast. Both the mast and the cables are steel with $E = 29 \times 10^3$ ksi (200×10^6 kN/m^2), and $E_c = 24 \times 10^3$ ksi (165×10^6 kN/m^2). It has been assumed that the plane containing H, if a horizontal load is present, and the plane in which the mast bends with or without H, coincides with the x-z plane, as defined in Fig. 1(*c*). This assumption results in the most critical loading conditions for the tower.

Numerical Results

Fixed Base.—Fig. 2 depicts typical post-buckling curves for fixed-base towers. The ratio of the applied load, P, to the critical load of a fixed-hinged column, P_f, is plotted against the ratio of the lateral displacement, δ_x, to the tower height, L. The cables that support the mast are assumed to have a small amount of pretension, sufficient to prevent the mast from buckling as a fixed-free column.

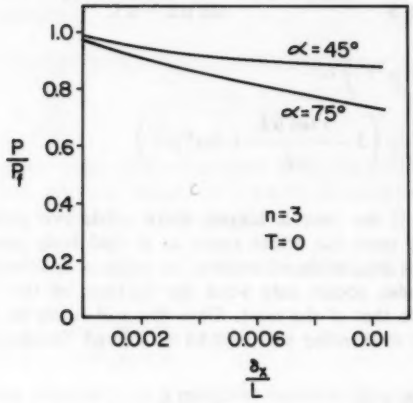

FIG. 2.—Post-Buckling Curves for Fixed-Base Towers

However, compared to the applied load, P, the tension in the cables at the onset of buckling is assumed to be negligible.

It is evident from the curves that buckling commences at a load very close to the critical load of a fixed-hinged column. This result agrees with the conclusions obtained using a linear analysis (1). In that analysis it was shown that only a minimum cable stiffness is required to produce a lateral restraint at the top of the mast that is nearly equivalent to a hinged support. The curves also indicate that the vertical load, P, which the tower can support, decreases gradually with increasing lateral deflection subsequent to the onset of buckling, and that this decrease in load becomes more pronounced as the initial slope of the cables, α, increases.

As the mast bends, an increasing tension force develops in the cables on the side opposite to the deflection. As a consequence, the mast is subjected to a compression force equal to the vertical components of these cable tension

forces, and the applied load, P, that the tower can support is accordingly reduced. The larger the initial slope of the cables, the larger the vertical components of the cable tension forces, and the larger the reduction in P with increasing lateral deflection. Except for towers with extremely flexible cables, which are rarely used, changes in the diameter of the cables or in the number of cables do not significantly affect the shape of the post-buckling curve of the system.

The curve in Fig. 3 depicts the effect of cable pretension on the buckling characteristics of the tower. It indicates that the presence of cable pretension reduces the critical load by an amount very nearly equal to the vertical components of the cable tension forces. In other words, for the system described in Fig. 3, the vertical components of the pretension forces add up to approximately $0.3P_f$ and the critical load is thus equal to $0.7P_f$.

Comparison of the curve in Fig. 3, with those in Fig. 2, also shows that the presence of cable pretension markedly affects the shape of the post-buckling

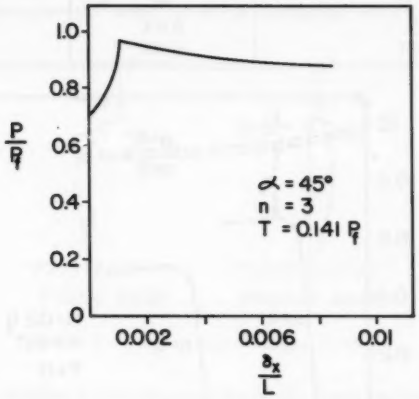

FIG. 3.—Effect of Cable Pretension on Post-Buckling Curves of Fixed-Base Towers

curve. Instead of a gradual decrease in P with increasing deflection, as was the case when no pretension existed, the curves now exhibit a sharp increase in P as the mast begins to buckle, followed by a gradual decrease in P as the deflection continues to increase. The system thus exhibits considerable post-buckling strength initially before it eventually becomes unstable.

The difference in behavior between towers that possess initial cable tension and those that do not can be explained by considering the relative values of δ_x and δ_z for the two cases in Table 1. For small deformations, the tower with initial cable tension, T, undergoes an axial shortening, δ_z, that is three times as large as the lateral displacement, δ_x. As a consequence, the cables shorten and most of the cable tension that originally existed disappears. This results in a decrease in C, the cable induced compression of the mast, and a corresponding increase in P. By comparison, in the tower with no initial cable tension, the lateral displacement, δ_x, exceeds the axial shortening, δ_z, of the mast, causing a buildup of tension in the cables resisting the deformation.

This subjects the mast to an increasing compression, C, and results in a reduction of the applied load, P, that the tower can support.

Fig. 4 depicts the effect of a horizontal load on the ability of a tower to support vertical load. The horizontal load is assumed to be applied first, and the vertical load thereafter. The solid curves in the figure represent the behavior of three- and four-cable systems with $H = 0.2P_f$. For comparison, systems with zero horizontal load are also included. They are indicated by the dashed curves.

For each of the two cases considered, the presence of horizontal load significantly reduces the ability of the tower to resist vertical load. The four-cable

TABLE 1.—Displacement at Top of Tower

Pretension T/P_f (1)	δ_x/L (2)	δ_x/L (3)
0	0.001	−0.0004
0.1	0.001	−0.003

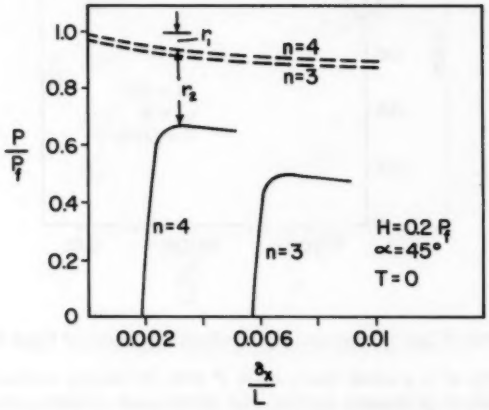

FIG. 4.—Effect of Horizontal Load on Carrying Capacity of Fixed-Base Towers

system with a horizontal load is able to support a maximum load of $0.67P_f$, and the three-cable system has its carrying capacity reduced to $0.51P_f$. A horizontal load, like a lateral deflection, causes tension forces to be developed in the aft cables. These forces, in turn, induce a compression force in the mast whose presence reduces the ability of the mast to support an external load, P.

It is evident that a greater reduction in the capacity to resist vertical load occurs for the three-cable system than for the four-cable system. This is due to the fact that a given horizontal load induces a vertical compression in the mast equal to $2H \tan \alpha$ for three cables, and $\sqrt{2}\ H \tan \alpha$ for four cables.

An increase in cable slope always increases the compression induced in the

mast by cable tension forces. Thus, the reduction in the carrying capacity of the tower due to the presence of a horizontal force will increase as α increases.

As indicated in the figure, the difference between the critical load of a tower without horizontal load, and the maximum carrying capacity with horizontal load, can be subdivided into two parts labeled r_1 and r_2. The first of these is the reduction in carrying capacity that results from the unstable post-buckling characteristics of the system. In other words, at the lateral deflection caused by H, the tower can resist less vertical load than it can at zero lateral displacement. The second reduction, r_2, is due to the compression induced in the mast by the cable tension forces required to resist H. While it is possible to obtain a very good approximation of r_2 by assuming the mast and the aft cables to behave like a truss, the value of r_1 can be obtained only from a nonlinear analysis of the system.

In the foregoing analysis of the effects of horizontal forces, it was assumed that the cables had zero pretension. If large cable pretensions are present they do not materially alter the effect of H. A horizontal force will still cause a

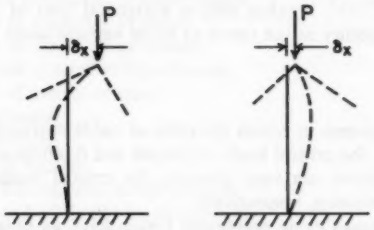

FIG. 5.—Deformation of Guyed Towers

reduction in the maximum carrying capacity of the tower because it still induces a sizable compression in the mast.

Hinged Base.—Except for the fact that the critical load of hinged-base towers is approximately half as large as that of fixed-base towers, the behavior of the two is very similar. The most significant difference between the two is that the decrease in P, with increasing lateral deflection, is much smaller for hinged-base towers than for fixed-base towers. In other words, the post-buckling curve of a hinged-base tower is almost horizontal. This difference in behavior is largely due to the different ways in which the two systems deform. As shown in Fig. 5, the fixed-base tower has a larger lateral deflection at its upper end than the hinged-base tower. As a consequence, buckling induces larger cable tensions and more mast compression in the fixed-base tower than in the hinged-base tower, and the former has a more unstable post-buckling curve than the latter.

Numerical Example.—Consider a fixed base tower consisting of a 6.625 in. (168.3 mm) diam pipe, and three 0.25 in. (6.4 mm) diam cables. The mast and cables have the following properties: $L = 100$ ft (30.5 m); $I = 28.1$ in.^{4} (11,690 mm^4); $A = 5.58$ in.^{2} (360 mm^2); $E = 30 \times 10^3$ ksi (200×10^6 kN/m^2); A_c

= .049 in.^{2} (3.2 mm^2); E_c = 24 × 10^3 ksi (165 × 10^6 kN/m^2); α = 45°; and T = 0.

Ref. 1 indicates that only a minimum cable stiffness is necessary to produce a lateral restraint at the top of the mast equivalent to a hinged support. Thus, the critical load of the given tower is close to that of a hinged-fixed column, i.e., $P_{cr} = 0.99P_f$ = 11.7 kips (52 kN). Since the cables are already producing the maximum lateral restraint possible, the critical load of the tower can be increased only by increasing the stiffness of the mast. An increase in mast diameter from 6.625 in. (16.83 cm) to 8.625 in. (21.91 cm) increases the critical load from 11.7 kips (52 kN) to 30.2 kips (134.4 kN).

According to Fig. 3, an initial cable tension of T = 1.2 K (5.3 kN) reduces the critical load from 11.7 kips (52 kN) to 8.2 kips (36.4 kN). However, as soon as the mast begins to bend, the carrying capacity of the tower increases to 11.2 kips (50 kN). Thus, even a relatively large cable pretension does not significantly decrease the carrying capacity of the tower.

Finally, Fig. 4 shows that a horizontal load of H = 2.4 kips (10.7 kN) reduces the vertical load that the tower can support by 50%. By comparison, if α is increased from 45°–75°, it takes only a horizontal load of H = 0.6 kips (2.7 kN) to reduce the ability of the tower to resist vertical loads by 50%.

Conclusions

1. Except for systems in which the ratio of cable stiffness to mast stiffness is extremely small, the critical loads of hinged and fixed-base towers with small cable pretension forces are very close to the critical loads of hinged-hinged and hinged-fixed columns, respectively.
2. Towers with small cable pretension forces have an unstable post-buckling curve. However, except for very steep guy wires, the decrease in vertical load with increasing deflection is relatively small. As a consequence, these systems will not be "imperfection-sensitive" and the actual buckling load of a real tower can be expected to be fairly close to the theoretically obtained critical load.
3. The presence of sizable cable pretension forces decreases the load at which buckling begins by an amount equal to the sum of the vertical components of the cable forces. However, as soon as the tower bends, the cable tension forces decrease rapidly with a corresponding increase in the capacity of the tower to support vertical load. The net effect is that a tower with large cable pretension forces can support a vertical load that is only slightly smaller than the load a tower without sizable cable pretension forces can support.
4. The presence of a horizontal load results in a significant decrease in the capacity of the tower to resist vertical load. Since this decrease is primarily caused by the compression that the horizontal load induces in the mast, increases in the magnitude of the horizontal load cause corresponding decreases in the ability of the tower to resist vertical load.

Appendix I.—References

1. Chajes, A., and Chen, W. S., "Stability of Guyed Towers," *Journal of the Structural Division*, ASCE, Vol. 105, No. ST1, Proc. Paper 14327, Jan., 1979, pp. 163–174.
2. Dym, C. L., and Shames, I. H., *Solid Mechanics: A Variational Approach*, McGraw Hill Book Co., Inc., New York, N.Y., 1973, pp. 467–470.

3. Goldberg, J. E., and Gaunt, J. T., "Stability of Guyed Towers," *Journal of the Structural Division*, ASCE, Vol. 99, No. ST4, Proc. Paper 9683, Apr., 1973, pp. 741–756.
4. Hull, F. H., "Stability Analysis of Multilevel Guyed Towers," *Journal of the Structural Division*, ASCE, Vol. 88, No. ST2, Proc. Paper 3091, Apr., 1962, pp. 61–80.
5. Ling, D., "Non-Linear Behavior of Guyed Towers," thesis presented to the University of Massachusetts, at Amherst, Mass., in 1980, in partial fulfillment of the requirements for the degree of Doctor of Philosophy.
6. Williamson, R. A., "Stability of Guyed Towers Under Ice Loads," *Journal of the Structural Division*, ASCE, Vol. 99, No. ST12, Proc. Paper 10242, Dec., 1973, pp. 2391–2408.

Appendix II.—Notation

The following symbols are used in this paper:

A = cross-section area of mast;
A_c = cross-section area of cable;
C = axial compression induced in mast by cable tension forces;
D = horizontal projection of cable length;
E = modulus of elasticity of mast;
E_c = modulus of elasticity of cables;
H = lateral load applied at top of mast;
I = moment of inertia of mast;
K = cable stiffness;
L = height of mast;
n = number of cables;
P = vertical load applied at top of mast;
P_f = critical load of fixed-hinged column;
r = radius of gyration;
r_1, r_2 = reduction in load carrying capacity due to horizontal load;
S = initial length of cable;
T = initial cable tension force;
U_c = strain energy in cables;
U_M = strain energy in mast;
u = displacement in z-direction;
w = displacement in x-direction;
x = coordinate axis normal to mast;
z = coordinate axis along mast;
α = initial angle between cable and horizontal plane;
β_i = angle between ith cable and x-z plane;
Δ_i = elongation of ith cable;
δ_x = horizontal displacement of mast top;
δ_z = vertical displacement of mast top;
ϵ = strain in mast due to bending and axial deformation;
μ = load parameter;
Π = total potential energy; and
Ω = potential energy of external loads.

Subscripts

c = cable; and
M = mast.

NONLINEAR DYNAMIC ANALYSIS BY MODAL SUPERPOSITION

By Louis F. Geschwindner, Jr.,[1] M. ASCE

INTRODUCTION

It is becoming more and more desirable to look into the nonlinear aspects of structural response to dynamic loads. In some instances this allows for refinement of our understanding of the behavior of a particular system, while in others, it is almost imperative if we are to have even a general appreciation of the response of a particular system. An example of the first case might involve the inclusion of partial rigidity of joints in a steel frame, while the second case might relate to the geometric nonlinearities associated with cable networks.

Numerous methods for dealing with the nonlinear dynamic analysis problem have been presented in the literature. Some implicit approaches have been proposed by Newmark (7), Houbolt (5), and Park (8). Explicit methods such as central difference predictors and the Runge-Kutta approach are also used. Each has its advantages and disadvantages. A good review of some of these methods is found in Ref. 1.

The method presented here uses the modal superposition approach, corrected to account for the nonlinear aspects of the system response. The method is presented by examining the results for cable network problems, where the changes in geometry under load provide the nonlinearity of the system.

EQUATIONS OF MOTION

The equations of motion for a nonlinear system may be written, in matrix form, as

$$[M]\{\ddot{\delta}\} + [K]\{\delta\} + \{R(\delta)\} = \{P(t)\} \quad \ldots\ldots\ldots\ldots\ldots\ldots\ldots\ldots (1)$$

in which $[M]$ = diagonal mass matrix; $[K]$ = linear stiffness matrix; $\{R(\delta)\}$ = nonlinear terms, as a function of displacements; $\{P(t)\}$ = dynamic loads, as a function of time; and δ, $\ddot{\delta}$ = displacements and accelerations, respectively.

[1]Asst. Prof. of Architectural Engrg., Pennsylvania State Univ., University Park, Pa.

Note.—Discussion open until May 1, 1982. To extend the closing date one month, a written request must be filed with the Manager of Technical and Professional Publications, ASCE. Manuscript was submitted for review for possible publication on December 3, 1980. This paper is part of the Journal of the Structural Division, Proceedings of the American Society of Civil Engineers, ©ASCE, Vol. 107, No. ST12, December, 1981. ISSN 0044-8001/81/0012-2325/$01.00.

If the nonlinear terms are neglected, the displacements and accelerations can be obtained as a combination of the independent patterns described by the mode shapes and corresponding modal amplitudes. They may be written as

$$\{\delta\} = [\Phi]\{Y(t)\} \quad \ldots (2)$$

and $$\{\ddot{\delta}\} = [\Phi]\{\ddot{Y}(t)\} \quad \ldots (3)$$

in which $[\Phi]$ = the matrix of mode shapes; and $Y(t)$ and $\ddot{Y}(t)$ = the modal amplitudes. Substitution of Eqs. 2 and 3 into Eq. 1, and reordering, leads to

$$[M][\Phi]\{\ddot{Y}(t)\} + [K][\Phi]\{Y(t)\} = \{P(t)\} - \{R(\delta)\} \quad \ldots (4)$$

If the right-hand side of Eq. 4 is defined as

$$\{Q(t,\delta)\} = \{P(t)\} - \{R(\delta)\} \quad \ldots (5)$$

Eq. 4 becomes

$$[M][\Phi]\{\ddot{Y}(t)\} + [K][\Phi]\{Y(t)\} = \{Q(t,\delta)\} \quad \ldots (6)$$

Since mode shapes from the linear analysis will be orthogonal, these equations may be uncoupled if the system is premultiplied by the transpose of the nth mode shape. Thus

$$\{X\}_n^T[M][\Phi]\{\ddot{Y}(t)\} + \{X\}_n^T[K][\Phi]\{Y(t)\} = \{X\}_n^T\{Q(t,\delta)\} \quad \ldots (7)$$

Due to the orthogonality of mode shapes, all but the nth terms vanish, which yields

$$\{X\}_n^T[M]\{X\}_n \ddot{Y}_n(t) + \{X\}_n^T[K]\{X\}_n Y_n(t) = \{X\}_n^T\{Q(t,\delta)\} \quad \ldots (8)$$

Eq. 8 may be written as

$$M_n \ddot{Y}_n(t) + K_n Y_n(t) = Q_n(t,\delta) \quad \ldots (9)$$

in which $$M_n = \{X\}_n^T[M]\{X\}_n \quad \ldots (10)$$

$$K_n = \{X\}_n^T[K]\{X\}_n \quad \ldots (11)$$

and $$Q_n(t,\delta) = \{X\}_n^T\{Q(t,\delta)\} \quad \ldots (12)$$

The terms M_n and K_n = the generalized mass and stiffness. They are the same for this nonlinear formulation as they would be for the linear formulation. The generalized load, $Q_n(t,\delta)$, however, is different and is the term through which the nonlinearity is modeled. Substitution of Eq. 5 into Eq. 12 yields

$$Q_n(t,\delta) = \{X\}_n^T[\{P(t)\} - \{R(\delta)\}] \quad \ldots (13)$$

If the nonlinear contribution were known ahead of time, the generalized load, $Q_n(t,\delta)$, could be determined, and Eq. 9 could be solved as a typical linear single-degree-of-freedom problem using any acceptable method. The nonlinear contribution, $\{R(\delta)\}$, is generally not known *a priori* and may be different at any time, t. Thus, it can be said that $\{R(\delta)\}$ is, actually, indirectly a function of time. In order to factor the time function out of Eq. 13, the nonlinear contribution is treated as a known load. Eq. 13 is then multiplied and divided by $\{X\}_n^T\{P_o\}$, in which $\{P_o\}$ = the vector of load amplitudes. Thus, Eq. 13 becomes

$$Q_n(t,\delta) = \{X\}_n^T \{P_o\} \left(\frac{\{X\}_n^T [\{P(t)\} - \{R(\delta)\}]}{\{X\}_n^T \{P_o\}} \right) \quad \ldots\ldots\ldots\ldots (14)$$

The bracketed term in Eq. 14 represents the variation in time, $fe_n(t)$, of the effective load, with the other term representing the generalized load, $(P_o)_n$. Thus

$$Q_n(t,\delta) = (P_o)_n fe_n(t) \quad \ldots\ldots\ldots\ldots\ldots\ldots\ldots\ldots\ldots\ldots (15)$$

The solution of Eq. 9, as given by the Duhamel integral, is given by

$$Y_n(t) = \frac{1}{M_n \omega_n} \int_o^t Q_n(\tau,\delta) \sin \omega_n (t-\tau)\, d\tau \quad \ldots\ldots\ldots\ldots\ldots\ldots (16)$$

Substitution of Eq. 15 into Eq. 16, and expansion of the integral, yields

$$Y_n(t) = \frac{(P_o)_n}{M_n \omega_n^2} \left[\omega_n \sin \omega_n t \int_o^t fe_n(\tau) \cos \omega_n \tau\, d\tau \right.$$

$$\left. - \omega_n \cos \omega_n t \int_o^t fe_n(\tau) \sin \omega_n \tau\, d\tau \right] \quad \ldots\ldots\ldots\ldots\ldots\ldots (17)$$

which simplifies to

$$Y_n(t) = (\mathrm{PF})_n (\mathrm{IAF})_n \quad \ldots\ldots\ldots\ldots\ldots\ldots\ldots\ldots\ldots\ldots (18)$$

in which $(\mathrm{PF})_n$ = the participation factor for mode n and remains constant for any time, t; and $(\mathrm{IAF})_n$ = the Instantaneous Amplification Factor. This IAF will differ from the linear IAF due to the inclusion of the $\{R(\delta)\}$ terms through the time variation of the effective load.

Procedure for Evaluation

After the natural frequencies and mode shapes are determined for a linear formulation, the nonlinear modal superposition scheme may be employed to determine the nonlinear forced vibration response. As can be seen from Eq. 17, the participation factors remain constant throughout the entire analysis and are the same as for a linear analysis.

Since the nonlinear terms are a function of displacement, and the displacements are small at the beginning of the response, an assumption that $\{R(\delta)\} = 0.0$ for the first time station is generally a good one.

The evaluation of the IAFs, the bracketed terms in Eq. 17, for a general time function, requires a numerical integration scheme if a closed solution for the integrals is not available. This holds for either the linear or nonlinear formulation. With the nonlinear problem, the complete effective time function, $fe_n(t)$, is not known at the beginning of the analysis, but is determined at each time interval from the bracketed term in Eq. 14 using the current values for $\{R(\delta)\}$. Assuming a parabolic variation of the effective time function, the integrals in Eq. 17 are evaluated and the IAFs for this trial are obtained. The modal amplitudes, $Y_n(t)$ and $\ddot{Y}_n(t)$, are then obtained in the same manner as for a linear analysis. The corresponding displacements and accelerations, δ and $\ddot{\delta}$, are calculated with Eqs. 2 and 3.

The nonlinear terms, $\{R(\delta)\}$, are then evaluated from Eq. 1 and compared with the assumed values. For the first time station, the nonlinear terms were taken initially as zero. The calculated terms are small and the difference between the assumed and calculated values is usually less than the set tolerance. If that is the case, the calculated displacements are accepted as correct and the calculated nonlinear terms are used to establish the continuous effective time function.

For the next time station, an assumption is needed for the nonlinear terms. It is possible to assume these terms to be zero; however, assuming them to be the same as those at the end of the calculations for the preceding time station will somewhat speed convergence. With these newly assumed terms, the process is repeated with trial IAFs and the resulting displacements and accelerations. When the difference between the assumed and calculated nonlinear terms is less than the permitted tolerance, the displacements for this time are accepted.

Essentially, this is the solution of a linear problem for each iteration, with the nonlinear terms applied as part of the time dependent loading. The modal superposition method for a linear problem allows for the evaluation of system response at any time, without evaluating the response for previous time stations, in cases where the integrals of Eq. 16 can be evaluated. For the general loading function, the integrals must be numerically evaluated. Thus, there will be some increment of time used to evaluate the IAFs. For the nonlinear problem, the effective loading function is not known prior to the evaluation of the nonlinear terms. This means there is a greater concern over the time increments for the nonlinear than the linear approach.

Results

The modified modal superposition method will be presented in comparison with Newmark's β method (7), since this is a well known technique for dynamic analysis.

The structure studied is the Aden Airways Building, Fig. 1, presented by Knudson (6), and previously used by the writer for parameter studies and forced vibration analysis (2,3). The static equilibrium configuration is given by

$$y = \frac{C_2}{b^2} z^2 - \frac{C_1}{a^2} x^2 + f \quad \ldots \ldots \ldots \ldots \ldots \ldots \ldots \ldots \ldots \ldots \ldots \ldots \ldots \quad (19)$$

in which $a = b = 57.5$ ft (17.5 m); C_1 = sag in x direction = 12.5 ft (3.81 m); C_2 = rise in z direction = 17.5 ft (5.33 m); and f = elevation at ($x = z = 0$) = 12.5 ft (3.81 m).

The additional structural data needed for an analysis are as follows:

Size of network—115 ft × 115 ft (35.1 m × 35.1 m);
Number of cables each way—7;
Properties of Cables (zinc-coated bridge strand):
Nominal diameter—1-13/16 in. (46.0 mm);
Area—1.97 in.^{2} (12.7 cm^2);
Mass per unit length—0.209 lb-sec^2/ft^2 (9.98 kg/m);

Breaking strength—404 kips (1,800 kN);
Modulus of elasticity—24,000 ksi (16,600 MN/m^2);
Horizontal component of initial cable tension:
x (longitudinal)—45.0 kips (200 kN);
z (transverse)—32.14 kips (143 kN);

The network has 75 degrees-of-freedom. The linear periods of vibration are given in Table 1. A complete study of the modes and frequencies for this network has been presented by the writer and West (2). They have also presented forced vibration studies for this network, using Newmark's β method (3). The

TABLE 1.—Natural Periods for Aden Airways Network

Number (1)	Period, in seconds (2)	Number (3)	Period, in seconds (4)	Number (5)	Period, in seconds (6)
1	0.191	26	0.022	51	0.006
2	0.160	27	0.022	52	0.006
3	0.158	28	0.017	53	0.006
4	0.152	29	0.017	54	0.006
5	0.143	30	0.017	55	0.006
6	0.139	31	0.016	56	0.006
7	0.135	32	0.012	57	0.006
8	0.129	33	0.011	58	0.005
9	0.128	34	0.011	59	0.005
10	0.120	35	0.011	60	0.005
11	0.119	36	0.011	61	0.005
12	0.113	37	0.011	62	0.005
13	0.106	38	0.009	63	0.005
14	0.100	39	0.009	64	0.005
15	0.096	40	0.009	65	0.005
16	0.090	41	0.009	66	0.005
17	0.087	42	0.008	67	0.005
18	0.082	43	0.008	68	0.005
19	0.076	44	0.006	69	0.005
20	0.066	45	0.006	70	0.004
21	0.066	46	0.006	71	0.004
22	0.062	47	0.006	72	0.004
23	0.061	48	0.006	73	0.004
24	0.059	49	0.006	74	0.004
25	0.053	50	0.006	75	0.004

formulation of the various components of Eq. 1 follows the development presented by the writer and West (2).

Time Increment.—Of particular interest in the development of any dynamic analysis is the required time increment for system stability and convergence. Knudson (6) and Goudreau (4) have presented studies relating to the selection of the time increment and the other factors associated with Newmark's β method. For a value of $\beta = 1/6$, the well known linear acceleration method, Newmark's β method, is unstable for a time increment, Δt, greater than $0.551T$, in which

T = the period associated with the largest frequency of the system.

If the Aden Airways network is subjected to a 2 kip transverse load ($+z$ direction in Fig. 1), with a duration of 0.08 sec as shown in Fig. 2, the response has been shown to be very nonlinear (3). In order to investigate the influence of the time interval, this system was studied with the Newmark linear and nonlinear methods, and the proposed method. The vertical displacements at joints 1 and 25, at a time $t = 0.06$ sec, are the same for both nonlinear approaches. The difference is seen in the number of iterations required to complete the analysis. Fig. 3 shows the relation between the number of iterations required and the time interval used for all three approaches. The Newmark approach

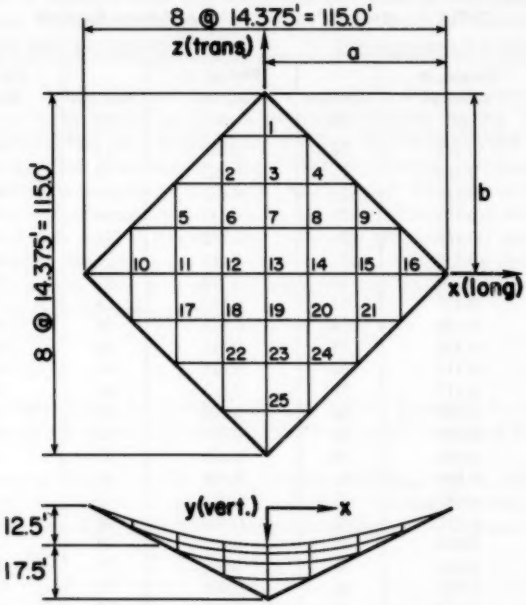

FIG. 1.—Aden Airways Network Geometry (1.0 ft = 0.305 m)

requires the same number of iterations for either the linear or nonlinear analysis. It is also seen that for a time interval greater than the previously discussed stability limit, this approach is unstable. The proposed method requires only two cycles, even for a time interval of approximately three times the Newmark stability limit.

Time Dependent Displacements.—The dynamic response of the Aden Airways network to loadings with the time variation of Fig. 2 has been presented in the literature (3). For cases where the loading is antisymmetric, a significant nonlinear response is seen. Figs. 4–6 give the response of selected joints of the Aden Airways network subjected to three different loading patterns. The

network is investigated for a vertical load of 2 kips per joint applied in an antisymmetric pattern about the main longitudinal cable, case I; a transverse load of 2 kips per joint in the z direction, case II; and, finally, a combination of the 2 kip transverse loading, with the 2 kip vertical load, case III. The forcing function is an impulse with the duration of 0.08 sec.

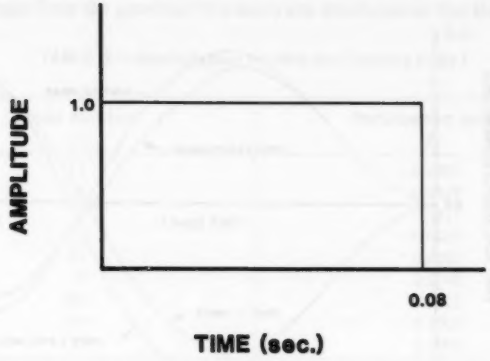

FIG. 2.—Amplitude Versus Time for Load Pulse

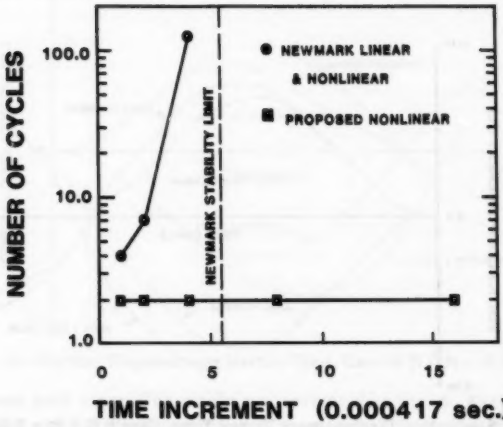

FIG. 3.—Iterations Versus Time Increment for Proposed Method and Newmark's β Method

For the loading of case I, joints 10–16 are not loaded, while an upward force of 2 kips is applied to joints 1–9, and a downward force of 2 kips is applied to joints 17–25. The dominant mode is mode 14 with a period $T = 0.100$ sec.

The participation factors corresponding to the nine most dominant modes, and the corresponding mode numbers, are given in Table 2.

The time dependent vertical displacements associated with joints 1 and 25, the joints which exhibit the greatest degree of nonlinearity, are presented in Fig. 4. In all cases, the analysis has been carried out using all modes. The figure shows the displacements for the nonlinear response, and the displacements

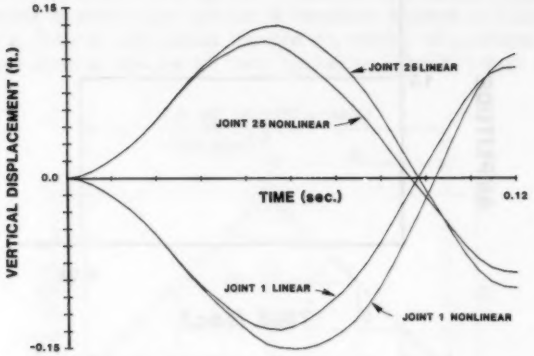

FIG. 4.—Vertical Displacement Versus Time, Case I (1.0 ft = 0.305 m)

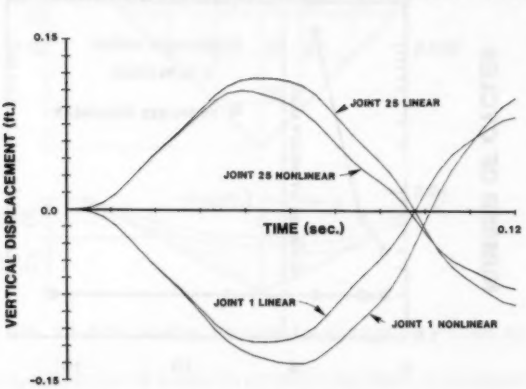

FIG. 5.—Vertical Displacement Versus Time, Case II (1.0 ft = 0.305 m)

from the linear modal superposition solution. The difference in stiffness between an upward displaced joint and a downward displaced joint results in a significant difference between the linear response, which cannot reflect this difference, and the nonlinear response.

The upward force applied at joint 1 is resisted by a longitudinal cable which it tends to put into reduced tension. Thus, the displacements are greater for

joint 1 in the nonlinear analysis than they are in the linear analysis. The opposite is true for the downward load on joint 25.

For case II, the 2 kip load applied at each joint in the transverse direction, the nonlinear response, is also evident in Fig. 5. As for case I, the linear and nonlinear response is given. For the transverse loading, mode 14 is again the dominant mode..

The loadings from the previous two cases are combined so that their responses

TABLE 2.—Participation Factors for Loading Case I

Mode number (1)	Participation factor (2)
14	−0.0901
16	0.0559
3	0.0417
18	−0.0267
11	0.0260
7	0.0090
26	0.0022
29	0.0009
35	0.0002

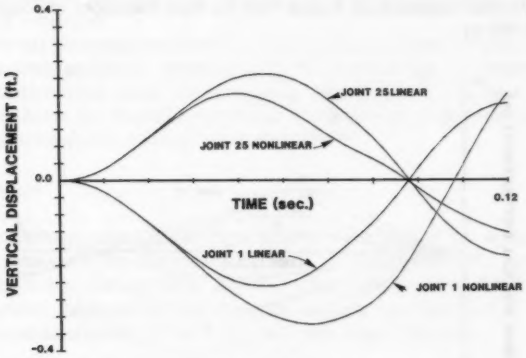

FIG. 6.—Vertical Displacement Versus Time, Case III (1.0 ft = 0.305 m)

will reinforce each other. The results are presented in Fig. 6. Again, the linear and nonlinear vertical displacements are presented. The amount by which the nonlinear solution varies from the linear solution is even greater in this combined loading than in any previous case.

Numerous authors have concluded that the linear solution to the dynamic response of cable networks is adequate; however, the results presented here, and previously (3), indicate that there are loading cases where consideration of the nonlinear response is necessary for an accurate analysis.

A direct comparison of the displacements obtained from the linear acceleration

method, and the proposed method, shows that the resulting displacements are essentially the same for all time stations.

Time Variation of Forcing Functions.—The variation of load magnitude, with time for four simplified time functions, yields the dynamic response indicated in Fig. 7. The loading pattern of case I, with three triangular pulses and the

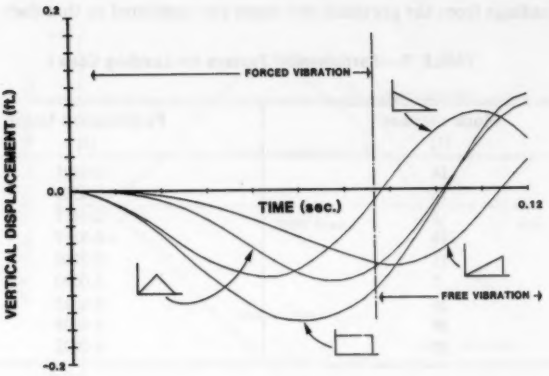

FIG. 7.—Vertical Displacement Versus Time for Four Variations of Forcing Function (1.0 ft = 0.305 m)

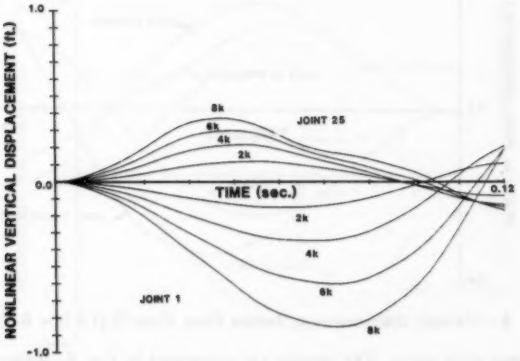

FIG. 8.—Vertical Displacement Versus Time for Four Load Magnitudes (1.0 ft = 0.305 m)

previously presented rectangular pulse, is used to determine the displacements of Fig. 7 which are the vertical displacements for joint 1. A comparison of the four curves indicates a response to the time variation as might be expected for a linear system, although the magnitudes are modified to reflect the nonlinearity of cable network.

Load Amplitude.—The response of the Aden Airways network to the 2 kip loading of case I is such that a few of the cables have a very low tension. If the load magnitude is increased to 4, 6 and 8 kips, and the elements are assumed to take compression, the resulting response is as indicated in Fig. 8. The time increment for these results was taken as 0.00333 sec. The analysis required two iterations at each time station.

The linear response, as predicted by the modal superposition approach, simply increases response amplitude while maintaining the period of the response. It can be seen that the nonlinear response reflects the changes over time of the system stiffness. Thus, the period of the response is not the same for all load magnitudes.

Summary and Conclusions

A hyperbolic paraboloid cable network has been used as the vehicle to present a new method for nonlinear dynamic analysis. Using this modified modal superposition approach, a number of response studies are carried out with simplified forcing functions and various loading patterns.

The proposed method has been shown to successfully determine the nonlinear dynamic response for systems which exhibit significant geometric nonlinearities. It accomplishes the analysis with much larger time increments and significantly fewer iterations than Newmark's β method, using the linear acceleration formulation. The results of this proposed method compare almost exactly with those of Newmark's method.

This study has presented a method for handling the nonlinear dynamic response of systems with geometric nonlinearities. Its applicability to problems with material nonlinearities needs to be treated. The method converged well and remained stable for the examples presented. Further study is required to establish the theoretical limits for stability and convergence.

Acknowledgment

The computations required for these studies were carried out using the IBM 370-3303 system of The Pennsylvania State University Computation Center, and the facilities of the Computer Aided Design Laboratory of the Department of Architectural Engineering. The financial support was provided by the Engineering Foundation under its Research Initiation Grant Program.

Appendix I.—References

1. Adeli, H., Gere, J. M., and Weaver, W., Jr., "Algorithms for Nonlinear Structural Dynamics," *Journal of the Structural Division*, ASCE, Vol. 104, No. ST2, Feb., 1978, pp. 263–280.
2. Geschwindner, L. F., and West, H. H., "Parametric Investigations of Vibrating Cable Networks," *Journal of the Structural Division*, ASCE, Vol. 105, No. ST3, Mar., 1979, pp. 465–479.
3. Geschwindner, L. F., and West, H. H., "Forced Vibrations of Cable Networks," *Journal of the Structural Division*, ASCE, Vol. 106, No. ST9, Sept., 1980.
4. Goudreau, G. L., "Evaluation of Discrete Methods for the Linear Dynamic Response of Elastic and Viscoelastic Solids," *SESM Report 69-15*, University of California, Berkeley, Calif., June, 1970.

5. Houbolt, J. C., "A Recurrence Matrix Solution for the Dynamic Response of Elastic Aircraft," *Journal of the Aeronautical Sciences*, Vol. 17, 1950, pp. 540–550.
6. Knudson, W. C., *Static and Dynamic Analysis of Cable-Net Structures*, thesis presented to the University of California, at Berkeley, Calif., in 1971, in partial fulfillment of the requirements for the degree of Doctor of Philosophy.
7. Newmark, N. M., "A Method of Computation for Structural Dynamics," *Transactions of the American Society of Civil Engineers*, Vol. 127, Part I, 1962, pp. 1406–1435.
8. Park, K. C., "An Improved Stiffly-Stable Method for Direct Integration of Nonlinear Structural Dynamic Equations," *Journal of Applied Mechanics, Series E*, American Society of Mechanical Engineers, June, 1975, pp. 464–470.

Appendix II.—Notation

The following symbols are used in this paper:

a = one-half of longitudinal span;
b = one-half of transverse span;
C_1 = sag in x direction;
C_2 = rise in z direction;
f = elevation at $x = z = 0$;
$fe_n(t)$ = time variation of effective load;
$(\text{IAF})_n$ = instantaneous amplification factor;
$[K]$ = linear stiffness matrix;
K_n = generalized stiffness;
$[M]$ = mass matrix;
M_n = generalized mass;
$(\text{P.F.})_n$ = participation factor;
$\{P(t)\}$ = time dependent joint loads;
$\{P_o\}$ = vector of load amplitudes;
$(P_o)_n$ = generalized load;
$\{Q(t, \delta)\}$ = equivalent load;
$Q_n(t, \delta)$ = generalized equivalent load;
$\{R\}$ = vector of terms nonlinear in displacements;
T = period;
t = time;
$\{X\}$ = mode shape vector;
x = longitudinal coordinate;
$\{Y(t)\}$ = modal displacement amplitude;
$\{\ddot{Y}(t)\}$ = modal acceleration amplitude;
y = vertical coordinate;
z = transverse coordinate;
$\{\delta\}$ = displacements;
$\{\ddot{\delta}\}$ = acceleration; and
$[\Phi]$ = mode shape matrix.

Optimization with Frequency Constraint

By William R. Spillers,[1] M. ASCE, Sohan Singh,[2] and Robert Levy[2]

Introduction

This paper is concerned with the most simple structural optimization problem with frequency constraints: Find a minimum weight truss for which the fundamental frequency is greater than some given value, given the structural configuration and the masses. This is, of course, not a new problem and the concern here is not with the development of an algorithm (although certainly there are implications in this area). The primary concern lies with attempting to explain why "allowable stress type" algorithms are successful when applied to problems of this nature.

There will be no attempt made here to review comprehensively the literature on optimization with frequency constraints. The interested reader could well begin with the recent paper of Cassis and Schmit (3), or the recent review of Venkayya (8), but will not, in any case, find it difficult to get into the literature. Neither is there concern here with finding a workable algorithm, since several different algorithms have been used to deal with this type of problem. Fox and Kapoor (4), for example, point out that the derivatives of eigenvectors and eigenvalues with respect to member stiffness were available in 1962, making any type of Newtonian algorithm feasible at that time, and Young and Christiansen (9) discuss an early aerospace application. In fact, since the problem under discussion is a basic nonlinear programming problem—a linear objective function with a single equality constraint—it is a candidate for solution by many of the classical procedures.

The concern here lies with "allowable stress" algorithms in general, and, in particular, with the fact that such algorithms have been successful when applied to problems of frequency constraints. "Allowable stress" algorithms have proven to be generally effective in dealing with a wide class of structural optimization problems. Their principal feature is that they tend to reduce the computations required for optimization to the repeated applications of methods of structural analysis, with repeated simple intermediate redesign steps. The

[1]Prof., Dept. of Civ. Engrg., Rensselaer Polytechnic Inst., Troy, N.Y. 12181.
[2]Grad. Student, Dept. of Civ. Engrg., Rensselaer Polytechnic Inst., Troy, N.Y. 12181.

Note.—Discusssion open until May 1, 1982. To extend the closing date one month, a written request must be filed with the Manager of Technical and Professional Publications, ASCE. Manuscript was submitted for review for possible publication on March 28, 1980. This paper is part of the Journal of the Structural Division, Proceedings of the American Society of Civil Engineers, ©ASCE, Vol. 107, No. ST12, December, 1981. ISSN 0044-8001/81/0012-2337/$01.00.

advantage of course is that the methods of analysis available today are *very* effective.

Venkayya and his colleagues at Wright-Patterson Air Force Base have been some of the most active proponents of "allowable stress" methods for optimization, and the scope of their applications (8) is quite remarkable. While this entire approach must on the whole be regarded as effective, "allowable stress" algorithms can have some theoretical difficulties when applied to situations of multiple loading conditions and, naturally enough, don't seem applicable to problems of optimal shape.

There has been some concern over "allowable stress" algorithms when it comes to motivation. They do not seem to relate directly to any of the standard mathematical programming algorithms and, for the most part, very little has been shown formally concerning their convergence. This, of course, takes nothing away from them since, in any actual application, the engineer can see whether or not the weight is being reduced.

This paper then attempts to determine why "allowable stress" algorithms work when they are applied to problems with frequency constraints. It extends earlier efforts (5–7) concerned with placing "allowable stress" algorithms within the realm of classical mathematical programming theory, and is built around the problem of minimizing the structural weight, given the mass, when the fundamental frequency of a structure is specified.

Following this introduction a formal problem statement is developed, the eigenvalue problem is discussed, properties of the algorithm (such as monotone behavior) are shown, a simplification using inverse iteration is indicated, and two examples are presented. It is hoped that through this simple optimization problem it will be possible to see more clearly the mechanisms at work and, thus, develop some intuition concerning both "allowable stress" algorithms and the structures to which they are applied.

Problem Statement

This paper is concerned with the problem of selecting an optimal stiffness matrix, given the matrix, so that the fundamental (lowest) frequency of the structure remains above some specified value. This will be written as

$$\text{minimize} \quad \Delta_a^2 \cdot \mathbf{K} \quad \text{subject to} \quad \omega^2(\mathbf{K}) \geq c \qquad (1)$$

Eq. 1 specifically refers to the truss problem in which Δ_a^2 = vector of the square of the member allowable length changes, i.e., $(\Delta_a^2)_i = (\sigma_a L_i/E)^2$ in which σ_a, L_i, and E = the allowable stress, member length, and Young's modulus, respectively; $\mathbf{K}$ = vector of member stiffnesses, i.e., $(\mathbf{K})_i = A_i E/L_i$ in which A_i = the area of member i; $\Delta_a^2 \cdot \mathbf{K} = \Sigma_i (\Delta_a^2)_i (\mathbf{K})_i = (\sigma_a^2/E) \Sigma_i A_i L_i$ is proportional to the sum of the volumes of the individual members; and ω^2 = square of the fundamental frequency which is to be larger than the given value c.

The member stiffnesses and the frequency come together in the (matrix) equation of free vibrations:

$$\mathbf{K}_e \delta = \omega^2 \mathbf{M} \delta \qquad (2)$$

in which $\mathbf{K}_e$ = structural stiffness matrix; $\mathbf{M}$ = mass matrix (which is given); and δ = eigenvector. Eq. 2 is called a generalized eigenvalue problem to distin-

guish it from the standard eigenvalue problem $Ax = \lambda x$.

In any case, to solve Eq. 1 it is necessary to find the member stiffnesses, $\mathbf{K}_e$, which minimize the structural volume and satisfy a single frequency constraint. It is assumed that the changes in structural volume do not significantly affect the mass matrix, **M**, which is taken to be fixed during the optimization. This is certainly the case for structures, such as buildings or bridges, when the mass is primarily due to nonstructural elements such as floor slabs.

With regard to other types of structures, there is clearly an identical plane (stress, strain) finite element analog to Eq. 1. Other formulations tend to be more complex than this system.

Eigenvalue Problem

For a general discussion of the structural eigenvalue problem, the reader can consult the recent paper of Bathe and Wilson (1). The purpose of this section is simply to collect some results which will be required later.

If only the fundamental frequency is of interest, Eq. 2 is equivalent to the Rayleigh quotient which states that the lowest frequency squared can be obtained as the minimum:

$$\omega^2 = \min_{\delta \neq 0} \frac{\tilde{\delta}\,\mathbf{K}_e\,\delta}{\tilde{\delta}\,\mathbf{M}\,\delta} \quad \text{or} \quad \omega^2 \leq \frac{\tilde{\delta}\,\mathbf{K}_e\,\delta}{\tilde{\delta}\,\mathbf{M}\,\delta} \qquad \ldots\ldots\ldots\ldots\ldots\ldots\ldots\ldots (3)$$

The minimum, of course, is achieved when δ corresponds to the first eigenvector, but the inequality is valid for any δ.

Several useful features of the eigenvalue problem now can be listed:

1. Scaling—If the structural stiffness matrix is multiplied by a scalar $\alpha \geq 0$, so are the frequencies, $\mathbf{K}_e \rightarrow \alpha\,\mathbf{K}_e \Rightarrow \omega^2 \rightarrow \alpha\,\omega^2$ This follows directly from Eq. 2.

2. Concavity—Beckenbach and Bellman (2) give an elegant proof of the old result by Courant that ω^2 is a concave function of the matrix $\mathbf{K}_e$, or that

$$\omega^2(\alpha\,\mathbf{K}_e' + (1-\alpha)\,\mathbf{K}_e'') \geq \alpha\,\omega^2(\mathbf{K}_e') + (1-\alpha)\,\omega^2(\mathbf{K}_e'') \qquad \ldots\ldots\ldots\ldots (4)$$

in which $\mathbf{K}_e'$ and $\mathbf{K}_e''$ = two different structural stiffness matrices. (This result follows directly from Eq. 3.)

3. Inverse Iteration—Given ω^2, the first eigenvector can be computed conveniently by iterating

$$\mathbf{K}_e\delta^{(n+1)} = \omega^2\mathbf{M}\delta^{(n)} \qquad \ldots\ldots\ldots\ldots\ldots\ldots\ldots\ldots\ldots\ldots (5)$$

(This is analyzed in Ref. 1.)

4. Homogeneous Functions—Let α be a scalar. Any scalar function f of a vector x which has the property

$$f(\alpha\mathbf{x}) = \alpha^n f(\mathbf{x}) \qquad \ldots\ldots\ldots\ldots\ldots\ldots\ldots\ldots\ldots\ldots (6)$$

is said to be homogeneous of degree n. It follows that

$$n\mathbf{f} = \mathbf{x}\cdot\nabla\mathbf{f} \quad \text{and} \quad (n-1)\,\nabla\mathbf{f} = \mathbf{H}\mathbf{x} \qquad \ldots\ldots\ldots\ldots\ldots\ldots (7)$$

in which **H** = Hessian matrix of the function f. Since the structural stiffness

matrix, $\mathbf{K}_e$, is linear in the member stiffnesses, $(\mathbf{K})_i$, the preceding property 1 implies that ω^2 is homogeneous of degree 1 in $\mathbf{K}$ or that

$$\omega^2 = \nabla\omega^2 \cdot \mathbf{K} \quad \ldots\ldots\ldots\ldots\ldots\ldots\ldots\ldots\ldots\ldots\ldots\ldots\ldots\ldots\ldots\ldots (8)$$

Furthermore, the vector $\nabla\omega^2$ then must be homogeneous of degree zero.

5. Derivatives of ω^2—The derivative of ω^2, with respect to any member stiffness, $(\mathbf{K})_i$, can be obtained in a relatively simple manner and is an identifiable structural term. Let the derivative $\partial/\partial(\mathbf{K})_i$ be indicated by a comma. Then

$$(\mathbf{K}_e - \omega^2\mathbf{M})\delta = 0 \Rightarrow (\mathbf{K}_{e,i} - \omega^2{}_{,i}\mathbf{M})\delta + (\mathbf{K}_e - \omega^2\mathbf{M})\delta_{,i} = 0 \quad \ldots\ldots\ldots\ldots (9)$$

Multiplying by δ now gives

$$\omega^2{}_{,i} = \frac{\tilde{\delta}\,\mathbf{K}_{e,i}\,\delta}{\tilde{\delta}\,\mathbf{M}\,\delta} \quad \ldots\ldots\ldots\ldots\ldots\ldots\ldots\ldots\ldots\ldots\ldots\ldots\ldots\ldots\ldots\ldots (10)$$

Eq. 10 can be simplified further. First of all, it is convenient to normalize

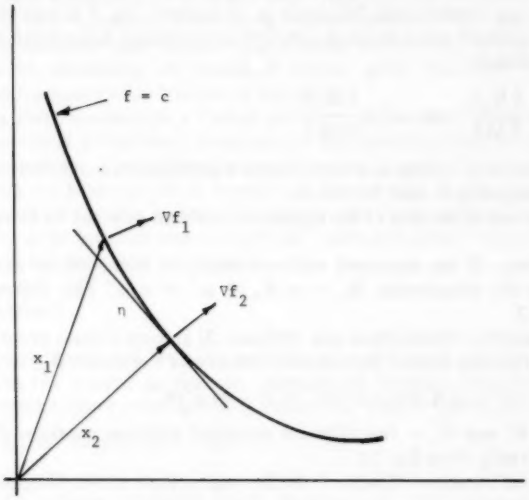

FIG. 1.—Concave Function

the eigenvectors with respect to the mass matrix and set

$$\tilde{\delta}\,\mathbf{M}\,\delta = 1 \quad \ldots\ldots\ldots\ldots\ldots\ldots\ldots\ldots\ldots\ldots\ldots\ldots\ldots\ldots\ldots\ldots (11)$$

Secondly, it is convenient to decompose the matrix $\mathbf{K}_e$ as

$$\mathbf{K}_e = \sum_i \tilde{N}_i(\mathbf{K})_i N_i \quad \ldots\ldots\ldots\ldots\ldots\ldots\ldots\ldots\ldots\ldots\ldots\ldots\ldots\ldots\ldots\ldots (12)$$

in which each term in the sum represents the contribution of member i to

the matrix $\mathbf{K}_e$ (see Ref. 6 for the detailed description of this decomposition). It follows directly that

$$\mathbf{K}_{e,i} = \tilde{N}_i N_i \quad \ldots \quad (13)$$

and that $$\frac{\partial \omega^2}{\partial (K)_i} = \omega^2{}_{,i} = \Delta_i^2 \quad \ldots \quad (14)$$

in which $\Delta_i = N_i \delta$ = the member displacement (length change for the truss).

Eq. 14 is a simple, but important, result. It identifies the derivative of ω^2 with respect to the member stiffness, $(K)_i$, as equal to the square of the member displacement associated with the normalized eigenvector, δ.

6. Concavity and Homogeneity—Let $f(x)$ be a concave, homogeneous function of degree 1 so that $f = \nabla f \cdot x$. Furthermore, let x_1 and x_2 be two points on the surface $f(\mathrm{x}_1) = f(\mathrm{x}_2) = c$ (Fig. 1), and η be $\perp$ to ∇f_2. It follows that since

$$\mathrm{x}_2 = \alpha \mathrm{x}_1 + \eta \quad (0 \le \alpha \le 1) \quad \ldots \quad (15)$$

$$\text{then} \quad \nabla f_2 \cdot \mathrm{x}_2 = \nabla f_2 \cdot (\alpha \mathrm{x}_1 + \eta) \le \nabla f_2 \cdot \mathrm{x}_1 \quad \ldots \quad (16)$$

$$\text{or} \quad \nabla f_1 \cdot \mathrm{x}_1 = \nabla f_2 \cdot \mathrm{x}_2 \le \nabla f_2 \cdot \mathrm{x}_1 \quad \ldots \quad (17)$$

Lagrange Multiplier Method

One possible approach to the solution of Eq. 1 is through the use of Lagrange multipliers which reduce constrained optimization problems to unconstrained problems. In this method, the Lagrangian is first formed as

$$\mathscr{L} = \Delta_a^2 \cdot \mathbf{K} + \lambda (c - \omega^2) \quad \ldots \quad (18)$$

Then, differentiation gives

$$\frac{\partial \mathscr{L}}{\partial \mathbf{K}_i} = 0 \Rightarrow \Delta_a^2 = \lambda \nabla \omega^2 \quad \ldots \quad (19)$$

$$\frac{\partial \mathscr{L}}{\partial \lambda} = 0 \Rightarrow \omega^2 = c \quad \ldots \quad (20)$$

Note: It is only necessary to consider the case of equality constraints in Eq. 1, since any solution with $\omega^2 > c$ can be reduced in weight by scaling to the surface $\omega^2 = c$. Let ϕ refer to the objective function

$$\phi = \Delta_a^2 \cdot \mathbf{K} \quad \ldots \quad (21)$$

and the asterisk denote an optimal point

$$\phi_* = \Delta_a^2 \cdot \mathbf{K}_* \quad \ldots \quad (22)$$

The optimal Lagrange multiplier, λ_*, can be computed by multiplying Eq. 19 by $\mathbf{K}_*$ as

$$\mathbf{K}_* \cdot \Delta_a^2 = \lambda_* \mathbf{K}_* \cdot \nabla \omega_*^2 = \lambda_* c \quad \ldots \quad (23)$$

$$\text{or} \quad \lambda_* = \frac{\phi_*}{c} \quad \ldots \quad (24)$$

In Eqs. 19 and 20, the optimization problem of Eq. 1 has been reduced to a nonlinear system which requires that $\nabla\omega^2$ be parallel to Δ_a^2. This fact is the basic motivation for treating Eq. 1 as an "allowable stress" problem. Since Eq. 14 shows that $\nabla\omega^2$ is proportional to the member displacement, and since the eigenvector, δ, can be assigned any length, δ could be scaled to give $\lambda = 1$, which would imply all members to be fully stressed for an optimal design. That scaling will not be used here since it tends to mask the basic features of the eigenvalue problem. In any case, the concept of a "fully stressed" algorithm remains useful and will be pursued in the next section.

From another point of view there is little reason to think of Eq. 1 as an allowable stress problem. Beyond Eq. 19, allowable stress problems are considerably different from Eq. 1 since they are concerned with nonhomogeneous equilibrium equations rather than homogeneous eigenvalue problems. This simply makes a study of "allowable stress" algorithms more interesting since they must then have a broader scope to include problems which are quite different.

It now can be shown that Eq. 1 is closely related to other problems with frequency constraints:

Problem 1.—Given a solution to Eq. 1, the solution for some other frequency, c', can be obtained simply by scaling $\mathbf{K} \rightarrow \mathbf{K}' = \mathbf{K}c'/c$. (This follows directly from the fact that $\nabla\omega^2$ is homogeneous of degree 0.)

Problem 2.—Given a solution of Eq. 1, the solution of the problem of maximizing the frequency, given the volume, follows directly by simply scaling $\mathbf{K}_*$ to the proper weight surface.

Let $\mathbf{K}$ be arbitrary, but such that it satisfies $\omega^2(\mathbf{K}) = c$, and $\mathbf{K}_*$ solve Eq. 1. Then it is possible to select an $\alpha \leq 1$ such that

$$\Delta_a^2 \cdot \mathbf{K}_* = \alpha\, \Delta_a^2 \cdot \mathbf{K} \leq \Delta_a^2 \cdot \mathbf{K} \quad \ldots\ldots\ldots\ldots\ldots\ldots\ldots\ldots\ldots\ldots \quad (25)$$

in which $\omega^2 = c$ is concave. Now scale point $\mathbf{K}$ down to $\alpha\mathbf{K}$ which has the same weight as $\mathbf{K}^*$. Since ω^2 is homogeneous of degree 1, it follows that

$$\omega^2(K^*) = \omega^2(\mathbf{K}) \geq \alpha\, \omega^2(\mathbf{K}) = \omega^2(\alpha K) \quad \ldots\ldots\ldots\ldots\ldots\ldots\ldots\ldots\ldots\ldots \quad (26)$$

An "Allowable Stress" Algorithm

As indicated in Fig. 2, to solve Eq. 1, it is necessary to find a point $\mathbf{K}_*$ on the surface $\omega^2 = c$ such that $\nabla\omega_*^2 \sim \Delta_a^2$. The "allowable stress" scheme to be discussed here iterates in the following manner, starting with an arbitrary $\mathbf{K}_{(0)}$:

Step 1. Given $\mathbf{K}_{(n)}$, solve the eigenvalue problem for $\omega_{(\mathbf{K})}^2$ and $\omega_{(n)}^2$ and scale to $\mathbf{K}'_{(n)}$ on the surface $\omega^2 = c$

$$\mathbf{K}'_{(n)} = \mathbf{K}_{(n)} \frac{c}{\omega_{(n)}^2} \quad \ldots\ldots\ldots\ldots\ldots\ldots\ldots\ldots\ldots\ldots\ldots\ldots\ldots\ldots \quad (27)$$

Step 2. Compute the new $\mathbf{K}_{(n+1)}$ so that

$$(\mathbf{K}_{(n+1)})_i \left(\sqrt{\nabla\omega_*^2}\right)_i = (\mathbf{K}'_{(n)})_i \left(\sqrt{\nabla\omega_{(n)}^2}\right)_i \quad \ldots\ldots\ldots\ldots\ldots\ldots\ldots\ldots \quad (28)$$

Since ω_*^2 is only known approximately until the problem is solved, it is necessary to compute replacing $\nabla\omega_*^2$ in Eq. 28 by its approximate value:

$$\nabla\omega_*^2 = \frac{\Delta_a^2}{\lambda_*} = \Delta_a^2\left(\frac{c}{\phi_*}\right) \sim \Delta_a^2\left(\frac{c}{\phi_{(n)}}\right) \quad \ldots\ldots\ldots\ldots\ldots\ldots \quad (29)$$

There are several properties of this algorithm which can now be demonstrated:

Property 1. The optimal point is a fixed point of the algorithm, i.e., $K_{(*+1)} = K_{(*)}$. This follows directly from Eqs. 27–28 in a somewhat trivial manner, but is, nevertheless, important.

Property 2. $\omega_{(n)}^2/c \le \phi_{(n)}/\phi_*$. This follows from the fact that

$$\omega_{(n)}^2 = \nabla\omega_{(n)}^2 \cdot \mathbf{K}_{(n)} \le \nabla\omega_*^2 \cdot K_n = \Delta_a^2 \cdot K_{(n)}\left(\frac{c}{\phi_*}\right) \quad \ldots\ldots\ldots\ldots\ldots \quad (30)$$

using the concavity property.

Property 3. In the vicinity of K_*, $\omega_{(n+1)}^2 \ge c$. This property uses the linear terms in a Taylor series expansion and is, thus, a local theorem. Since ω^2

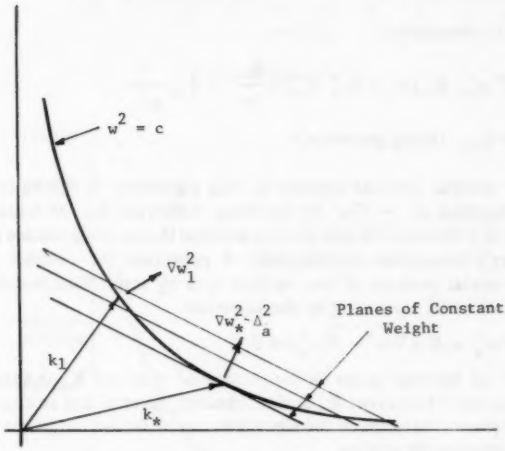

FIG. 2.—Surface of Constant Frequency

is a homogeneous function of degree 1 in $\mathbf{K}$, it follows, from a Taylor series expansion about some point $\mathbf{K}_o$, that

$$\omega^2(\mathbf{K}) \simeq \omega^2(\mathbf{K}_o) + \Delta\omega^2(\mathbf{K}_o)\cdot(\mathbf{K} - \mathbf{K}_o) \quad \ldots\ldots\ldots\ldots\ldots\ldots \quad (31)$$

$$\text{or} \quad \omega^2(K) \sim \nabla\omega^2(K_o)\cdot K \quad \ldots\ldots\ldots\ldots\ldots\ldots\ldots\ldots \quad (32)$$

But the iteration scheme (Eq. 28) implies that

$$\sum_i (\sqrt{\nabla \omega^2_{(n)}})_i (\mathbf{K}_{(n+1)})_i (\sqrt{\nabla \omega^2_*})_i = \sqrt{\frac{\phi_n}{\phi_*}}\, c \quad \ldots\ldots\ldots\ldots\ldots\ldots \quad (33)$$

Squaring Eq. 33 and applying Schwartz's inequality, it follows that

$$\left[\sum_i (\nabla \omega^2_{(n)})_i (\mathbf{K}_{(n+1)})_i\right]\left[\sum_i (\nabla \omega^2_*)_i (K_{(n+1)})_i\right] \geq \frac{\phi_n}{\phi_*}\, c^2 \quad \ldots\ldots\ldots\ldots \quad (34)$$

or that (using Property 2):

$$\omega^2_{(n+1)} \geq c \quad \text{when} \quad \phi_n \geq \phi_* \quad \ldots\ldots\ldots\ldots\ldots\ldots\ldots\ldots \quad (35)$$

Property 4 (Monotone Behavior). In the vicinity of K_*, $\phi_{(n+1)} \leq \phi_{(n)}$. From Eqs. 27–28 it follows that

$$(\mathbf{K}_{(n+1)})_i \sqrt{\frac{(\Delta_a)_i}{\lambda_{(n)}}} = (\mathbf{K}'_n)_i \sqrt{(\nabla \omega^2_{(n)})_i} \quad \ldots\ldots\ldots\ldots\ldots\ldots \quad (36)$$

Multiplying by $(\Delta_a)_i$, rearranging, and squaring them gives

$$\phi^2_{(n+1)} = (\Delta^2_a \cdot \mathbf{K}_{n+1})^2 = \left[\sum_i (\Delta_a)_i (\mathbf{K}'_{(n)})_i \sqrt{(\nabla \omega^2_{(n)})_i}\, \lambda^{1/2}_{(n)}\right]^2 \quad \ldots\ldots\ldots \quad (37)$$

(by Schwartz's inequality)

$$\leq (\Delta^2_a \cdot \mathbf{K}'_n)(\nabla \omega^2_{(n)} \cdot \mathbf{K}'_n)\lambda_n = (\Delta^2_a \cdot K'_n)\, c\, \frac{\phi_{(n)}}{c} = \phi^2_{(n)} \frac{c}{\omega^2_{(n)}} \quad \ldots\ldots\ldots\ldots \quad (38)$$

$$\text{or} \quad \phi_{(n+1)} \leq \phi_{(n)} \quad \text{(using property 3)} \quad \ldots\ldots\ldots\ldots\ldots\ldots \quad (39)$$

There are several peculiar aspects of this algorithm. It attempts to satisfy the vector equation $\Delta^2_a \sim \nabla \omega^2$ by iterating, following Eq. 28 which contains square roots. It is thus Schwarzian in the sense that the square roots are compatible with Schwarz's inequality. Furthermore, it possesses the peculiar feature of equating the scalar product of two vectors term by term. This is quite unusual but can be motivated somewhat by the equation

$$(K_* - K) \cdot \nabla \omega^2_* = K \cdot (\nabla \omega^2 - \nabla \omega^2_*) \leq 0 \quad \ldots\ldots\ldots\ldots\ldots\ldots \quad (40)$$

in which $\mathbf{K}$ = an arbitrary point on the surface $\omega^2 = c$; and $\mathbf{K}_*$ is again optimal. In some sense, Eq. 31 involves K_* as the unknown, given $\mathbf{K}$ and an approximation of ω^2_*. The square root terms of the algorithm can be forced out of the right-hand side of this equation by writing

$$(\nabla \omega^2)_i - (\nabla \omega^2_*)_i = [\sqrt{(\nabla \omega^2)_i} - \sqrt{(\nabla \omega^2_*)_i}]\,[\sqrt{(\nabla \omega^2)_i} + \sqrt{(\nabla \omega^2_*)_i}] \quad (41)$$

which might be regarded as a useful device when $\mathbf{K} \to \mathbf{K}_*$. Finally, the algorithm behaves like a Newtonian algorithm but does not require as many derivatives.

Inverse Iteration and Examples

Figs. 3 and 4 show two truss problems to which this "allowable stress" algorithm has been applied. In both cases $\omega^2 = 1{,}757\ (\text{rad/sec})^2$, and in both cases the convergence is quite good. (In the case of Fig. 3, convergence is

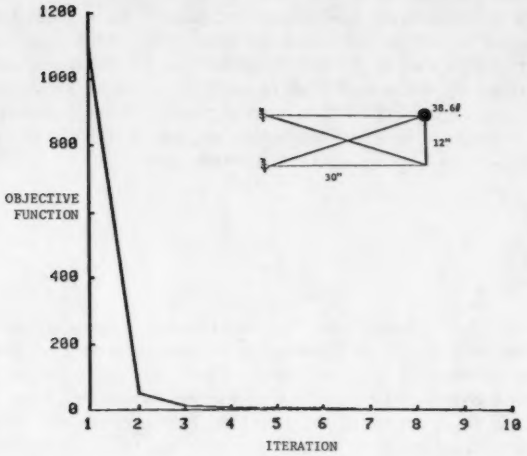

FIG. 3.—Example 1

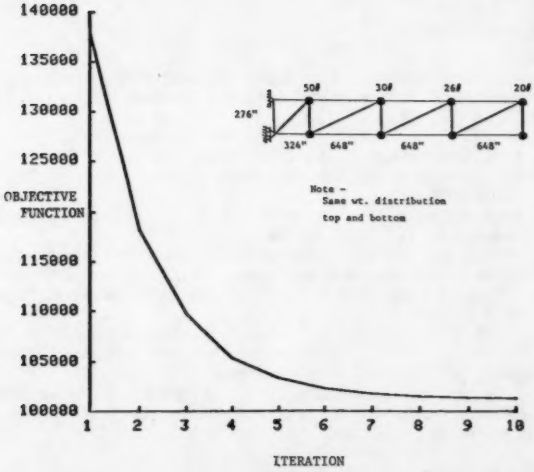

FIG. 4.—Example 2

to 2.71, while Fig. 4 converges to 101,310.) What is not shown in these figures is that fact that they were computed twice: Once as described above, and once using inverse iteration with almost identical results.

In order to maintain the analysis-redesign point of view, it is natural to turn to the method of inverse iteration rather than some canned eigenvalue routine, since inverse iteration can be carried out using a structural analysis computer program after only minor modifications. In terms of the algorithm stated above, the only change required, in addition to performing an inverse iteration (a structural analysis) rather than an exact eigenvalue analysis, is to replace at each step the term $\omega^2_{(n)}$ by its Rayleigh quotient approximation:

$$\omega^2_{(n)} \sim \frac{\bar{\delta}_{(n)} \mathbf{K}_{(n)} \delta_{(n)}}{\bar{\delta}_{(n)} M \delta_{(n)}} \quad \ldots \ldots \ldots

E = Young's Modulus;
$\mathbf{K}$ = vector of member stiffness;
$\mathbf{K}_e$ = structural stiffness matrix;
L_i = length of member i;
$\mathbf{M}$ = mass matrix;
Δ_a^2 = vector of square of member "allowable" length changes;
δ = eigenvector;
σ_a = allowable stress; and
ω^2 = square of fundamental frequency.

Strength of Old Wood Joists

By Ross M. Lanius, Jr.,[1] F. ASCE, Robert Tichy,[2] A. M. ASCE, and William M. Bulleit[3]

Introduction

Recycling, conservation—these terms are now being heard in the building field. Old buildings, historic buildings, and some not-too-old buildings are being altered and revamped for new uses. In all cases, the structural adequacy must be evaluated. While architects and engineers have always been called on to evaluate the strength of old buildings, the number of structural investigations of this type is increasing. This paper provides architects and engineers with a procedure for examining wood joists in an existing structure, and for making reasonable judgements concerning the structural adequacy of those joists.

In this study, a wood framed barn constructed in 1925 was examined. Two nondestructive grading techniques were investigated: The conventional visual method and a longitudinal stress wave method. Utilizing these techniques to develop a procedure for examining the joists, the basic questions are: (1) How is joist strength determined from either grading technique; and (2) how do the two systems compare?

Little has been published in the past several decades addressing the problem of evaluating old wood structures. Lee (14,15), and Wen, et al. (20) report using longitudinal stress waves to evaluate the strength of in situ wood. However, much of the work in this area has relied on a visual assessment of building strength.

More recently, dynamic measurement techniques for the evaluation of the modulus of elasticity for wood have been given extensive consideration. The dynamic approach can take several forms, e.g., transverse vibrations and longitudinal stress waves. Following is an overview of the elementary aspects of the longitudinal stress wave propagation theory as it applies to the evaluation of the modulus of elasticity in wood.

A simplification of the governing differential equation for wave propagation

[1]Assoc. Prof., Dept. of Civ. and Environmental Engrg., Univ. of New Haven, W. Haven, Conn.

[2]Mgr., Engrg. Research and Development, Western Wood Products Assoc., Portland, Oreg.

[3]Struct. Engr., Howard, Needles, Tammen, & Bergendoff, Bellevue, Wash.

Note.—Discussion open until May 1, 1982. To extend the closing date one month, a written request must be filed with the Manager of Technical and Professional Publications, ASCE. Manuscript was submitted for review for possible publication on December 8, 1978. This paper is part of the Journal of the Structural Division, Proceedings of the American Society of Civil Engineers, ©ASCE, Vol. 107, No. ST12, December, 1981. ISSN 0044-8001/81/0012-2349/$01.00.

through an isotropic, elastic, homogeneous material results in the one-dimensional stress wave equation for long, slender prismatic bars. It gives a relationship between the stress wave propagation rate, the material's dynamic modulus of elasticity, and the mass density:

$$c = \left(\frac{E_d}{\rho}\right)^{1/2} \quad \ldots\ldots\ldots\

The compression wave traveling through the wood is cohesive in nature, i.e., a wave front does not separate or disintegrate at discontinuities. The wave propagation rate is greatest along the major axis of a piece of lumber (i.e., along the grain). In the transverse direction, propagation rate is slower due to the changes in density from earlywood to latewood (spring wood to summer wood). As a wave encounters a grain deviation in its path, the wave velocity reduces depending on the severity of the deviation. If one were to look at the components of the stress wave in the direction of travel and along the direction of the cross grain, a relationship might be established as to the degree of resistance a grain deviation would produce. As a wave encounters a knot, there are local grain deviations around the knot and the abrupt discontinuity at the knot. Fig. 1 shows a plot of a wave front passing through a piece of structural lumber containing knots. The portion of the wave that contacts the discontinuity lags behind the rest of the wave, and, in the case of a knot, it wraps itself around the knot and eventually becomes continuous again.

A common method for obtaining the propagation time is through the use of accelerometers clamped against the member. An accelerometer is a device which contains piezoelectric material (usually quartz) that is activated as the wave passes the point of contact. Fig. 2 is a schematic representation of a typical stress-wave timing system.

The stress wave causes the first accelerometer to produce on electrical signal which turns on the timer. The electrical signal produced by the second accelerometer turns off the counter and the time interval is stored. With this time interval and the board density, the board's apparent E_d can be calculated. It should be noted that the value obtained is an average E_d over the distance between accelerometers; furthermore, it is only an apparent E_d because Eq. 2 ignores Poisson's effect for lateral strains. Despite the simplifying assumptions to the governing wave equation, Eq. 2 has been shown to be useful in determining E_d for structural lumber (5,8,9).

Procedure

The barn that was examined was constructed in 1925 for the College of Agriculture, Washington State University, Pullman, Washington. It was primarily used as an animal shelter on the ground floor, and for hay storage on the second floor. The inspection was confined to the nominal 2 × 12 in. (50 × 300 mm) floor joists in the south bay of the barn where hay storage was believed to be the primary use.

Two methods of inspection were performed to determine the allowable working stresses for the joists: (1) The conventional visual grading technique; and (2) the stress-wave technique. The implementation of the stress-wave technique to evaluate in-place strength requires a means of relating the strength properties to the stiffness properties of the individual members. Through the use of a linear regression, the dynamic modulus, E_d, was adjusted to the static modulus, E_s, which was ultimately related to an allowable extreme fiber stress in bending, F_b.

To corroborate the findings of others concerning the correlation between E_d and E_s, a random 30 piece sample of Douglas-fir (Pseudotsuga menziesii), nominal 2 × 6 in. (50 × 150 mm) wood joists were examined in the laboratory.

The lumber was tested by both the stress-wave method, and by static third point loads to determine E_d and E_s, respectively. The regression run on this data was the vehicle used to determine the static modulus of elasticity, E_s, of joists in the barn.

Specimen selection in the barn consisted of a random sampling of approx 50% of the total number of joists in the south bay of the barn (the parent sample). Independent subsamples of 5, 10, 20, and 30% were chosen from the parent sample, with replacement, to allow for comparisons in later analyses. The intent here was to determine an appropriate sample size for this type of

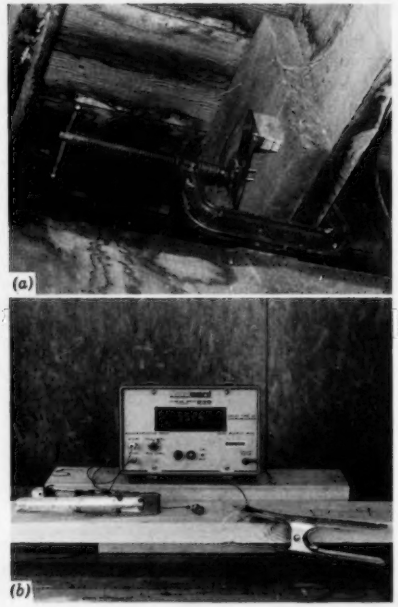

FIG. 3.—Stress Wave Timing System: (*a*) Anvil; (*b*) Timing Unit with Accelerometers and Clamps

investigation. For a study of this type, it would have been far better to sample 100% of the joists rather than only 50%, but due to time and financial constraints the smaller level was selected.

With the parent sample distinctly numbered, a visual assessment of the joists ensued. Based on the Western Wood Products Association (WWPA) grading rules (11), each joist was assigned to a grade and its corresponding design value. Next, stress wave time intervals for the joists were recorded. Two accelerometers were clamped to the joist with a specific distance between them. The signal was introduced by impacting a specially designed anvil (Fig. 3(*a*)) with a hammer. The start accelerometer was located at least 6 in. (150 mm)

in front of the anvil. Fig. 3(*b*) shows the timer, accelerometers, and clamps that were used. The time for the leading edge of the first pulse to travel between the two accelerometers was recorded. In order to calculate E_d, the density of the member was determined. Small blocks were cut from overhangs on about two-thirds of the samples for determination of density and moisture content. The moisture content of all joists in the sample was measured by using a moisture meter. The densities were compared to values listed in Ref. 21. Evaluation of this data results in reasonable allowable design values and some indication of an acceptable sample size.

Data Analysis

The data are discussed in two distinct sections. The first section consists of data obtained from laboratory tests of 30 Douglas-fir joists. Their moduli

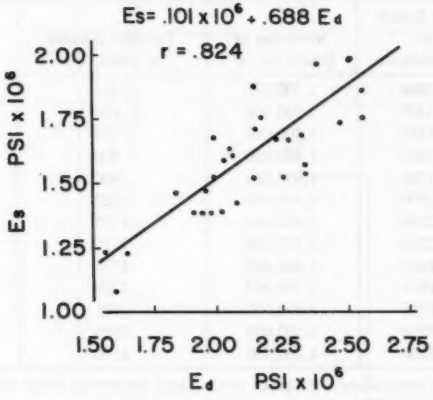

FIG. 4.—Regression of E_s Versus E_d (Laboratory Tests)

of elasticity were found using the stress-wave equipment, and by a third point loading static bending test. The second section consists of the stress wave and visual grading data obtained in the field which were used to determine the moduli of elasticity and allowable bending stress of the barn joists.

Section One.—The wood tested in the laboratory was nominal 2 × 6 in. (50 × 150 mm) Douglas-fir (Pseudotsuga menziesii) joists consisting of visually graded No. 1 and No. 2 lumber. The longitudinal stress wave propagation time was taken over a 90 in. (2.29 m) span for all boards. The density was determined by weighing and measuring overall dimensions of each sample, and moisture content was measured using an electrical resistance meter. Since all boards had moisture contents of approx 7%, it was not necessary to adjust the mechanical properties to a standard moisture content. The dynamic moduli were calculated from this data.

Each board was statically tested as a joist in third point loading. The center-point

deflection obtained from this testing was used to calculate E_s. The E_s values were modified to a span to depth ratio of 21, and a uniformly distributed load (3).

A linear regression was performed to relate E_s and E_d. The plot of the data and the regression line are shown in Fig. 4. The regression equation is

$$E_s = 0.101 \times 10^6 + 0.688 E_d \quad \ldots \ldots \ldots

stress wave data, and the average density for the sample, the dynamic modulus of elasticity, E_d, was calculated from Eq. 2.

An approximate average moisture content for the joists of 15% was measured, using an electric resistance moisture meter, with the appropriate corrections for temperature and species as per the manufacturer's specifications. This value seemed high for a covered, unheated structure in the month of November. Therefore, a second moisture content measurement was made by oven drying samples cut from the joist overhangs. This average moisture content of 13.6% was used in the study for computational purposes. The moisture meter value can be used for practical purposes. The joists in the barn were a mixture of Douglas-fir and Western larch (Pseudotsuga menziesii and Larix occidentalis).

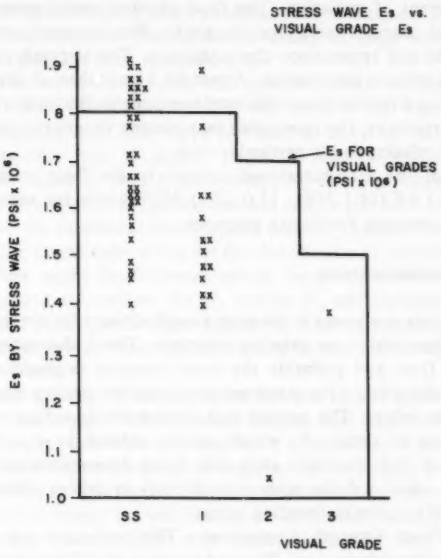

FIG. 5.—Stress Wave E_s upon Visual Grade E_s

With E_d for the sample determined, E_s values were obtained by using the regression Eq. 3. The E_s obtained was for a moisture content of 13.6%, and was adjusted to a moisture content of 19%, which is the maximum allowable in use moisture content for tabulated design values (7). The average E_s was 1.639×10^6 psi (11.3 GPa), and s, the standard deviation of the mirror image of the lower half of the distribution (16), was 0.186.

All the joists in the sample were visually graded in order to compare E_s from the stress-wave method, to that derived from the visual grading method. Fig. 5 shows that the average stress wave, E_s, is less than the E_s assigned using visual grading criteria, i.e., E_s stress wave is conservative, in this case, compared to the visual assessment of E_s. It is possible to utilize these test

results to construct a machine-stress-rated (MSR) grade of lumber for a floor system. MSR lumber is classified into $F_b - E$ groupings (Table 1). The F_b (extreme allowable fiber stress in bending) that is associated with each E class is derived from a regression function of bending strength versus modulus of elasticity.

There are some physical requirements which must also be satisfied, for a particular set of lumber to meet an MSR grade, e.g., the average edge modulus of elasticity ($\bar{E}_s$ in our case) must equal or exceed the modulus of elasticity assigned to that grade, E_g (16). A second requirement is that the lower fifth percentile of the sample modulus of elasticity distribution must equal or exceed 82% of the modulus of elasticity assigned to that grade (i.e., $E_{5th} \geq 0.82\ E_g$) (16). The factor 0.82 assures that the grade being assigned has no more than an 11% coefficient of variation. The final physical requirement refers to the allowable visual characteristics for the grade. This category includes strength reducing defects and appearance characteristics. The strength reducing characteristics are of primary importance. Appendix I describes all the visual characteristics which can override the mechanical assessment. Because we are concerned with existing structures, the researcher may choose to ignore some of the visual restrictions not relating to his particular case.

Application of the aforementioned criteria to the floor joist data suggests that a $2050F_b$, $1.6E$ (14.1 MPa, 11.0 GPa) MSR grade for repetitively spaced joists might be assigned for design purposes.

Analysis and Recommendations

The intent of this study was to develop a methodology for determining strength of wood members within an existing structure. Three alternative methods are proposed. The first, and probably the most common in practice today, is the process of visually grading the members and using the grading rules to determine allowable design values. The second and third methods utilize the stress wave timing equipment to obtain E_d which can be related to E_s. These last two methods differ in their resultant allowable stress determinations, i.e., one uses the MSR grade rules, and the other goes directly to curves relating E_s to mode of rupture (MOR), (ultimate bending stress).

Method 1—Visual Strength Assessment.—This technique requires strict adherence to a grading rule manual. Size and location of defects must be accurately characterized to ensure against high grading or low grading the material. A common problem is the subjectiveness of this approach. Experienced persons must do the grading. Frequently the material in older structures can be weathered, rough sawn, or both, which makes precise identification of the strength reducing characteristics difficult. Another drawback of this system is the inability to look at all faces and edges of the member. Often the top edge of a joist is inaccessible; consequently, one is not able to do a complete job of visual estimation.

Once the visual grade has been assigned it is a simple matter of reading the allowable stresses from the grading rules. Using current grading rules, the joists in this study were a grade mixture, with 95% No. 1 or better. One No. 2 joist and one No. 3 joist were found in the sample.

The discovery of the No. 3 joist in the sample penalized all of the other

joists, if one wished to assign allowable stresses to the joists. If this joist is strengthened, then the joists may be graded as No. 2 and better, with F_b and E values of 1,450 psi (10.0 MPa) (repetitively spaced), and 1.7×10^6 psi (11.7 GPa), respectively. Alternatively, if the two joists below the No. 1 grade were strengthened, the floor system could be assigned No. 1 stresses for repetitively spaced members, i.e., 1,750 psi (12.1 MPa) for F_b, and 1.8×10^6 psi (12.4 GPa) for E.

Method 2—Stress Wave—MSR Assessment.—Utilizing the stress-wave technique removes the personal subjectiveness from the process. It gives a mechanical means of characterizing defects. A visual override must still be employed along with other limitations that are listed in the grading rules (11). Members with obvious failures must be noted and replaced. The stress-wave technique is also valuable for indicating defects not readily visible, such as incipient decay, sloping grain, and insect infestations. The extent of decay in large wood arches by stress-wave techniques has been reported (13).

When using stress-wave equipment, one must be aware of the fact that a hole or a partial failure (horizontal split) in the member will have little effect on the wave propagation rate. The wave will tend to travel in the sound wood, essentially ignoring this type of defect. It should also be noted that the E_d derived from these types of tests is an average E_d over the distance between accelerometers. If necessary, the accelerometers can be placed at short intervals which would allow the determination of a low point E_d value. The stress-wave assessment gives the investigator a feel for the distribution of material properties.

A procedure that might be followed would begin with calibration of the stress-wave equipment to confirm the E_s versus E_d relationships. Inspect all members for decay, failure, and other limitations. The writers recommend that all joists that are decayed, have failed, or are below the desired grade be strengthened or replaced.

Upon elimination of the obviously failed specimens and those with visual decay, data collection begins. Wood species, density, and moisture content must be determined. Species can be confirmed by a local Wood Technologist, the U.S. Forest Products Laboratory, or through an identification key in a basic wood technology book (6,18). The most accurate methods of density and moisture content determination would be with actual wood blocks removed from some *safe* location. If this is impossible, the writers found that Ref. 22, and the electrical resistance meter both gave conservative measures of these properties.

A note about densities taken from Ref. 21 should be made here. Handbook values which most appropriately characterize the material being investigated should be used, e.g., a structure constructed in 1925 would be built with material from a pre-1925 resource consequently, the edition of the *Wood Handbook* nearest that date should be used. This is done in consideration of our changing resource base. The densities from Ref. 21 are conservative because the bulk density (wood fiber and moisture) (10) is used in Eq. 2, while densities in the *Wood Handbook* are of the wood only. Appropriate corrections can be made if desired.

The final variable needed to calculate E_d is the stress-wave time interval. This is obtained as described in the procedure section of this report. Using this information, E_d is computed and modified to an E_s value as shown in Fig. 4. The sample can then be analyzed according to the procedure previously

outlined, and a MSR grade can be assigned.

In recognition of the fact that MSR machines monitor the low point, E, of each piece, as well as its average, it may be necessary to provide some assurance that the sample does not have an unrealistic E value based only on the average E obtained from the stress-wave technique. If the low point cannot be determined, a conservative approach to assigning F_b values would be to assign a MSR grade based on a minimum or near minimum E_s value from the sample. For this study one might address this by applying a nonparametric analysis to the sample E_s data, e.g., using the second order statistic for E_s (1.37×10^6 psi, 9.4 GPa), it can be stated with 71% confidence that 95% of the E_s values of the population of floor joists equals or exceeds the second order statistic (4). Tables exist such that one can select the order statistic,

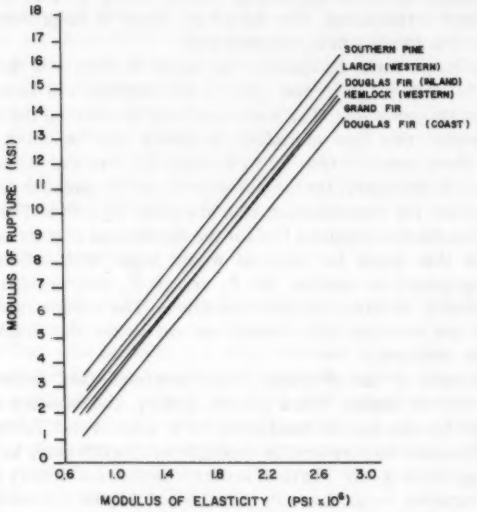

FIG. 6.—Confidence Limit for Mean Value of MOR given an E_o

with its associated confidence level commensurate with the objectives of the evaluation process. Using this joist data, the conservative approach yields a MSR graded of 1,750 F_b, 1.4E (12.1 MPa, 9.7 GPa) for repetitively spaced joists.

There are, however, two inherent problems with utilizing the MSR approach. The first is that the MSR allowable stress values include a size correction which is monitored at the sawmill through daily in-plant quality control procedures. For visually graded lumber, the size effect is incorporated into the published design values (2), but for MSR lumber the size effect has not been explicitly identified. A second problem relates to the visual grading requirements which may override the grade as determined by E alone (16). A suitable correction of the stress wave raw data for these problems, if required, is unknown.

Nonetheless, the MSR table values for F_b are based on an adjusted lower 5% exclusion level, using the reduction factors specified in Ref. 2.

Method 3—Stress Wave-MOR Assessment.—This method is a more empirical approach not relying upon the grading rules manual. This technique relies solely upon the grading rules manual. This technique relies solely on the relationships between E_s and E_d, and E_s versus MOR. For method 3 to be used by the architect or engineer, further refinement is necessary. Allowable stresses must be derived. This can be done in the following manner.

The least squares procedure used in the general linear model produces a regression line fitting the data by minimizing the sum of squared residuals (deviations) about that line. Often it is useful to compute confidence limits for the mean response (in our case MOR), given a selected independent variable, E_s. Pictorially this can be described by Fig. 6. Using Fig. 6, it is possible to determine the allowable stress: simply multiply MOR_0 by 1/2.1 as in Ref.

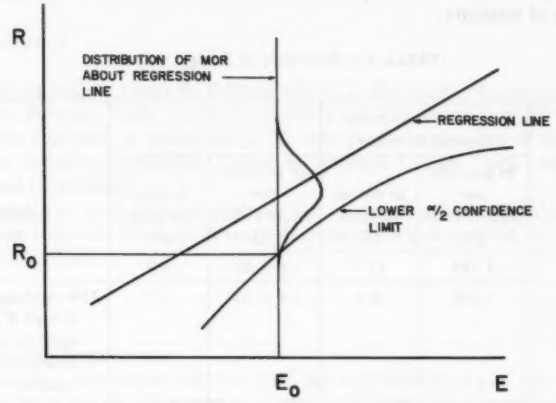

FIG. 7.—E_s versus MOR for Common Species of Structural Lumber

1. A nice feature about this method is that the engineer can select a level of confidence suitable to his particular needs, i.e., it may be necessary to choose a very high degree of confidence in his analysis; therefore, he may choose the appropriate confidence limit.

Another interesting feature about this method is seen upon noting the similarity of the E–MOR regression lines shown in Fig. 7 (17). As can be seen, there are only slight differences in the slopes and locations of the lines for the six species considered. This would indicate that "master curves," i.e., one or two curves for all structural species, might be developed; thus, greatly simplifying the design process. The allowable bending stress from method 3 can be compared with methods 1 and 2, by solving Eq. 4:

$$F_b = \frac{1}{2.1}(X_0 - t_{\alpha/2}s)(1.15) \quad \ldots\ldots\ldots\

in which X_0 = 6,300 psi at $E = 1.4 \times 10^6$ (Fig. 7 for Douglas-Fir); s = 1,600 psi (17); and $t_{\alpha/2} = 1.645$ at the lower 5% exclusion level (normal distribution). The 1.15 factor is the allowable stress increase for repetitive member use. F_b is found to be 2,000 psi (13.8 MPa).

The writers feel method 3 is of special interest because of the direct nature in which allowable stresses can be derived. We feel further development of this technique is warranted and encourage additional investigation toward this end.

Conclusions

Procedures for estimating the strength of in situ structural members are in demand because of increased restorations, refitting, and repair of existing structures. This initial study presents procedures for estimating the strength of repetitively spaced wood joists, based on nondestructive measures and the modulus of elasticity.

TABLE 2.—Summary of Design Values

Method (1)	F_b for Repetitively Spaced Members		E_s		Remarks (6)
	in pounds per square inch (2)	in mega-pascals (3)	in pounds per square inch (4)	in giga-pascals (5)	
1	1,750	12.1	1.4×10^6	9.7	
2	1,750	12.1	1.4×10^6	9.7	71% confidence that 95% of E values equal or exceed the second order statistic
	2,050	14.1	1.6×10^6	11.0	by machine-stress-rated procedure
3	2,000	13.8	1.4×10^6	9.7	

Table 2 summarizes the allowable design values determined by the different methods. Method 2, the stress wave-MSR assessment, yielded values equal to or larger than method 1, the visual strength assessment. Method 3 yielded comparable results but needs additional investigation.

One important advantage of stress wave measurement is the ability to detect the low strength members. These members can be reinforced or replaced and the overall structural capacity can be increased.

After eliminating failed joists by visual inspection it was found that a random sample of 10% of the joists was statistically adequate for this investigation. However, it may be impossible to randomly select the specimens for the sample. For practical purposes all joists need to be examined, whenever possible, in order to locate and strengthen low-grade pieces.

The objective nature of the Nondestructive Testing (NDT) stress-wave inspec-

tion complements the subjective: necessary visual grading procedures are required. Future work is needed to refine the instrumentation into a convenient package that can be used easily in the field by investigators. The method of arriving at allowable stress for in situ joists needs further study. Future test programs should include field testing and then the removal of joists to a laboratory for static testing. The results will provide direct correlation between E_d and allowable stresses.

A question of greater concern in a timber structure is the strength of large primary members—solid beams and glulam beams. Solid beams are found in pre-World War II structures, while glulam beams have had increased use in post-World War II structures. Is the response of large members to stress waves similar to the response of nominal 2 in. (50 mm) joists?

It is obvious that no one method is a panacea, but it is felt that the stress-wave techniques show considerable merit and deserve further consideration and development.

Acknowledgments

The writers wish to thank R. Pellerin and R. J. Hoyle, Jr., Washington State University, Pullman, Wash. for their comments and suggestions during this study. The writers also wish to acknowledge the constructive comments of the ASCE reviewers, including Donald M. Onysk of Forintek Canada Corp., who were helpful and appreciated.

The first writer wishes to acknowledge the receipt of a Professional Development Grant from the National Science Foundation which enabled him to take part in this project.

Appendix I

Visual Grading Requirements

Mechanically stress-rated lumber must be well manufactured and visually graded to limit certain characteristics even though the actual strength is not affected. All pieces shall be visually graded to assure that the characteristics affecting strength are no more serious than the following limiting characteristics:

Checks—Seasoning checks not limited. Through checks at ends limited as splits.

Shake—On ends limited to 1/2 the thickness. Away from ends through heart shakes up to 2 feet long, well separated. If not through, single shakes may be 3 feet or up to 1/4 the length, whichever is greater.

Skips—Hit and miss, and in addition 5% of the pieces may be hit or miss or heavy skip not longer than 2 feet. See Section 720.000(e), (f) and (g).

Splits—Equal in length to 1 1/2 times the width of the piece.

Wane—1/3 thickness, 1/3 width, 5% of pieces may have wane up to 2/3 thickness and 1/2 the width for 1/4 the length.

Warp—Light. See table, Section 752.000.

In addition to the visual limitations listed, knots, knot holes, burls, distorted

grain or decay partially or wholly at edges of wide faces, must not occupy more of the net cross section than:

Fb Class

1/2 for 0–900
1/3 for 950–1450
1/4 for 1500–2050
1/6 for 2100 and over

Reprinted under Permission of the Western Wood Products Association.

Appendix II.—References

1. American Society for Testing and Materials, *Standard Methods for Establishing Clear Wood Strength Values*, Part 22, ASTM D 2555, 1978, p. 734.
2. American Society for Testing and Materials, *Standard Methods for Establishing Structural Grades and Related Allowable Properties for Visually Graded Lumber*, Part 22, ASTM 245, p. 139.
3. American Society for Testing and Materials, *Standard Method for Evaluating Allowable Properties for Grades of Structural Lumber*, Part 22, ASTM 2915, p. 824.
4. Bendtsen, B. A., and Rattner, F., "Tables for Developing Nonparametric Estimates of Near Minimum Property Values," *Research Paper* FPL *134*, U.S.D.A. Forest Service, 1970.
5. Bertholf, L. D., *Use of Elementary Stress Wave Theory for Predication of Dynamic Strain in Wood*, Bulletin No. 291, Washington State Institute of Technology, Washington State University, 1965.
6. Core, H. A., Côté, W. A., and Day, A. C., *Wood Structure and Identification*, 2nd ed., Syracuse University Press, Syracuse, N.Y., 1979.
7. *Design Values for Wood Construction*, National Forest Products Association, Apr., 1980, 1619 Massachusetts Ave., N.W., Washington, D.C.
8. Galligan, W. L., and Courteau, P. W., "Measurement of Elasticity of Lumber with Longitudinal Stress Waves and the Piezoelectric Effort of Wood," *Second Symposium on the Nondestructive Testing of Wood*, Washington State University, 1965, pp. 223–244.
9. Galligan, W. L., and Pellerin, R. F., "Dynamic Tests for Nondestructive Analysis of Lumber Quality," *Proceedings of the 5th International Conference on Nondestructive Testing*, Montreal, Canada, 1967.
10. Gerhards, C. C., "Stress Wave Speed and MOE of Sweetgum Ranging from 150 to 15% MC," *Forest Products Journal*, Vol. 25, No. 4, Apr., 1975, pp. 51–57.
11. *Grading Rules for Western Lumber*, Western Wood Products Association, 1500 Yeon Building, Portland, Oreg., 1977.
12. Hoyle, R. J., "Background to Mechanical Stress Grading," *Forest Products Journal*, Vol. 18, No. 4, Apr., 1968, pp. 87–97.
13. Hoyle, R. J., Jr., and Pellerin, R. F., "Stress Wave Inspection of a Wood Structure," *Fourth Nondestructive Testing of Wood Symposium*, Washington State University, Pullman, Wash., 1978, pp. 33–45.
14. Lee, I. D. G., *Nondestructive Tests on Structural Timber in an 18th Century Mansion*, Timber Development Assoc., E/TR/15, 1958.
15. Lee, I. D. G., "Ultrasonic Pulse Velocity Testing Considered as a Safety Measure for Timber Structures," *2nd Symposium on the Nondestructive Testing of Wood*, Washington State University, Pullman, Wash., 1965, pp. 185–203.
16. *Machine Stress-Rated Lumber Procedures for Qualification and Quality Control*, Western Wood Products Association, 1980, 1500 Yeon Building, Portland, Oreg.
17. McKean, H. B., Hoyle, R. J., "Stress-Grading Method for Dimension Lumber," *ASTM Special Technical Publication 353*, 1964, p. 3–18.
18. Panshin, A. J., and deZeevw, C., *Textbook of Wood Technology*, 3rd ed., McGraw-Hill Book Co., Inc., New York, N.Y., 1970.
19. Pellerin, R. F., and Kaiserlik, J. H., "Grading of Wood Products by Stress Waves,"

Presented at International Union of Forestry Research Organizations, Div. 5, Delft, Holland, 1965.
20. Wen, R. K., Henley, B. F., and Hsiu, F., "Modulus of Elasticity of Timber Members," *Journal of the Structural Division*, ASCE, Vol. 103, No. ST12, Proc. Paper 13385, Dec., 1977, pp. 2399–2404.
21. *Wood Handbook*, Forest Service Agricultural Handbook No. 72, U.S. Department of Agriculture, 1935.
22. *Wood Handbook*, Forest Service Agricultural Handbook No. 72, U.S. Department of Agriculture, 1974.

Appendix III.—Notation

The following symbols are used in this paper:

c = velocity;
E = allowable design modulus of elasticity;
E_d = dynamic modulus of elasticity;
E_g = modulus of elasticity assigned grade;
E_s = static modulus of elasticity in bending on edge;
$\bar{E}_s$ = average edge modulus of elasticity;
F_b = allowable design extreme fiber stress in bending;
r^2 = coefficient of determination;
s = standard deviation of mirror image of lower half of distribution;
$t_{\alpha/2}$ = students', t, statistic with $n - 2$ degrees of freedom;
X_o = MOR_0 for a given E value; and
ρ = material mass density.

DYNAMIC COLLAPSE OF FRAMES UNDER WIND DISTURBANCES

By Kiyotaka Morisako,[1] Shuzo Ishida,[2] Tsuneyoshi Nakamura,[3] and Hatsuo Ishizaki[4]

INTRODUCTION

In the evaluation of design wind loads, a considerable number of attempts have been made to take into account the dynamic behavior of structures when subjected to fluctuating wind pressure. In the latter half of the 1960's, procedures for evaluating design wind loads for structures as a function of their mass distribution, flexibility, damping, and size were proposed by, e.g., Davenport (2), Vellozzi and Cohen (14), and Vickery (15). These papers adopted the same spectral approach for the estimation of the dynamic response of a linear system. They differ in detail, e.g., the estimation of spatial characteristics of the turbulence by Vellozzi et al. is different from those in the aerodynamic admittance by Davenport and by Vickery. Each of them has proposed a factor defined as the ratio of the maximum expected value of a structural displacement response to its mean value. The factor has been called "gust loading factor (2)," or "gust response factor (14)." Many studies (e.g., 6, 7, 13) have since been carried out with the intent to place the evaluation of design wind loads on a more rational basis.

Only two papers have dealt with the plastic behavior of structures under wind action. Vickery's investigation on the behavior of simple elastic-perfect plastic structures is an approximate linear spectral approach and includes numerical analysis (16). He has proposed "the damage rate defined as the rate of accumulation of permanent set." The "rate of accumulation of plastic damage," similar to the damage rate, has been examined by Wyatt and May on a bilinear hysteretic model (17).

In order to establish a rational plastic design method of wind-resistant buildings, it is indispensible to accumulate a large number of data on dynamic characteristics of wind, and to accurately investigate dynamic collapse behavior of structures.

[1]Asst., Dept. of Architecture, Kyoto Tech. Univ., Kyoto, Japan.
[2]Prof., Dept. of Architecture, Kyoto Tech. Univ., Kyoto, Japan.
[3]Prof., Dept. of Architecture, Kyoto Univ., Kyoto, Japan.
[4]Prof., Disaster Prevention Research Inst., Kyoto Univ., Kyoto, Japan.

Note.—Discussion open until May 1, 1982. To extend the closing date one month, a written request must be filed with the Manager of Technical and Professional Publications, ASCE. Manuscript was submitted for review for possible publication on September 3, 1980. This paper is part of the Journal of the Structural Division, Proceedings of the American Society of Civil Engineers, ©ASCE, Vol. 107, No. ST12, December, 1981. ISSN 0044-8001/81/0012-2365/$01.00.

At present, the accumulation of data on strong wind, and the development of the methods of dynamic large-deflection analysis, enable one to carry out numerical analysis of dynamic collapse behavior of multistory frames subjected to strong winds. Some characteristics of the dynamic collapse behavior of strain-hardening frames have been analyzed by the senior writers (3,5). The numerical method used by them has been developed on the basis of the combined nonlinear finite element method, and of the combined use of the transfer matrix method (3,12,18).

This paper clarifies what strengths are to be assigned to the members of a frame so that it can withstand a fluctuating wind disturbance. The effect of a wind disturbance on the collapse of the frame is estimated with respect to the following two scales on the overall strength of the frame (Fig. 1): (1) α by means of simple plastic theory; and (2) β by means of the refined numerical analysis. The concept of the "dynamic collapse gust load factor" proposed by the senior writers (5) is examined more closely. A plane six-story frame

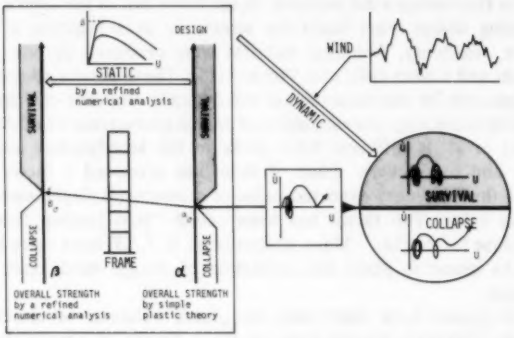

FIG. 1.—Numerical Approach to Dynamic Collapse Gust Load Factor

of one bay is adopted here as a model frame. Model wind disturbances are generated by amplifying a recorded fluctuating wind pressure. By means of the numerical approach, as shown in Fig. 1, several frames with different overall strengths are tested consecutively as to whether each will survive or collapse under a model disturbance. From this approach, a critical frame with the boundary strength is found. This boundary strength provides a rational basis for a safety factor for the frame to be designed with respect to the wind disturbance. The work presented herein is viewed as a first step toward the development of a more sound foundation for determining the safety factor of structures subjected to wind loads.

Model Wind Disturbances and Frames

Model Disturbances Representing Wind Pressure Fluctuation.—For a simulation study of dynamic collapse processes, it is desirable to apply realistic wind disturbances to frames. The fluctuating wind pressure record of Typhoon No.

7209 on July 22, 1972 (4), has been utilized here. This record was taken at a height of 10 m above ground in the Shionomisaki Wind Effect Laboratory of the Disaster Prevention Research Institute of Kyoto University. The maximum 10 min mean wind pressure was 126 N/m^2 (12.8 kgf/m^2). In the present study,

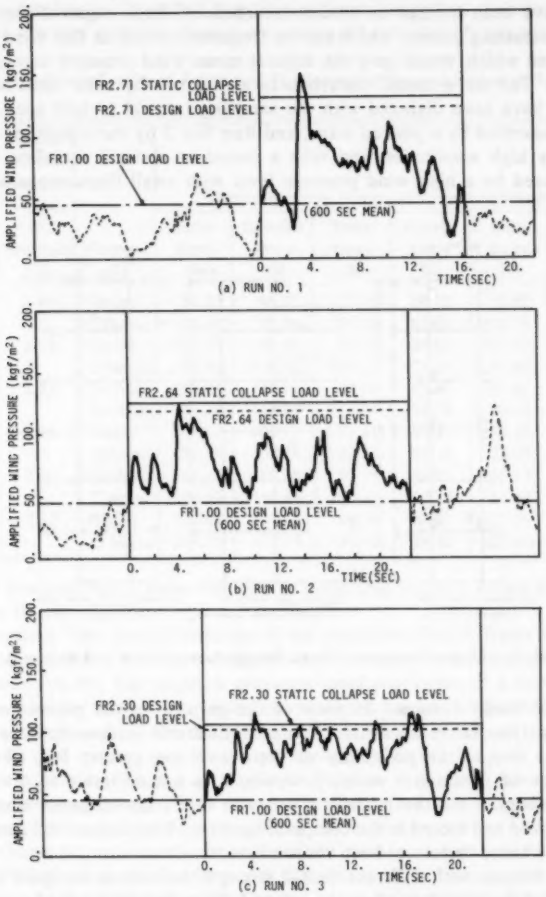

FIG. 2.—Model Wind Disturbances (1 N/m^2 = 9.81 kgf/m^2)

the original record was so amplified that the resulting 10 min mean wind velocity at a height of 10 m above ground would amount to 30 m/sec. It is assumed, for the sake of this numerical analysis, that the windward wall is subjected to the wind pressure in proportion to $(h/h_0)^{0.5}$ in which h_0 and h represent

1 m and the height, in meters, above ground, respectively, and that 75% of the total wind pressure on the windward wall is uniformly distributed over the leeward wall. This is a deliberately simplified model that could be modified in subsequent studies.

In the numerical analysis, three segments of the amplified wind pressure record have been utilized as model disturbances. Each segment represents a typical fluctuating pattern which can be frequently found in this wind pressure record, and which would give the highest mean wind pressure among similar segments. The three model disturbances are shown by solid lines in Fig. 2. The data have been digitized with the sampling interval of 0.04 sec. Run No. 1 is characterized by a peaked wave, and Run No. 2 by the repetition of waves with fairly high amplitudes, and with a period of about 2 sec. Run No. 3 is characterized by a high wind pressure level with small fluctuations about the mean.

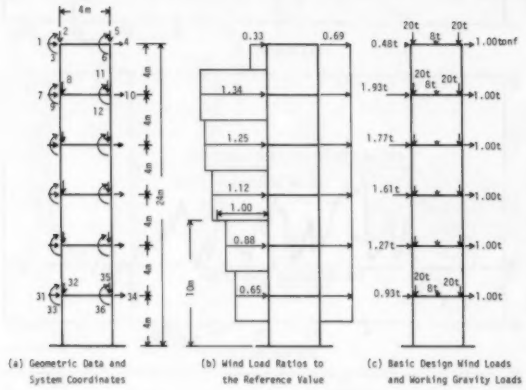

FIG. 3.—Model Frame and Basic Design Loads (1 kN = 9.81 ton f)

Design of Model Frames.—In view of the purpose of the present nonlinear dynamic analysis, fairly tall, slender frames are desirable as representative models, particularly due to the possibility of their involving greater P-Δ effect. For the purpose of parametric study, however, it is not desirable to involve too many members, since the hysteretic behavior of all the elements would have to be analyzed and stored in the computer memory. The geometrical data shown in Fig. 3(*a*) have, therefore, been chosen here.

Several frames, with different overall strength, have been designed consecutively to find the boundary strength, and each frame has been tested numerically for survival or collapse under the model disturbance defined here. The nodal force introduced by the pressure, corresponding to the 10 min mean wind velocity of 30 m/sec at a height of 10 m above ground, has been adopted as the reference value of the wind loads. The wind-load ratios to the reference value at each node are shown in Fig. 3(*b*). These ratios have been estimated on the basis of the spatial distribution assumed here. The "basic design wind loads" are

defined by the reference value and the wind-load ratios. Fig. 3(*c*) shows the basic design wind loads, together with the working gravity loads. Each frame has been designed using simple plastic theory so as to support the two sets of loads: One, consisting of the working gravity loads, and α times the lateral loads shown in Fig. 3(*c*); and the other, 1.4 times the working gravity loads only. The number, α, is called the "design load factor" in the sense that it represents the gust level for design, as compared with the 10 min mean level.

TABLE 1.—Cross-Sectional Areas and Fundamental Natural Period of Frames

Frame (1)	Fundamental natural period, in seconds (2)	Member (3)	Cross-Sectional Areas, in square centimeters					
			First story (4)	Second story (5)	Third story (6)	Fourth story (7)	Fifth story (8)	Sixth story (9)
FR1.00	3.15	Girder	54.29	45.58	35.48	24.70	15.97	12.54
		Column	116.33	95.54	74.68	53.89	35.78	29.56
FR2.00	2.59	Girder	108.58	91.15	70.96	48.61	28.08	12.54
		Column	172.65	141.08	109.35	77.79	47.57	29.56
FR2.20	2.52	Girder	119.43	100.27	78.07	53.50	30.41	12.54
		Column	183.94	150.19	116.31	82.59	50.36	29.56
FR2.40	2.46	Girder	127.62	107.15	83.41	57.15	32.13	12.54
		Column	192.43	157.06	121.53	86.18	53.09	29.56
FR2.60	2.40	Girder	141.21	118.56	92.29	63.22	35.00	12.54
		Column	206.52	168.46	130.21	92.15	55.85	29.56
FR2.80	2.32	Girder	152.04	127.65	99.36	68.07	37.31	12.54
		Column	217.75	177.54	137.12	96.92	58.60	29.56

A frame designed for α times the lateral loads (Fig. 3(*c*)) is called FRα, e.g., the frame for $\alpha = 2.70$ is designated as FR2.70.

The required fully plastic moments of the members of each frame have been found under the two loading conditions by assuming over complete collapse mechanisms (10,19). The in-plane cross-sectional properties of a member may be represented by those of an equivalent idealized sandwich member (19). The equivalent depths of all the beams and all the columns adopted here are 40 cm and 30 cm, respectively. For a prescribed value of the yield stress, the area of an equivalent flange may readily be found so as to satisfy the interaction yield condition represented by a square (9). The larger area between the two, determined for the two-loading conditions, has been adopted for each member. Table 1 shows the cross-sectional areas of the members of several frames from FR1.00–FR2.80, and the fundamental periods of their frames. All the other values have been omitted since they turned out to be almost equal to the values obtained by a linear interpolation.

Method of Numerical Analysis

The method of numerical analysis developed in Refs. 3, 12, and 18 has been applied to the present wind response analysis. The following approximations

have been introduced in generating the system stiffness matrix.

1. A cross-section is idealized as an equivalent sandwich section consisting of two flanges, each possessing a concentrated area of half the actual total area, and located at the radius of gyration.
2. Each flange obeys the bilinear hysteretic stress-strain relation, with Young's modulus of 206 kN/mm^2 (2,100 ton f/cm^2), the yield stress of 2.35 N/mm^2 (2.4 ton f/cm^2), and the strain-hardening modulus of 0.005 times Young's modulus.
3. Each member consists of several beam-column elements connected in series, and only the representative, or averaged flange stress and strain of an element, obeys the relation in assumption 2. The basic element length used here is 40 cm.

Only the buffeting response in the plane of a frame is analyzed by employing the system coordinates shown in Fig. 3(*a*). The following approximations have been introduced for dynamic analysis.

4. The generalized mass matrix consistent with the displacement functions of a member in the initial elastic range has been generated and held constant.
5. The viscous damping matrix is 0.01 times the system stiffness matrix, and the aerodynamic damping has been neglected in comparison with the former.
6. A modified version of the Wilson-Clough method (1) has been utilized for direct integration of the equation of motion. After a convergence study, the time step of 0.01 sec has been adopted here.

Static Behavior under Lateral Loads Proportional to Design Wind Loads

The lateral loads proportional to the design wind loads have been applied to the several frames and increased under the constant gravity loads. Fig. 4 shows the base shear-top lateral displacement diagram. The dropping portion of each curve has been obtained by the displacement-controlled incremental

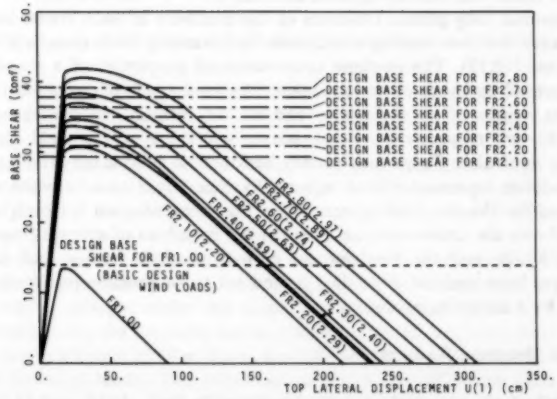

FIG. 4.—Base Shear—Top Lateral Displacement Diagram (1 kN = 9.81 ton f)

analysis (11) and demonstrates the negative stiffness, reflecting the effect of gravity loads or P-Δ effect.

The ratio, β, of the maximum base shear to that due to the basic design wind loads is called the *static collapse load factor*. The values of β have been indicated by the numbers in the round brackets in Fig. 4. The value of β for each frame is slightly greater than its α value. In general, the β value for a frame may not be equal to its prescribed α value.

Dynamic Behavior under Model Disturbances

The problem here is to clarify what strengths are to be assigned to the members of a frame so that it can withstand a fluctuating wind disturbance during a

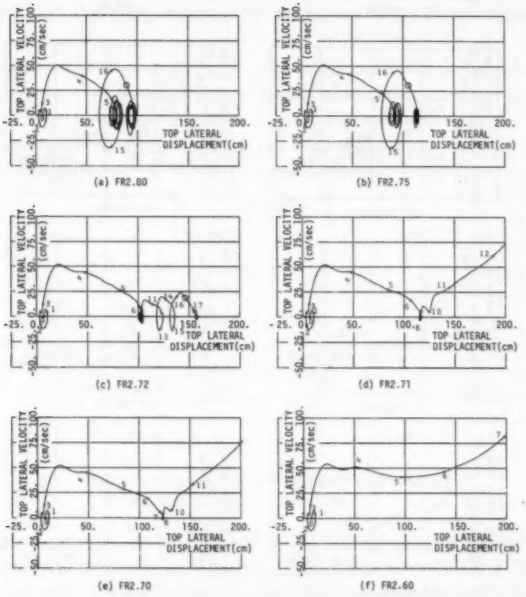

FIG. 5.—Phase Plane Diagrams (Run No. 1)

windstorm. For this purpose, the standard state of a frame is defined as that state which is subjected to the gravity loads and to the mean wind pressure. A frame under the standard state is subjected to one of the three model disturbances. When this disturbance is terminated, the frame is brought under the mean pressure level again. Numerical simulation of this process was conducted on all the frames designed in the preceding section, and the dynamic collapse behavior and survival behavior of the frames were investigated. Some frames may or may not exhibit the critical or precarious behavior during the application

of a fluctuating disturbance. In order to investigate whether or not a frame would collapse during the autonomous state after the fluctuation was terminated, the numerical analysis of the behavior was continued for 10 sec under the mean wind pressure. The analysis was also terminated if the top lateral displacement exceeded 5 m.

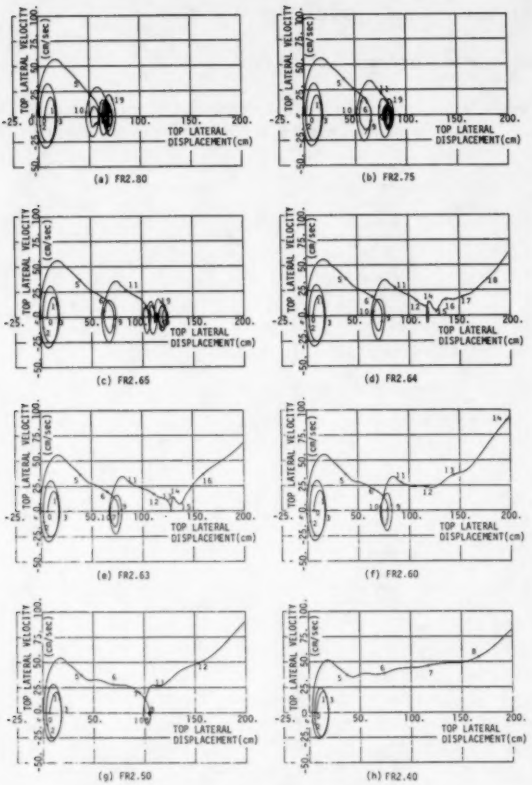

FIG. 6.—Phase Plane Diagrams (Run No. 2)

While frames have been subjected here, tentatively, to only three model wind disturbances, it is necessary to conduct a similar numerical analysis with respect to more realistic disturbances. Therefore, this work is viewed as a first step toward the development of a more sound foundation for determining the safety factor of structures subjected to wind loads.

Phase Trajectories.—Figs. 5, 6, and 7 show the phase trajectories on the top lateral velocity-top lateral displacement planes. In these diagrams, the symbol

"*o*" indicates the time when the wind pressure fluctuation is over, and each number along a trajectory indicates the time in seconds.

The dynamic behavior of simple elastic-plastic structures has been studied previously with respect to the phase trajectories (8,20). Sun et al. (8) studies the gravity effect on the dynamic behavior of an undamped single degree-of-freedom inelastic system in free vibration, subjected to given initial conditions, and in forced vibration to an earthquake input. Yokoo et al. (20) has also analyzed a definition of the dynamic stability limit of a simple bilinear hardening column model, and the engineering significance of stability under a finite disturbance.

In this paper, phase trajectories will also play an important role in studying the dynamic behavior of frames subjected to model disturbances. But it would be extremely difficult to investigate the dynamic behavior given here with the analytic approach used in the preceding studies. A phenomenological examination of Figs. 5–7 will therefore have to be attempted first. These trajectories are

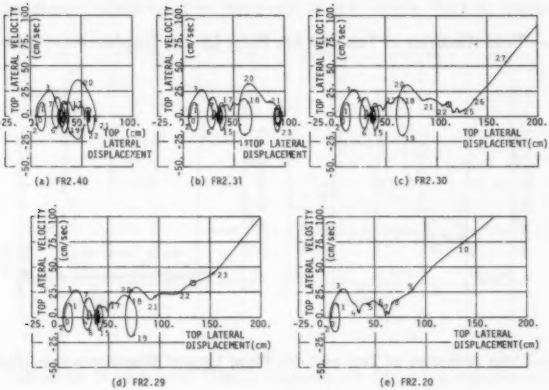

FIG. 7.—Phase Plane Diagrams (Run No. 3)

substantially composed of *some or all* of the following three typical processes: (1) A process represented by a spiral in the neighborhood of a point on the displacement axis; (2) a process represented by a segment from one spiral to the next; and (3) a process such that both displacement and velocity components of the trajectory exhibit a tendency of divergence within the region of the response given here. The three processes correspond to the following patterns of the behavior of frames:

(1) Elastic Vibration-like Behavior.—Process 1 represents an approximate elastic vibration of the frame virtually without the work dissipated for the plastic deformation. The pattern of the behavior of the frame represented by this process will, therefore, be called "elastic vibration-like behavior."

(2) One-way Bounded Plastic Deformation Behavior.—Process 2 means that some plastic regions have been developed in some parts of the frame, but the corresponding one-way displacements are still bounded. The pattern of the

behavior of the frame by this process, followed by process (1), will therefore be called "one-way bounded plastic deformation behavior."

(3) One-way Unbounded Plastic Deformation Behavior.—Process 3 represents a tendency in which the plastic deformation of the frame, and the corresponding

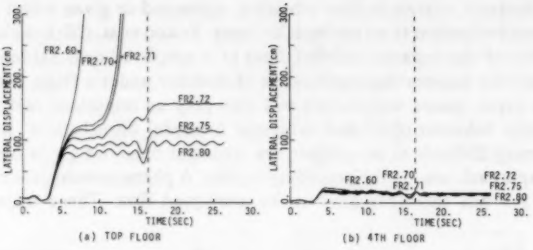

FIG. 8.—Time Histories of Top and 4th Floor Lateral Displacements (Run No. 1)

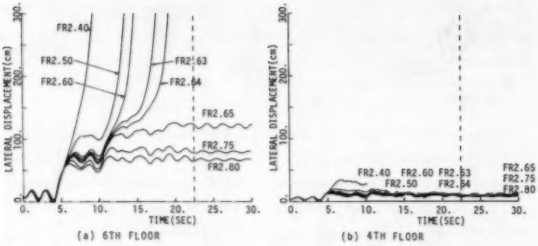

FIG. 9.—Time Histories of Top and 4th Floor Lateral Displacements (Run No. 2)

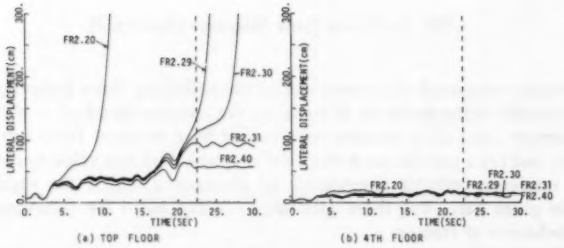

FIG. 10.—Time Histories of Top and 4th Floor Lateral Displacements (Run No. 3)

nodal displacements, will keep on increasing unboundedly during the time interval considered here. The pattern of the behavior of the frame represented by this process will therefore be called "one-way unbounded plastic deformation behavior."

Run No. 1.—The trajectories of FR2.80, FR2.75, and FR2.72 (Figs. 5(*a*)–(*c*)) eventually represent the elastic vibration-like behavior. On the other hand, the trajectories of FR2.71, FR2.70, and FR2.60 (Figs. 5(*d*)–(*f*)) eventually represent the one-way unbounded plastic deformation behavior. Even while the wind pressure varies at a relatively low level after 10 sec in (Fig. 2(*a*)), the trajectory of FR2.71 represents the one-way unbounded plastic deformation behavior. The trajectories of FR2.71 and FR2.70 exhibit a cusp-like process with a small loop, followed by Process 3, after the Process 2, from 3–7 sec. This process indicates that there exists such a point as a saddle point for an autonomous system.

Run No. 2.—The trajectories of FR2.80, FR2.70, and FR2.65 (Figs. 6(*a*)–(*c*)) eventually represent the elastic vibration-like behavior. On the other hand, the trajectories of FR2.64, FR2.63, FR2.60, FR2.50, and FR2.40 (Figs. 6(*d*)–(*h*)) eventually represent the one-way unbounded plastic deformation behavior. In the trajectories of FR2.64 and FR2.63, there also exist such cusp-like processes as those observed in the trajectories of FR2.71 and FR2.70 (Run No. 1). FR2.60 exhibits the elastic vibration-like behavior twice, while FR2.40 does so only

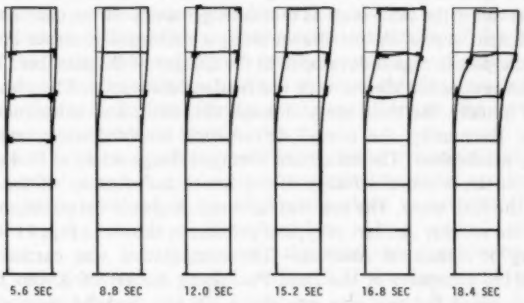

FIG. 11.—Deflected Shapes and Plastic Regions for FR2.64 Subjected to Run No. 2 (In Real Proportional Scale)

once. The one loop process of FR2.50 is a degenerated version of the second elastic vibration-like behavior of FR2.60. Among those frames whose α values are between 2.40 and 2.50, there will probably exist a frame whose trajectory exhibits a clearer cusp-like process as a limiting case of the one loop process (Fig. 6(*g*)).

Run No. 3.—The trajectories of FR2.40 and FR2.31 (Figs. 7(*a*) and (*b*)) eventually represent the elastic vibration-like behavior. On the other hand, the trajectories of FR2.30, FR2.29, and FR2.20 (Figs. 7(*c*)–(*e*)) eventually represent the one-way unbounded plastic deformation behavior. The trajectory of FR2.30 is mostly similar to that of FR2.31 until 21 sec, but the displacement component of FR2.30 thereafter appears to keep on increasing. In the autonomous state after the wind fluctuation is over, the trajectory of FR2.30 is considerably similar to a saddle-like trajectory for an autonomous system.

For all the frames and within the duration of the analysis, the maximum response nodal velocities have been very small compared to the mean wind velocity of 30 m/sec.

Displacement Response.—Figs. 8, 9, and 10 show time histories of top and fourth floor lateral displacements. The broken line in each diagram indicates the time when each wind pressure fluctuation is over.

The following characteristics have been observed in these diagrams.

1. Even if a frame exhibits the one-way unbounded plastic deformation behavior, the lateral displacement of the fourth floor hardly increases.
2. A set of displacement response curves of the top floor looks as if bundled threads were becoming loose. For instance, the curves for Run No. 2, shown in Fig. 9(*a*), have been bundled initially, but they are divided into two groups at about 6 sec. One is composed of the curves whose displacement components appear to keep on increasing rapidly, and the other is composed of the subsequent wave-shaped curves. The latter is further divided into two groups.
3. Once the top lateral displacements exhibit a tendency of divergence, within several seconds they exceed the prescribed displacement limit of 5 m.

Overall Deformation and Growth of Plastic Regions.—Fig. 11 shows the deformed configurations of FR2.64 subjected to Run No. 2, drawn at several second intervals in the same scale as the frame geometry without any amplification of displacement scales. A line drawn along a deformed member indicates the extent of the plastic region developed in the flanges of the member. The overall deformation proceeded almost with the fundamental mode. The plastic regions developed initially the third story through the sixth, and subsequently in the fifth story. Eventually, the overall deformation involved some tendency of a story-sway mechanism. The maximum averaged flange strain at 18.4 sec is 9.3% in tension at the windward flange of the lower end element of the windward column in the fifth story. The one-way unbounded plastic deformation processes of frames are roughly similar. A typical process is shown in Fig. 11 for FR2.64.

Efficiency of Numerical Analysis.—The computation was carried out on a FACOM-M190 computer at the Data Processing Center of Kyoto University. The time required for one case was about 300 sec, and the memory required was about 400 KB.

Dynamic Collapse Behavior and Dynamic Collapse Gust Load Factor

In view of the numerical results, frames designed for various design load factors, α, are divided into two classes according to the dynamic behavior under a fluctuating wind pressure disturbance. One class of frames is characterized by the elastic vibration-like behavior at the final stage of the analysis. The other is characterized by the one-way unbounded plastic deformation behavior within the duration of the analysis. The latter is unbounded in the sense that both lateral displacement and velocity components of at least one story exhibit a tendency of divergence within the region of the response given here. Since all the displacement components of a frame will be eventually bounded after the frame has completely crushed or overturned, the trajectory must also be bounded. If the analysis were continued a little longer, the trajectory might turn out to be bounded. For practical purposes, however, the one-way unbounded plastic deformation behavior may be regarded as a collapse behavior, possibly leading to a final state, and is called the *dynamic collapse behavior*. On the other hand, the elastic vibration-like behavior at the final stage of the analysis

appears to represent a survival behavior against the wind disturbance.

This classification of the nonautonomous systems, with respect to their trajectories, roughly corresponds to the well-known classification of the trajectories of an autonomous system, and is supported by the phase trajectories which almost indicate the existence of such a point as a saddle point for the autonomous system. It is natural to expect, therefore, that there also exists a watershed trajectory dividing a saddle-like cluster of trajectories, for the present nonautonomous systems. This potentially existent saddle point may be called a *dynamic collapse point*. It is assumed that there exists a frame whose phase trajectory passes through such a dynamic collapse point. The corresponding value of α, denoted by α_c, may be called the *dynamic collapse gust load factor* of the frame to be designed with respect to the fluctuating wind pressure disturbance. The frame designed for the α_c value is a critical frame which exhibits the dynamic collapse behavior.

The effect of wind disturbances on the collapse of frames may be estimated with respect to the overall plastic strength of their frames. The design load factor α due to the simple plastic theory does not represent the true strength of the frame. The static collapse load factor β, evaluated by the present refined numerical method, will provide a more accurate estimate of the effect. The β value of the critical frame designed for the α_c value is denoted by β_c. Then the value of α_c may be called a nominal value of the dynamic collapse gust load factor. However, for the purpose of the initial design, the nominal value α_c will be more convenient in practice.

Even if such a dynamic collapse point is not found numerically, it is possible and, for practical purposes, sufficient to determine the upper and lower bound values of α_c from α values of the neighboring phase trajectories. The highest lower bound and the lowest upper bound are denoted by α_c^L and α_c^U, respectively, and $\alpha_c^L < \alpha_c < \alpha_c^U$. For the present, three numerical examples, values of α_c^L and α_c^U are given by: $\alpha_c^L = 2.71$, $\alpha_c^U = 2.72$ for Run No. 1; $\alpha_c^L = 2.64$, $\alpha_c^U = 2.65$ for Run No. 2; and $\alpha_c^L = 2.30$, $\alpha_c^U = 2.31$ for Run No. 3. Similarly, for a more accurate value, β_c, of the dynamic collapse gust load factor, values of β_c^L and β_c^U are given by: $\beta_c^L = 2.90$, $\beta_c^U = 2.91$ for Run No. 1; $\beta_c^L = 2.80$, $\beta_c^U = 2.82$ for Run No. 2; and $\beta_c^L = 2.40$, $\beta_c^U = 2.41$ for Run No. 3.

The solid straight line and the broken straight line in Fig. 2 indicate the pressure level corresponding to the β_c^L value and the α_c^L value, respectively. The peaked wave characterizing Run No. 1 goes beyond the solid line. The pressure level corresponding to the β_c^U value for FR2.72, which has not exhibited the dynamic collapse behavior, is slightly above the solid line. The external forces represented by the peaked wave do not have sufficient intensity and duration for inducing the dynamic collapse behavior of FR2.72. The frame has therefore exhibited the elastic vibration-like behavior against the subsequent wind pressure fluctuation of lower level. In this sense, the increment appears to represent the toughness of the frame. Run No. 2 represents the wind fluctuation obviously below the solid line. The decrement appears to represent the unfavorably dynamic effect of the wind pressure fluctuation on the frame. In Run No. 3, the peaks of the wind disturbance are almost on the same level as the solid line. In this case, it has been difficult to observe the effect of the wind pressure fluctuation on the frame.

The gust factors proprosed by Davenport (2), and others (14,15), have been

introduced for the purpose of estimating the effect of the resonant amplification of structural displacement response to gusts in simple static design criteria. The calculation involves a spectral analysis of the dynamic response of a linear system. On the other hand, the dynamic collapse gust load factor of a frame, with respect to a wind pressure disturbance as defined here, reflects the effect of the wind pressure fluctuation on the dynamic collapse behavior of the frame.

Summary and Conclusions

A parametric numerical analysis has been conducted on strain-hardening multistory frames subjected to wind disturbances generated by amplifying a recorded fluctuating wind pressure. The effect of spreading and diminishing of the strain-hardening regions has been taken into account in the one-dimensional finite element formulation employed here. The following facts should be noted:

1. The dynamic behavior, including, in particular, the dynamic collapse behavior, has been extensively examined and the details are presented, for the first time, of strain-hardening multistory frames subjected to fluctuating wind pressure disturbances. A phase trajectory is composed of *some or all* of the following three typical processes: (1) A spiral trajectory represents the elastic vibration-like behavior of the frames; (2) a segment of a trajectory from one spiral to the next represents the one-way bounded plastic deformation behavior; and (3) a divergent trajectory within a given duration represents the one-way unbounded plastic deformation behavior of the frame. The one-way unbounded plastic deformation behavior has been regarded as a dynamic collapse behavior.
2. Under a fluctuating wind pressure disturbance, frames designed for various design loads are divided into two classes: one in which frames exhibit the elastic vibration-like behavior at the final stage of a given loading duration, and the other in which frames exhibit the one-way unbounded plastic deformation behavior within the given duration. This classification of the nonautonomous systems with respect to their trajectories roughly corresponds to the well-known classification of the trajectories of an autonomous system. There exist a couple of frames whose trajectories almost indicate the existence of such a point as a saddle point for the autonomous system. The trajectories of those frames appear to be quite close to the watershed trajectory dividing the elastic vibration-like behavior and the one-way unbounded plastic deformation behavior.
3. The concept of the dynamic collapse gust load factor proposed by the senior writers (5) has been more thoroughly examined with respect to the three typical patterns of a recorded wind disturbance. The effect of a fluctuating wind disturbance on a frame may be represented by the required overall plastic strength, and therefore measured by a multiplier (load factor) of the basic wind loads. There exists a critical frame which just exhibits the dynamic collapse behavior under a wind disturbance. The corresponding critical value of the multiplier has been called the dynamic collapse gust load factor. There are two methods for evaluating the dynamic collapse gust load factor. The factor evaluated by a refined numerical analysis is more accurate than the nominal value due to the simple plastic theory. However, for the purpose of the initial design, the nominal value will be more convenient in practice. The dynamic

collapse gust load factor provides a rational basis for a practical safety factor and is, therefore, recommended for a more rational method of wind resistant design of ductile structures.

Appendix.—References

1. Clough, R. H., "Analysis of Structural Vibrations and Dynamic Response," *Recent Advances in Matrix Method of Structural and Design*, R. H. Gallagher, Y. Yamada, and J. Tinsley Oden, eds., The University of Alabama Press, Alabama, 1971, pp. 441–486.
2. Davenport, A. G., "Gust Loading Factors," *Journal of the Structural Division*, ASCE, Vol. 93, No. ST3, Proc. Paper 5255, June, 1967, pp. 11–34.
3. Ishida, S., "A Method of Static and Dynamic Large Deflection Analysis of Elastic-Plastic Frames," (in Japanese), thesis presented to Kyoto University, at Kyoto, Japan, in 1975, in partial fulfillment of the requirements for the degree of Doctor of Engineering.
4. Ishizaki, H., Murota, T., and Yoshikawa, Y., "On the Behavior of the Glass Pane under Natural Wind," (in Japanese), *Proceedings of the 2nd Symposium on Wind Effects on Structures in Japan*, 1972, pp. 67–72.
5. Ishizaki, H., Nakamura, Tsuneyoshi, Ishida, S., and Okuhira, T., "The Analysis of Dynamic Collapse Behavior of Strain-Hardening Multi-Story Frames Subjected to Strong Gusts," (in Japanese), *Proceedings of the 4th Symposium on Wind Effects on Structures in Japan*, 1976, pp. 109–116.
6. Simiu, E., "Revised Procedure for Estimating Along Wind Response," *Journal of the Structural Division*, ASCE, Vol. 106, No. ST1, Proc. Paper 15111, Jan., 1980, pp. 1–10.
7. Soize, C., "Gust Loading Factors with Nonlinear Pressure Terms," *Journal of the Structural Division*, ASCE, Vol. 104, No. ST6, Proc. Paper 13844, June, 1978, pp. 991–1007.
8. Sun, C., Berg, G. V., and Hanson, R. D., "Gravity Effect on Single-Degree Inelastic System," *Journal of the Engineering Mechanics Division*, ASCE, Vol. 99, No. EM1, Proc. Paper 9565, Feb., 1973, pp. 183–200.
9. Tanabashi, R., and Nakamura, Tsuneyoshi, "An Approach to the Last Hinge Point Design of Tall Multi-Story Frames," *Proceedings of 11th Symposium on Bridge and Structural Engineering (1964), External Forces and Structural Design of High-rise and Long-span Structures*, 1965, pp. 169–179.
10. Tanabashi, R., and Nakamura Tsuneyoshi, "The Minimum Weight Design of A Class of Tall Multi-Story Frames subjected to Large Lateral Forces I, II," *Transactions*, Architectural Institute of Japan, Vol. 118, 1965, pp. 10–18, and Vol. 119, 1966, pp. 37–44.
11. Tanabashi, R., Kaneta, K., Nakamura, Tsuneyoshi, and Ishida, S., "To the Final State of Rectangular Frames," *Proceedings of the 4th World Conference on Earthquake Engineering (1969)*, Santiago, Chile, Vol. 2, A-4, 1969, pp. 179–194.
12. Tanabashi, R., Nakamura, Tsuneyoshi, and Ishida, S., "Gravity Effect on the Catastrophic Dynamic Response of Strain-Hardening Multi-Story Frames," *Proceedings of the 5th World Conference on Earthquake Engineering (1973)*, Rome, Italy, Vol. 2, 1974, pp. 2140–2154.
13. Vaicaitis, R., Shinozuka, M., and Takeno, M., "Response Analysis of Tall Buildings to Wind Loadings," *Journal of the Structural Division*, ASCE, Vol. 101, No. ST3, Proc. Paper 11194, Mar., 1975, pp. 585–600.
14. Vellozzi, J., and Cohen, E., "Gust Response Factors," *Journal of the Structural Division*, ASCE, Vol. 94, No. ST6, Proc. Paper 5980, June, 1965, pp. 1295–1313.
15. Vickery, B. J., discussion of "Gust Response Factors," by Joseph Vellozzi, and Edward Cohen, *Journal of the Structural Division*, ASCE, Vol. 95, No. ST3, Proc. Paper 6430, Mar., 1969, pp. 494–501.
16. Vickery, B. J., "Wind Action on Simple Yielding Structures," *Journal of the Engineering Mechanics Division*, ASCE, Vol. 96, No. EM2, Proc. Paper 7204, Apr., 1970, pp. 107–120.
17. Wyatt, T. A., and May, H. I., "The Ultimate Load Behavior of Structures under

Wind Loading," *Proceedings of 3rd International Conference on Wind Effects on Buildings and Structures*, Tokyo, 1971, pp. 501–510.

18. Yokoo, Y., Nakamura, Tsuneyoshi, Ishida, S., and Nakamura Takashi, "Cyclic Load-Deflection Curves of Multi-Story Strain-Hardening Frames subjected to Dead and Repeated Alternating Lateral Loads," *Preliminary Report of the International Association for Bridge and Structural Engineering Symposium on Resistance and Ultimate Deformability of Structures Acted on by Well Defined Repeated Loads*, Lisbon, Portugal, 1973, pp. 81–87.
19. Yokoo, Y., Nakamura, Tsuneyoshi, and Keii, M., "The Minimum Weight Design of Multi-Story Building Frames Based upon the Axial Force-Bending Moment Interaction Yield Condition," *Proceedings of the International Union of Theoretical and Applied Mechanics Symposium on Optimization in Structural Design (1973)*, Warsaw, Poland, 1975, pp. 497–517.
20. Yokoo, Y., Nakamura, Tsuneyoshi, and Denda, M., "Analysis of Dynamic Stability Limits of Elastic-Plastic Structures by Incremental Perturbation Method," (in Japanese), *Summaries of Technical Papers of Annual Meetings of the Architectural Institute of Japan*, 1975, pp. 693–694.

BUCKLING OF REINFORCED CONCRETE SHELLS

By Endre Dulácska[1]

INTRODUCTION

A stability analysis of shells is generally carried out by comparing the expected load magnitude to a theoretical critical load divided by a safety factor. This safety factor used to be much greater than that applied for other structures. The reason is that there are several secondary effects decreasing the critical load of shells much more than that of other structures, and these secondary effects have not been clarified so far.

Shells of reinforced concrete present various special problems. For example, the stiffness of reinforced concrete decreases due to cracks while it increases due to the reinforcement. Thus, an additional stiffness of shell caused by a double layer reinforcement has been evident but it could not be taken into account. We believe that the research of these secondary effects has advanced so much that a dimensioning procedure, for which the safety factor will conform to that of common structures, can be developed. Such a dimensioning procedure will be more correct and reliable for the various destabilizing secondary effects can be considered at their correct places with their effective values.

When considering a shell of perfect geometry, the differential equations of equilibrium and compatibility restricted to small deflections lead to a linear eigenvalue problem. The lowest eigenvalue obtained is the critical force based on linear theory, or bifurcation force of the shell ($N_{\text{crit}}^{\text{lin}}$). The surface load belonging to that shell is the linear critical load of the shell. However, experimental observations indicated that cylinders and spherical domes buckle at a load magnitude much lower than the bifurcation one, and the buckling deflection is no longer small. Therefore, nonlinear terms relating to nonlinear deflections were introduced to the differential equations. Thus, equations became applicable to describe the linear as well as the nonlinear (postcritical) behavior.

Investigations by the energy method presented the following features:

1. The load carrying capacity of some shells does not decrease, but increases after reaching the bifurcation state. If there is an initial imperfection of amplitude w_o, the shell has no bifurcation load any more, and its carrying capacity increases

[1]Struct. Lead Engr., Planning Office, BUVATI of Budapest, Budapest, Hungary.

Note.—Discussion open until May 1, 1982. To extend the closing date one month, a written request must be filed with the Manager of Technical and Professional Publications, ASCE. Manuscript was submitted for review for possible publication on March 8, 1977. This paper is part of the Journal of the Geotechnical Engineering Division, Proceedings of the American Society of Civil Engineers, ©ASCE, Vol. 107, No. ST12, December, 1981. ISSN 0044-8001/81/0012-2381/$01.00.

with increasing deflections. Shells of this type are not sensitive to initial imperfections. Generally those shells exhibit such a behavior at which a qualitative change in the stress distribution occurring at p_{crit}^{lin} stabilizes the shell, thus it becomes more rigid than before. Some hypar shells and some shells without edge beams are known as belonging to this type.

2. In other cases, the carrying capacity of the perfect shell decreases until the deflection due to buckling reaches a value, w_{crit}, then it increases again.

The force and load belonging to w_{crit} are called the lower critical force, N_{crit}^{low} and the lower critical load, p_{crit}^{low}, respectively [this notation was used by Kármán (20)]. Shells of this type are referred to as shells of decreasing carrying capacity. Generally, cylinders, cones, spheres, and domes belong to this type. However, not even this value of p_{crit}^{low} was confirmed by experiments. Failure loads appeared between the bifurcation load and the lower critical one.

Further investigations pointed out that the reason for which cylindrical and spherical shells buckle at a load smaller than the bifurcation was their initial imperfection. The maximum amplitude of imperfection will be denoted by w_o.

TABLE 1.—Ratio of Snap-Through Critical Load and Bifurcation Load

w_o/t (1)	$\rho_{hom} = p_{crit}^{u}/p_{crit}^{lin}$ (2)
0	1.00
0.1	0.60
0.2	0.45
0.3	0.35
0.4	0.30
0.5	0.25
1.0	0.20

Investigations of shells with initial imperfections were carried out as well. The essense of the results was that the initial deformation increases with the load intensity. The load magnitude reaches a maximum value, after that, it decreases with increasing deformations. This maximum is denoted by N_{crit}^{sn} (snap-through critical load). Actually, cylinders and spheres buckle at the snap-through critical load.

The Ratio of Snap-through and Bifurcation Load.—Referring to radially loaded spheres and axially compressed cylinders, can be estimated by using the results found in Refs. 1, 4, 5, 8, 19, 21, 22, 23, 28 and 34. For different values of w_o/t, the ratio $p_{crit}^{sn}/p_{crit}^{lin}$ is given in Table 1. Here t is the shell thickness. An approximate formula for the ratio considered fairly good for $w_o/t < 0, 6$ can be stated as follows:

$$\frac{p_{crit}^{sn}}{p_{crit}^{lin}} = \frac{1}{1 + F\dfrac{w_o}{t}} \quad \ldots\ldots\ldots\ldots\ldots\ldots\ldots\ldots\ldots\ldots\ldots\ldots\ldots\ldots\ldots\ldots (1)$$

For various types of shells F assumes different values. For radially compressed

cylinders and radially loaded spheres $F = 6$, for radially loaded long cylinders $F = 0.6$, and for short ones, $F = 1.4$. For hypar shells on square ground plan, the value of F is zero. For hyperboloids of revolution, the value of F depends on geometrical ratios, namely, how much the current geometry differs from that allowing an inextensional deformation.

Initial deformation (imperfection) consists of two parts: (1) Deformation which can be calculated, $w_{o,\text{calc}}$; and (2) random initial imperfection, $w_{o,\text{ran}}$. The average value of experimental failure loads measured on spherical and cylindrical models having random initial imperfections can be approximated by the formula

$$\frac{p_{\text{crit}}^{\text{an}}}{p_{\text{crit}}^{\text{lin}}} = \frac{1}{1 + \sqrt{3}\,\dfrac{R}{1{,}000t}} \quad \ldots\ldots\ldots\

also exists. Consequently, the "elastic" modulus of concrete E_c appearing in the ideal elasto-plastic stress-strain diagram serving as the approximation of the real one, depends on whether loads have been acting for a long or short while. In the case of long time loading, viscous deformations can fully develop while this is not possible when the load acts instantaneously, or for a short time (proof load). Thus $E_{c,l}$ and $E_{c,s}$ for long and short time loading, respectively, are the characteristic moduli for the ideal elasto-plastic model of material. Long time loading means more than one year of action. During such a while viscous deformations can almost fully develop.

In the case of instantaneous loading (e.g., vibration), there is no viscous deformation at all, thus the modulus of the concrete can be considered equal to its elastic modulus.

Characteristics of the cracked cross section of reinforced concrete are modelled as it were of homogeneous ideal elasto-plastic material. These characteristics can be determined from various deformation factors calculated for the two parts of the cross section (tensile reinforcement, compression zone of concrete).

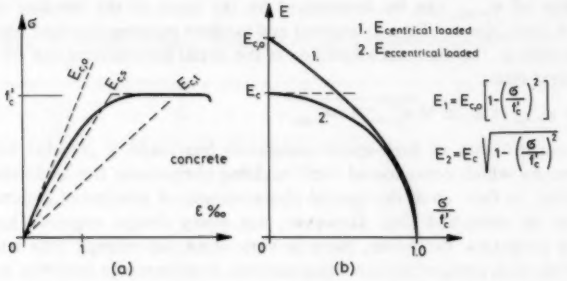

FIG. 1.—(*a*) Stress (Σ) – Strain (ϵ) Diagrammes of Concrete; (*b*) Change of Deformation Modulus of Concrete E_c Plotted against Stress Σ

As both the reinforcement and concrete are regarded as ideal elasto-plastic materials, the cracked reinforced concrete cross section also has a similar behavior. Actually, the start of yield in the cross section is influenced (besides the geometrical data) by the quantity of reinforcement as well. This is automatically taken into account, however, in the usual computation of the reinforced concrete cross section.

In summary, the reinforced concrete differs from the elastic homogeneous material in the following ways:

1. Viscous deformation (linear creep) of the concrete.
2. Plastic deformation (nonlinear creep) of the concrete.
3. Tensile cracks in the concrete (stiffness of the cross section drops off, and the reinforcement becomes of particular relevance).

Deformation Properties of Concrete

Modulus of Elasticity ($E_{c,o}$).—The modulus of elasticity, $E_{c,o}$, characterizes

instantaneous behavior, e.g. vibration. Its mean value can be obtained from the generally used formula:

$$E_{c,o} = 6{,}750\sqrt{f'_c}\ \mathrm{N/mm^2} \quad (6.9\ \mathrm{kN/m^2} \equiv 1\ \mathrm{psi}) \quad \ldots\ldots\ldots\ldots\ldots\ldots (4)$$

Here, f'_c denotes the specified compressive strength of the concrete, that can be assumed for 80% of the cube strength, thus:

$$f'_c = 0.80 f'_{c,\mathrm{cube}} \quad \ldots\ldots\ldots\ldots\ldots\ldots\ldots\ldots\ldots\ldots\ldots\ldots\ldots\ldots (5)$$

In practice, the deviation of the modulus of elasticity is taken into account by using a nominal strength value in Eq. 4. The nominal strength is a threshold value belonging to the desired quantile.

Viscous Deformation (Linear Creep).—The buckling deformation of a concrete shell depends on viscous deformations of the concrete as well. Although, viscous deformation does not alter the instantaneous modulus of elasticity, its effect (buckling deformation increases with time while load remains unchanged) can be taken into account by reducing the value of $E_{c,o}$ (see Refs. 9, 35).

The phenomenon of the linear creep is commonly described by the creep function, $\phi(t) = \epsilon_{\mathrm{creep}}(t)/\epsilon_{\mathrm{elastic}}$.

The asymptotical maximum of the creep function is the creep factor $\phi^{(t)}_{t\to\infty} = \phi_c$. Its value depends on the thickness of the structure, the quantity and quality of the cement applied, the water-cement ratio, and the surrounding of the concrete (6). For normal circumstances ϕ_c depends only on the type of concrete as follows:

$$\phi_c = 4 - 2\log_{10} f'_c \quad \ldots\ldots\ldots\ldots\ldots\ldots\ldots\ldots\ldots\ldots\ldots\ldots\ldots\ldots (6)$$

Values of ϕ_c for some cases are given in Table 2.

Modulus of Deformation E_c.—The critical load influenced by linear creep was determined exactly for some structures (9,18). The results obtained there, confirm that the approximate consideration of the creep effect, by using a reduced modulus of deformation, $E_{c,\ell}$, instead of its instantaneous value, $E_{c,o}$, (E_c is the average value of secant modulus) is always on the safe side.

This reduced modulus is generally computed as (6,9,35):

$$E_{c,\ell} = \frac{E_{c,o}}{1+\phi_c}. \quad \ldots\ldots\ldots\ldots\ldots\ldots\ldots\ldots\ldots\ldots\ldots\ldots\ldots\ldots (7)$$

If loads are applied on the structure only for a short while (i.e., a few hours), then only a part of the creep deformation develops (6).

By considering this part of the creep deformation together with the straightening of the $\Sigma(\epsilon)$ diagram, the modulus of deformation for short time loading, $E_{c,s}$, could be taken as the 70% of the elastic modulus, $E_{c,o}$:

$$E_{c,s} \approx 0.7 E_{c,o} = 4{,}730\sqrt{f'_c} \quad \mathrm{N/mm^2} \quad \ldots\ldots\ldots\ldots\ldots\ldots\ldots (8)$$

Later on in this paper, E_c will always denote the value of the modulus of deformation corresponding to the loading time. That is, $E_c = E_{c,\ell}$ for long time loading, $E_c = E_{c,s}$ for short time loading, and $E_c = E_{c,o}$ for instantaneous loading vibration.

Effect of Plasticity.—As is well known, the buckling of centrally compressed bars built of nonlinearly elastic or plastic material can be investigated by using

the theory I. of Engesser, substituting the nonlinear stress-strain diagram by its tangent at the point in question. Shells built of materials of plastic properties buckle in central compression similarly to straight bars (3). Thus, the theory I. of Engesser can also be applied for shells. In the stability analysis of centrally compressed structures, and for concretes of good quality used for shells, a formula for the elastic modulus E varying with the stress is available in the form (see Ref. 10):

$$E = E_{c,o}\left[1 - \left(\frac{\Sigma}{f'_c}\right)^2\right] \quad \ldots\ldots\ldots\ldots\ldots\ldots\ldots\ldots\ldots\ldots\ldots\ldots\ldots\ldots (9)$$

The value of E is depicted by the curve 1 in Fig. 1(*b*). For the computation of deformations due to eccentric loads, instead of the elastic modulus $E_{c,o}$,

TABLE 2.—Values of ϕ_c Creep Factor

f'_c, in Newtons per square millimeters (pounds per square inch) (1)	ϕ_c (2)
10 (0.69×10^3)	2.7
14 (0.97×10^3)	1.7
20 (1.38×10^3)	1.4
28 (1.93×10^3)	1.1
40 (2.76×10^3)	0.8

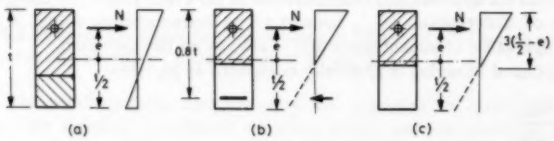

FIG. 2.—Stresses in Eccentrically Compressed Homogeneous, Concrete, and Reinforced Concrete Cross Sections

the modulus of deformation E_c is used. This value cuts off the parabolic line in the figure by a dotted line.

Since formulae must meet continuously in the limiting case, we introduce the ellipse:

$$E = E_c\sqrt{1 - \left(\frac{\Sigma}{f'_c}\right)^2} \quad \ldots\ldots\ldots\ldots\ldots\ldots\ldots\ldots\ldots\ldots\ldots\ldots\ldots\ldots (10)$$

approximating the preceding condition [line 2 in Fig. 1(*b*)]. In this formula Σ means the axial membrane stress in elastic buckling. Rewriting the formula for loads, we obtain:

$$\left(\frac{p_{cr}^{pl}}{p_{cr}^{sh,el}}\right)^2 + \left(\frac{p_{cr}^{pl}}{p_{pl}}\right)^2 = 1 \quad \ldots\ldots\ldots\ldots\ldots\ldots\ldots\ldots \quad (11a)$$

$$\text{or} \quad p_{cr}^{pl} = (p_{cr}^{sn,el}) \sqrt{\frac{1}{1 + \left(\frac{p_{cr}^{sn,el}}{p_{pl}}\right)^2}} = (p_{cr}^{sn,el})\,\zeta \quad \ldots\ldots\ldots\ldots \quad (11b)$$

in which p_{cr}^{pl} = critical load taking plastic features also into account; $p_{cr}^{sn,el}$ = snap-through critical load assuming linearly elastic material; and p_{pl} = the strength of the shell if buckling didn't occur. The same expressions were also obtained for shells of ideal elasto-plastic material. Thus, to compute p_{cr}^{pl}, the critical load based on elastic theory must first be obtained.

Stiffness Data for Concrete and Reinforced Concrete Cross Sections

Generally, the real dimensions of concrete and reinforced concrete structures differ from those planned values. A long series of measurements carried out in the Hungarian Institute of Building Research (25 and 33) pointed out that the thickness of plates and shells are, in an average, 1.05 times bigger and are, at worst, by 10 mm (0.4 in.) less than their planned values. In buckling, the average value of the thickness is the relevant, while the influence of the weakest cross sections is to be felt only at rupture. Thus, in the stability analysis of shells, similarly to that of other structures of reinforced concrete, cross-sectional properties may be taken into account with their planned dimensions.

The shell stiffness can be given according to the explanation given in Eq. 12:

$$K = \sqrt{BD} \quad \ldots\ldots\ldots\ldots\ldots\ldots\ldots\ldots\ldots\ldots\ldots\ldots\ldots\ldots \quad (12)$$

Here, B and D mean the flexural and extensional stiffness of the shell, respectively. These two stiffnesses preventing the buckling of shell, are combined in the shell stiffness K. For the homogene shell plate is $K = \sqrt{BD} = \sqrt{Et^3}\,(12\,(Et) = Et^2)\sqrt{12}$.

Stiffness data are computed on the basis of State II. of the reinforced concrete cross section, i.e., when the cross section is cracked but still behaves ideal elastically.

In cross sections of concrete and reinforced concrete, the flexural and extensional stiffness depend on the reinforcement and on the eccentricity of the axial compression force, because the cross section cracks more and more as the eccentricity increases.

Consider the cross sections, in Fig. 2. The upper one shows the stress diagram of an eccentrically compressed, uncracked cross section of linearly elastic concrete. In this case, the flexural and extensional stiffness, respectively, neglecting the contraction factor (Poisson's ratio), are:

$$B_{conc}^{uncr} = \frac{E_c\,t^3}{12} = E_c \times I_{conc}^{uncr} \quad \ldots\ldots\ldots\ldots\ldots\ldots\ldots\ldots \quad (13)$$

$$D_{conc}^{uncr} = E_c\,t = E_c \times A_{conc}^{uncr} \quad \ldots\ldots\ldots\ldots\ldots\ldots\ldots\ldots \quad (14)$$

in which I = the moment of inertia per unit width; and A = the area per unit width. Thus, the shell stiffness of the uncracked cross section of concrete is:

$$K_{\text{conc}}^{\text{uncr}} = \frac{E_c t^2}{\sqrt{12}} \quad \ldots \ldots \ldots

$$B = \frac{Et^3}{12}\,[1 + 3n\mu\,(1 - 2\eta)^2] \quad \ldots\ldots\ldots\

$$D^{\text{crack}}_{\text{reinf.conc}} = E_c \times A^{\text{crack}}_{\text{reinf.conc}} = Et(\xi + \lambda_{ts} n\mu) \quad \ldots\ldots\ldots\ldots\ldots\ldots \quad (24)$$

in which λ_{ts} = the factor of tension stiffening (see Appendix I). The stiffnesses, $B^{\text{crack}}_{\text{reinf.conc}}$ and $D^{\text{crack}}_{\text{reinf.conc}}$, differ from $B^{\text{uncr}}_{\text{reinf.conc}}$, and $D^{\text{uncr}}_{\text{reinf.conc}}$, respectively, because the stiffness due to the uncracked concrete in tension gets lost as the concrete cracks. Thus, the shell stiffness referring to large eccentricities can be computed as:

$$K^{\text{crack}}_{\text{reinf.conc}} = E_c \sqrt{A^{\text{crack}}_{\text{reinf.conc}} \times I^{\text{crack}}_{\text{reinf.conc}}} \quad \ldots\ldots\ldots\ldots\ldots\ldots\ldots\ldots \quad (25)$$

By applying the notations $x/h = \xi$, $A_s/bh = \mu$, and we restrict ourselves to the commonly used symmetrical reinforcement, the values of $I^{\text{crack}}_{\text{rein.conc}}$ and $A^{\text{crack}}_{\text{reinf.conc}}$ can be expressed with the use of the theory (13) of reinforced concrete. Substituting these into Eq. 25, $K^{\text{crack}}_{\text{reinf.conc}}$ for $e \to \infty$ (pure bending) can be obtained. This value may be used in the cases $e_o/t > 0{,}5$.

Introduce now the expression

$$K^{\text{crack}}_{\text{reinf.conc}} = \psi_\infty \times K^{\text{uncr}}_{\text{conc}} \quad \ldots\ldots\ldots\ldots\ldots\ldots\ldots\ldots\ldots\ldots \quad (26)$$

and let's express the value ψ_∞ from Eq. 26:

$$\psi_\infty = \sqrt{12(\lambda_{ts} n\mu + \xi)\left[\frac{\xi^3}{3} + \frac{\lambda_{ts} n\mu}{2}(1 + 2\xi^2 + 2\eta^2 - 2\xi - 2\eta)\right]} \quad \ldots\ldots \quad (27)$$

The relative height of the compression zone in pure bending is obtained from that condition, the statistical moment is to be zero. From this condition:

$$\xi = \lambda_{ts} n\mu \left(\sqrt{1 + \frac{1}{\lambda_{ts} n\mu}} - 1\right) \quad \ldots\ldots\ldots\ldots\ldots\ldots\ldots \quad (28)$$

The computed values of $\psi_{\infty,1}$ and $\psi_{\infty,2}$ referring to $\eta = 0.5$ and $\eta = 0.2$, respectively, are shown in Table 3, and also in Fig. 3.

Linear interpolation in the Table is allowed. Index "o" refers to the case $(e_o/t) = 0$, while index ∞ refers to the case $(e_o/t) > 0.5$. Indexes "1" and "2", however, refer to single mesh and double mesh of reinforcement, respectively.

If there is no reinforcement in the cross section, tension force disappears when the tension zone of the cross section cracks. Thus, bending moment can be balanced only by compression forces. For concrete cross sections, consequently, the resultant compression force must be inside the cross section. Due to shrinkage, cracks may also appear in concretes. Thus, for being on the safe side, the tension strength of the cross section is to be neglected even for the lower values of loads.

The compression area of a cross section of unit width is according to the lower drawing in Fig. 2(c):

$$A^{\text{crack}}_{\text{conc}} = 3\left(\frac{t}{2} - e\right) \quad \ldots\ldots\ldots\ldots\ldots\ldots\ldots\ldots\ldots \quad (29)$$

and the extension stiffness is:

$$D^{\text{crack}}_{\text{conc}} = E_c\left[3\left(\frac{t}{2} - e\right)\right] \quad \ldots\ldots\ldots\ldots\ldots\ldots\ldots\ldots\ldots \quad (30)$$

Here e denotes the eccentricity of the compressive force, related to the initial centroid of the cross section. During shell buckling, we assume $e = cw$, $c = 1.0$ for cylindrical shells, and $c = 0.5$ for doubly curved shells (approximately). The curvature due to deflections is to be generally computed as:

$$\mathrm{K} = \frac{M}{EI} \quad \ldots \ldots \ldots

continuous and dotted lines, in the upper part of Fig. 5, are obtained. The maximum values of these curves give the critical loads based on elastic theory belonging to the considered eccentricity, for reinforced concrete and concrete shells. It can be expressed as:

$$p_{crit}^{sn,el} = \rho_{hom} \times p_{crit}^{lin} \quad \ldots\ldots\ldots\

Consider, e.g., the critical load of an isotropic concrete shell (without tension strength) for which $w_{crit} = 2\,t$, and $p_{crit}^{low} = 0.25\,p_{crit}^{lin}$. The resulting curve computed by the aforementioned method can be seen in Fig. 6, drawn by the continuous line.

As cracks in concrete appear at discrete distances, the shell stiffness is somewhat greater than that of a shell without any tension strength. Considering these, the exact results obtained for a shell with no tension strength can be well approximated with the following formula:

$$\rho_{conc} = \left(1 - \frac{2\,e_o}{t}\right)^3 \quad \ldots\ldots\ldots\ldots\ldots\ldots\ldots\ldots\ldots\ldots\ldots\ldots \quad (36)$$

This is shown by the dotted line, in Fig. 6. Obviously, for $e_o/t > 0.5$, $\rho_{conc} = 0$.

At $e_o/t = 0.5$, the stiffness of the concrete cross section is zero. When dealing with stiffness characteristics of the reinforced concrete cross sections we mentioned that, the shell stiffness value of reinforced concrete cross sections, in case of $e_o/t > 0.5\,t$, can be calculated by multiplying that of the homogeneous shell by the factor ψ_∞. Thus

$$\rho_{reinf.conc}\left(\frac{e_o}{t} > 0.5\right) = \psi_\infty\,\rho_{hom} \quad \ldots\ldots\ldots\ldots\ldots\ldots\ldots\ldots\ldots\ldots \quad (37a)$$

For the cases in which $e_o/t \le 0.5$, the values of $\rho_{reinf.conc}$ are between those of ρ_{conc} and ρ_{hom}. On the base of more detailed investigations, the following expression can be written:

$$\rho_{reinf.conc}\left(\frac{e_o}{t} \le 0.5\right) = \psi_o \times \rho_{conc} + \psi_\infty(\rho_{hom} - \rho_{conc}) \quad \ldots\ldots\ldots\ldots\ldots \quad (37b)$$

Thus, finally, the snap-through critical load of an elastic reinforced concrete shell can be computed as follows:

$$p_{crit,reinf.conc}^{sn,el} = \rho_{reinf.conc} \times p_{crit,conc}^{lin} \quad \ldots\ldots\ldots\ldots\ldots\ldots\ldots\ldots\ldots\ldots \quad (38)$$

Supposing that $\psi_o \approx 1$, and introducing the quotient

$$\beta = \frac{\rho_{reinf.conc}(\psi_\infty)}{\rho_{reinf.conc}(\psi_\infty = 1)} \quad \ldots\ldots\ldots\ldots\ldots\ldots\ldots\ldots\ldots\ldots\ldots\ldots \quad (39)$$

we can compute the critical load for the axially compressed cylinder, also in the following manner:

$$p_{crit,reinf.conc}^{sn,el} = \beta \times p_{crit,hom}^{sn,el} \quad \ldots\ldots\ldots\ldots\ldots\ldots\ldots\ldots\ldots\ldots\ldots\ldots \quad (40)$$

Values of β are depicted in Fig. 7. With the use of these values of β, the snap-through critical load of reinforced concrete shells can also be well approximated when $p_{crit}^{low} \neq 0.25\,p_{crit}^{lin}$.

Snap-through Critical Load for Reinforced Concrete Shells of Plastic Behavior

Plastic behavior of reinforced concrete shells can be considered by using the factor given in Eq. 11. Thus, when we finally consider all the effects (i.e.,

cracks, reinforcement, creep, and plasticity) described in the foregoing, we arrive at the formula of the critical load as is given in the following equation:

$$p^{sn,pl}_{crit,reinf.conc} = \zeta\, p^{sn,el}_{crit,reinf.conc} \approx \zeta\beta\, p^{sn,el}_{crit,hom} \quad \ldots\ldots\ldots\ldots\ldots\ldots\ldots\ldots (41)$$

In the preceding formula, $p^{sn,pl}_{crit,reinf.conc}$ denotes the snap-through critical load of a reinforced concrete shell, plastic behavior included.

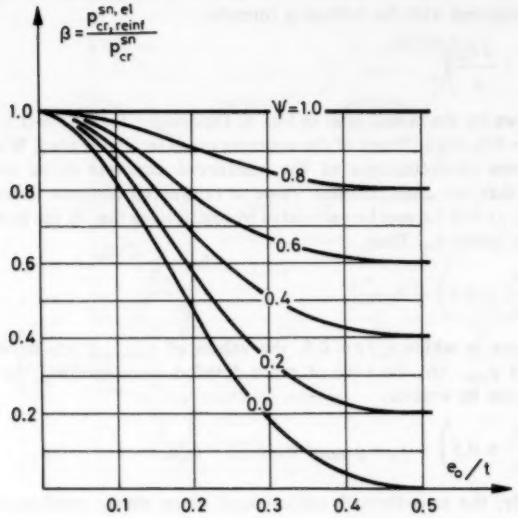

FIG. 7.—Values of β Plotted against ψ and e_o/t

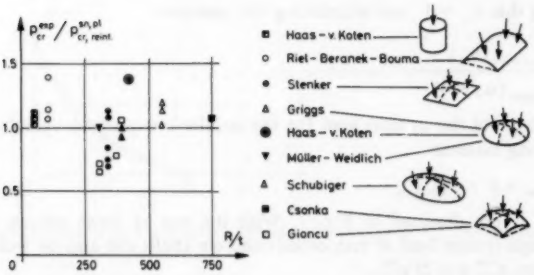

FIG. 8.—Values of Ratio $p^{experiment}_{cr}/p^{sn,pl}_{cr,reinf.}$ for Shell Models

In an earlier paper (11), we computed buckling loads for the experimental shells that had been published in Refs. 15, 17, 32, 31, 7, 16, 29, 14 and 27. We used Eq. 41 and made comparison between the results of our computation

and the experimental ones. These values plotted against R/t are seen, in Fig. 8. The mean of the quotients of the experimental and computed values is 1.02 while the standard deviation is 20%. This shows that our procedure presented here is fairly realistic.

Safety Factor

The procedure proposed in this paper gives a probable mean value for the buckling (failure) load. Uncertainties must be taken into consideration by applying a safety factor. According to the probability theory the safety factor can be expressed as follows:

$$k = \frac{k_o}{1 - \alpha S_r} \quad \ldots \ldots \ldots

For the cylinder and dome experiments investigated in Eq. 43, we found a deviation of 20%. As the number of cases investigated was rather low, we consider here a deviation of $1.1 \times 20 = 22\%$, instead. With common reinforced concrete constructions the deviations of the no-buckling failure loads is about 10%, thus we set $S_{pl} = 0.1$ and then S_{cr} can be expressed as $S_{crit} = \sqrt{(1.1 \times 0.2)^2 - 0.1^2} = 0.20$.

Finally, the resultant deviation is: $S_r \approx \sqrt{0.1^2(3)} = 0.25$. Thus, from Eq. 42 we obtain for imperfection-sensitive shells:

$$k \geq \frac{1.25}{1 - 2(0.25)} = 2.50 \quad \ldots\ldots\ldots\ldots\ldots\ldots\ldots\ldots\ldots\ldots \quad (44)$$

Consequently, the value of the safety factor must be $k = 2.5$ at least, and it should be greater if there are any more uncertainties.

We computed critical loads for several erected domes of great dimensions, and depicted these in Fig. 9. These data show that the use of safcty factors $2.5 < k < 3.5$ give fairly satisfactory results.

For structures with a constant post-buckling load-bearing capacity are $S_{cr} \approx 0.1$, $S_r = 0.17$, and $k \approx 1.90$. In the case of an increasing post-buckling load-bearing capacity are $S_{cr} = 0$, $S_r = 0.14$, and $k = 1.75$.

Numerical Example

Let's investigate Griggs (15) spherical dome models, made of concrete and rigidly built-in around their support. Griggs used the formula

$$p_{crit} = c\frac{\sqrt{3}}{2}\left(\frac{Et^2}{R^2}\right) \quad \ldots\ldots\ldots\ldots\ldots\ldots\ldots\ldots\ldots\ldots \quad (45)$$

to compute the critical load of his shell.

On plastic models just so formed as the aforementioned ones, experimental results $c = 0.57$ and $c = 0.63$ were obtained. It conforms to the theoretical results of (36). Data:

$$R = \frac{(84.0 \text{ in.})}{2{,}134 \text{ mm}};$$

$$t = \frac{(0.25 \text{ in.})}{6.4 \text{ mm}};$$

$$f'_c = \frac{(4.17 \times 10^3 \text{ psi})}{28.8 \times 10^3 \text{ kN/m}^2};$$

$$E_c = \frac{(3.16 \times 10^6 \text{ psi})}{21.7 \times 10^6 \text{ kN/m}^2};$$

$$\frac{w_{o,ran}}{t} = \frac{\frac{R}{3{,}500}}{t} = 0.117; \quad \frac{e_o}{t} = \frac{1}{2} w_{o,ran} = 0.059 \quad \ldots\ldots\ldots\ldots\ldots \quad (46)$$

From the bending theory:

$$e_{o,\text{calc}} = \frac{M_{\max}}{N} = \frac{p\dfrac{Rt}{30}}{p\dfrac{R}{2}} = 0.067\,t \quad \ldots\ldots\ldots\ldots\ldots\ldots\ldots\ldots \quad (47)$$

$$\text{Thus:} \quad \frac{e_o}{t} = \sqrt{\left(\frac{e_{o,\text{ran}}}{t}\right)^2 + \left(\frac{e_{o,\text{calc}}}{t}\right)^2} = \sqrt{0.059^2 + 0.067^2} = 0.089 \quad \ldots \quad (48)$$

As there was no reinforcement in the concrete

$$\psi_o = 1.0; \quad \psi_\infty = 0 \quad \ldots\ldots\ldots\ldots\ldots\ldots\ldots\ldots\ldots\ldots \quad (49)$$

$$\text{and from Eq. 35,} \quad \rho_{\text{conc}} = \left(1 - 2\frac{e_o}{t}\right)^3 = (1 - 2 \times 0.089)^3 = 0.55 \quad \ldots\ldots \quad (50)$$

$$p_{\text{crit}}^{\text{lin}} = \frac{\sqrt{3}}{2}\left(\frac{3.16 \times 10^6 \times 0.25^2}{84^2}\right) = 32.2 \text{ psi } (222 \text{ kN/m}^2) \quad \ldots\ldots\ldots \quad (51)$$

$$p_{\text{crit}}^{\text{sn,el}} = \rho_{\text{conc}} \times p_{\text{crit}}^{\text{lin}} = 0.55 \times 32.2 = 17.9 \text{ psi } (123 \text{ kN/m}^2) \quad \ldots\ldots\ldots \quad (52)$$

$$p_{\text{pl}} = 2\frac{t \cdot f_c'}{R}\left(1 - 2\frac{e_o}{t}\right) = \frac{2 \times 0.25 \times 4.17 \times 10^3}{84}(1 - 2 \times 0.089)$$

$$= 19.1 \text{ psi } (152 \text{ kN/m}^2) \quad \ldots\ldots\ldots\ldots\ldots\ldots\ldots\ldots\ldots \quad (53)$$

$$\zeta = \sqrt{\frac{1}{1 + \left(\dfrac{p_{\text{crit}}^{\text{sn,el}}}{p_{\text{pl}}}\right)^2}} = \sqrt{\frac{1}{1 + \left(\dfrac{17.9}{19.1}\right)^2}} = 0.73 \quad \ldots\ldots\ldots\ldots \quad (54)$$

$$\text{and} \quad c = \rho_{\text{conc}} \times \zeta = 0.5 \times 0.73 = 0.40 \quad \ldots\ldots\ldots\ldots\ldots\ldots \quad (55)$$

From failure of the two shell models, the results $c = 0.36$ and $c = 0.38$ were obtained.

Summary and Conclusions

The results of the nonlinear shell buckling theory has been extended to apply to the reinforced concrete shells. A simple relation is derived for the snap-through critical load of reinforced concrete shell. The solution contains the special properties of reinforced concrete, i.e., cracks, plasticity, creep, and quantity of reinforcement. The proposed method adequately describes the results and the situation of erected domes.

The main results of the research are the following:

1. The shell buckling stiffness was seen to be composed of two parts; the bending and the axial stiffness of the reinforced concrete cross section.
2. The critical load is reduced by the plasticity and the imperfections.
3. The critical load of the reinforced concrete shells decreases by the cracks of concrete and increases by the reinforcement.

APPENDIX I.—FURTHER EQUATIONS

The parameter, λ_{ts}, of tension stiffening.

The parameter λ_{ts} is computed as the ratio of the steel elongation, ϵ_s, to the mean elongation, ϵ_{sm}, of the reinforcement:

$$\lambda_{ts} = \frac{\epsilon_s}{\epsilon_{sm}} \quad \ldots \ldots \ldots

Appendix II.—References

1. Almorth, B. O., "Influence of Imperfections and Edge Restraint on the Buckling of Axially Compressed Cylinders," *NASA-CR-432*, Apr., 1966.
2. Árbócz, J., "The Effect of General Imperfections on the Buckling of Cylindrical Shells," *Journal of Applied Mechanics*, Vol. 30, 1969, pp. 28–38.
3. Batterman, Wt. C., "Plastic Stability of Spherical Shells," *Journal of the Engineering Mechanics Division*, ASCE, Vol. 95, No. EM2, Proc. Paper 6512, Apr. 1969, pp. 433–446.
4. Budiansky, B., and Amazigo, J. C., "Initial Postbuckling Behavior of Cylindrical Shells under External Pressure," *Journal of Mathematics and Physics*, Vol. 47, 1968, pp. 223–235.
5. Bushnell, D., "Nonlinear Axisymmetric Behaviour of Shells of Revolution," *AIAA Journal*, Vol. 5, 1967, pp. 432–439.
6. "CEB-FIP Model Code for Concrete Structures," 3rd ed., CEB-FIP International Recommendation, 1978.
7. Csonka, P., "The Buckling of a Spheroidal Shell Curved in Two Directions," *Acta Technica Academic Science (Hungary)*, Vol. 14, Budapest, Hungary, 1956, pp. 425–437.
8. Donnell, L. H., and Wan, C. C., "Effect of Imperfections on Buckling of Thin Cylinders and Columns under Axial Compression," *Journal of Applied Mechanics*, Vol. 17, 1950, pp. 73–83.
9. Dulácska, E., "The Influence of Creep on the Stability of Shells," *IASS Symposium, 1980*, Acta University, Oulu, Oulu, Finland, C 16, 1980, pp. 87–97.
10. Dulácska, E., "Praktische Stabilitätsuntersuchung von zentrisch gedrückten Tragwerken aus Material mit veränderlichen Elastizitätsmodul," *Bautechnik*, Vol. 10, W. Germany, 1972, pp. 340–345.
11. Dulácska, E., "Investigation of the Local Buckling of Concrete and Reinforced Concrete Shell Structures (in Hungarian), *Müszaki Tudomány*, Vol. 48, Budapest, Hungary, 1974, pp. 415–464.
12. Dulácska, E., "Der Steifigkeitskennwert der Schalenbeulung," *Acta Technica Academic Science (Hungary)*, Vol. 87, Budapest, Hungary, 1978, pp. 457–467.
13. Dunham, C. W., *The Theory and Practice of Reinforced Concrete*, McGraw-Hill Publishing Co., Inc., New York, N.Y., 1966.
14. Gioncu, V., "Cercetari experimentale privind stabilitatea dupelelor pe contur patrat," *St. Cerc. Mec. Apl.*, Vol. 32, No. 3, 1973, pp. 641–651.
15. Griggs, H., "Buckling of Reinforced Concrete Shells," *Journal of the Engineering Mechanics Division*, ASCE, Vol. 97, No. EM3, Proc. Paper 8173, June, 1971, pp. 687–700.
16. Haas, A. M., and Van Koten, H., "On the Buckling Behavior of Doubly Curved Shells," *RILEM Symposium*, Buenos Aires, Argentina, 1971.
17. Haas, A. M., and Von Koten, H., "The Stability of Doubly Curved Thin Shells," *RILEM Symposium*, Buenos Aires, Argentina, 1971.
18. Huang, N. C., "Nonlinear Creep Buckling of Some Simple Structures," *Report IRPA-66-80*, University of California, San Diego, California, 1960.
19. Hutchinson, J. W., "Imperfection Sensitivity of Externally Pressurized Spherical Shells," *Journal of Applied Mechanics*, Vol. 34, 1967, pp. 49–55.
20. Kármán, Th., Tsien, H. S., "The Buckling of Spherical Shells by External Pressure," *Journal of Aeronautical Sciences*, Vol. 7, 1939, p. 43.
21. Koga, T., and Hoff, N. J., "The Axisymmetric Buckling of Initially Imperfect Complete Spherical Shells," *International Journal of Solids and Structures*, Vol. 5, 1969, pp. 679–697.
22. Koiter, W. T., "The Effect of Axisymmetric Imperfections on the Buckling of Cylindrical Shells under Axial Compression," *Proceedings Royal Netherlands Academy of Sciences*, Amsterdam, The Netherlands, Series B. 66, 1963, pp. 265–279.
23. Koiter, W. T., "The Nonlinear Buckling Problem of a Complete Spherical Shell under Uniform External Pressure," *Proceedings of the Acad. Netherland*, Series B, Vol. 72, 1969, pp. 40–123.
24. Kollár, L., "Remarks on the Safety Factor against Shell Buckling and on the Influence of Creep on the Critical Load," *IASS-Symposium on Pipes and Tanks*, Weimar, W. Germany, 1968.

25. Korda, J., and Móna, J., "Dimensional defects measured at erected reinforced concrete structures," Report of *Épitöipari Miuöseguizsgàlà Intèzet*, (in Hungarian), *Buildings Quality Control Institute*, Budapest, Hungary, 1969.
26. Lin, Ch-Sh., and Scordelis, A. C., "Nonlinear Analysis of RC Shells of General Form," *Journal of the Structural Division*, ASCE, Vol. 101, No. ST3, Proc. Paper 11164, Mar., 1975, pp. 523–538.
27. Müller, F. P., and Weidlich, C., "An Experimental Investigation of the Stability of Shallow Spherical Shells of RC Subjected to Uniformly Distributed Load," *Nonlinear Behaviour of RC, Proceedings if IASS Symposium Spatial Structures*, Vol. 99, 1978, Darmstadt, W. Germany, Werner Verlag, W. Germany, Düsseldorf, W. Germany, 1978, pp. 319–328.
28. Madsen, W. A., and Hoff, N. J., "The Snap—through and Postbuckling Equilibrium Behaviour of Circular Cylindrical Shells under Axial Load," *Report No. 227*, Stanford University Department of Aeronautics and Astronautics, Stanford, Calif., 1965.
29. Riel, A. C., Beranek, W. J., and Bouma, A. L., "Tests on Shell Roof Models of Reinforced Mortar," *Proceedings of the Second Symposium on Concrete Shell Roof Construction*, Teknis Ukeblad, Oslo, Norway, July, 1957.
30. Ros, M., "Die materialtechnischen Grundlagen und Probleme des Eisenbeton im Hinblick auf die zukünftige Gestaltung der Stahlbeton-Bauweise," *EMPA-Bericht*, Nr. 162, 1950.
31. Schubiger, E., "Die Schalenkuppeln im Vorgespannten Beton der Kirche Felix und Regula in Zürich," *Schweitzerische Bauzeitung*, Vol. 68, Zurich, Switzerland, 1950, pp. 223–228.
32. Stenker, H., "Gesamtbericht von Gro versuchen an doppelt gekrümmten Montageschalen für raumabschlie endre Geschossdecken," *Wissenschaftliche Zeitschrift Hochschule für Architektur und Bauwesen*, Weimar, W. Germany, Vol. 2, 1961, pp. 181–202.
33. Szepesszentgyörgyi, O., Scientific report on the theme of International Standard Organization referring to steady load, worked out in the Intitute *Épitöipari Miuöseguizgàlà Intèzet*, (in Hungarian), *Buildings Quality Control Institute*, Budapest, Hungary, 1966.
34. Thompson, J. M. T., "The Elastic Instability of a Complete Spherical Shell," *Aeronautical Quarterly*, Vol. 13, 1962, pp. 189–201.
35. Vandepitte, D., Rathé, J., and Weymeis, G., "Experimental Investigation into the Buckling and Creep Buckling of Shallow Spherical Caps Subjected to Uniform Radial Pressure," *Proceedings, International Association of Shell Structures World Congress*, Vol. 1, Madrid, Spain, 1979, 1.1–1.15.
36. Weintschke, H. J., "On Asymmetric Buckling of Shallow Shells," *Journal of Mathematics and Physics*, Cambridge, England, Vol. 44, London, England, 1965, pp. 141–163.
37. Wolmir, A. S., "Biegsame Platten und Schalen," *Verlag für Bauwesen*, Berlin, W. Germany, 1962.

Appendix III.—Notation

The following symbols are used in this paper:

B = bending stiffness;
D = tensile stiffness;
E = elastic modulus;
$E_{c,o}$ = elastic modulus for concrete, at start of loading;
$E_{c,s}; E_{c,\ell}$ = moduli of deformation belonging to short time loading and long time loading, resp.;
f'_c = compressive strength of concrete;
$f'_{c,\text{cube}}$ = compressive strength of concrete cube;
$K = \sqrt{BD}$ = shell buckling stiffness;
$l_x; l_y$ = length of buckling waves in x and y directions;
$n = E_s / E_c$ = ratio of the moduli of steel and concrete;

$N^{lin}_{crit}; p^{lin}_{crit}$ = critical compression force and load of shell based on linear theory, or bifurcation load;

$N^{low}_{crit}; p^{low}_{crit}$ = lower critical force and load of geometrically perfect shell computed by nonlinear theory (with large deflections);

$N^{sn}_{crit}; p^{sn}_{crit}$ = snap-through critical force and load of the imperfect shell, v.e. maximal carrying capacity computed by nonlinear theory;

$p^{sn,el}_{crit,reinf.conc}$ = snap-through critical load of reinforced concrete or concrete shell of linearly elastic behavior;

$p^{sn,pl}_{crit,reinf.conc}$ = snap-through critical load of reinforced concrete or concrete shell of elasto-plastic behavior;

p_{pl} = load intensity at which stresses in shell reaches the strength of material (without buckling);

R = shell radius;

t = shell thickness;

w = maximum amplitude of buckling deflection;

w_o = maximum amplitude of initial deformation;

$w_{o,ran}; w_{o,calc}$ = random and calculated parts of deformation;

x, y = coordinate axes; referring to direction of axis when used in index;

$\psi_o; \psi_\infty$ = factors used in the computation of shell (index 1 and 2 refer to the number of meshes of reinforcement);

ϕ_c = creep factor;

λ_{ts} = factor of tension-stiffening;

μ = ratio of cross sections of steel and concrete; and

$\rho_{reinf.conc}; \beta$ = factors used in computation of snap-through critical load of elastic reinforced concrete shells.

SHEAR REINFORCEMENT FOR CONCRETE SLABS[a]

By Walter H. Dilger[1] and Amin Ghali,[2] Members, ASCE

INTRODUCTION

Concrete flat plates are subjected to large bending moment and shearing force at their connections with columns. Their combined effect can cause failure by punching of the slab.

In flexure, reinforced concrete slabs exhibit a great deal of ductility; extensive deformations occur before their ultimate strength is reached. Design codes place increasing reliance on this ductile behavior which enables slab systems to redistribute moments. Complete redistribution of bending moments can generally be achieved in a slab system prior to failure provided that shear failure is prevented. It is, therefore, important that in design, when considering punching, attention be given to both strength and ductility.

Perhaps the greatest source of problems for slabs in practice, apart from excessive deflection, is shear. The so-called punching shear failure of slabs without shear reinforcement occurs suddenly without warning so that, normally, no remedial measures can be applied prior to failure. Several such failures have been reported in the literature (9,6).

The development of the concrete design codes in North America in the last two decades and the extensive use of prestressed concrete in slab construction have resulted in the design of thinner and thinner slabs. Particularly if we use prestressed concrete, we can eliminate problems related to deflections which may govern the design of reinforced slabs and, therefore, the main criterion for the design is "punching shear." In addition, the architects may require openings for ducts in the vicinity of the columns which may substantially weaken the punching shear resistance of the slab around the column.

If the design of a slab is found adequate for flexure, but not for punching shear, and an increase of the depth or use of higher concrete strength in the whole slab are not desired, three possibilities exist to increase the shear strength: (1) Increase the slab thickness in the vicinity of the column (provide a drop

[a]Presented at the April 14–18, 1980, ASCE Convention and Exposition, held at Portland, Oreg. (Preprint).

[1,2]Prof. of Civ. Engrg., The Univ. of Calgary, Calgary, Alberta, Canada, T2N 1N4.

Note.—Discussion open until May 1, 1982. To extend the closing date one month, a written request must be filed with the Manager of Technical and Professional Publications, ASCE. Manuscript was submitted for review for possible publication on June 24, 1980. This paper is part of the Journal of the Structural Division, Proceedings of the American Society of Civil Engineers, ©ASCE, Vol. 107, No. ST12, December, 1981. ISSN 0044-8001/81/0012-2403/$01.00.

panel); (2) if this is not enough, flare the top of the column (i.e., use a column capital); and (3) provide shear reinforcement.

In many cases drop panels and column capitals are unacceptable. For example, in apartment buildings where the bottom surface of the concrete slab is the ceiling of the rooms, a drop panel would be unfitting for esthetic reasons. Column capitals are also not suitable for many types of buildings. In addition, they complicate the formwork and the construction process. In recent years, the so-called "flying forms" have been introduced which employ formwork panels of approximately the same size as the floor panels and are moved in their entirety from one floor to the next. If these large panel forms cannot be used for constructing the slab or if they have to be modified to accommodate drop panels, a substantial increase in cost results. This leaves only the shear reinforcement as a possible alternative for many structures.

Different Types of Shear Reinforcement

There have been many attempts to develop effective shear reinforcement for slabs. It was, however, recognized that shear reinforcement for slabs creates special problems because of the relatively small slab thickness. Many different types of shear reinforcement have been investigated, most of which are summarized in an excellent paper by Hawkins (8), who gives a comprehensive list of references. The different types may be grouped into four different categories: (1) Bent-up bars; (2) stirrups (closed and U-shaped); (3) shearhead cages; and (4) shearheads.

The first type of shear reinforcement was first investigated by Graf, and later by Elstner and Hognestad, Franz, Anderson, Rosenthal and Yitzhaki. Closed and open stirrups were tested by Franz, Wantur, Carpenter, Keefe and Narasinham. Shearhead cages were used by Moe, Anderson and Leonhardt. Shearheads consisting of structural steel plates or structural steel sections, or both, were investigated by Tasker and Wyatt, Corley, and Hawkins. A few typical examples are shown in Figs. 1 to 4 (exstensive lists of references are given in 8 and 9).

In many of these tests it is found that the shear reinforcement consisting of bars is not fully effective, which means that it does not reach the yield strength at failure. The reason is that the anchorage of the bent bars or stirrup is not sufficient to develop the full capacity of the bars. In case of bent-up bars, the tensile force in the inclined leg is associated at the bends with compressive stresses higher than the concrete strength and with a pull-out effect of the horizontal portion of the bar. This leads to an increase in width of the shear crack, which when extending to the compression zone results in the destruction of the concrete shear compression resistance before the shear reinforcement reaches its yield capacity. Similar observations have been made on stirrups. A 90° bend at the end of a vertical stirrup generates high concrete compressive stresses under the bend and also a certain pull-out effect of the horizontal leg under high stress in the vertical leg. A vertical slip of more than 0.04 in. (1.0 mm) has been measured in beam shear tests. In beams, this is normally not critical, but in thin slabs the slip explains why it is difficult or, perhaps, impossible to develop the yield strength of the stirrups. The need for special care for anchorage details for shear reinforcement in slabs has been emphasized by many researchers.

Anchorage slip in shear reinforcement made up of welded wire fabric was measured by Seible, et al. (12). To monitor the vertical movement of the shear reinforcement, small studs were tack welded to the bars and their vertical movement relative to the surrounding concrete was measured by means of dial gages. A typical set of results is shown in Fig. 5. In order to reduce this pull-out effect, Leonhardt (11) proposed that the vertical bars be welded to rings of

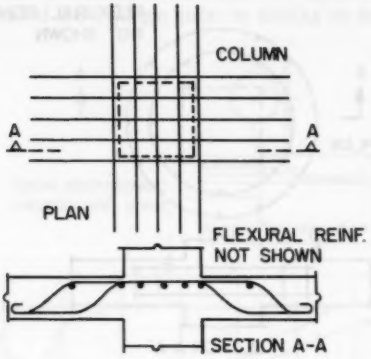

FIG. 1.—Bent-Up Bars

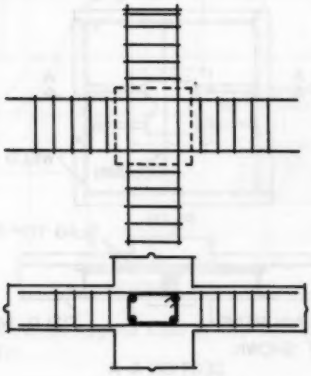

FIG. 2.—Stirrups

round bars as shown in Fig. 3. But to thread all the flexural steel through one or more such rings is a difficult task at the construction site.

In order to make normal stirrups reasonably effective, they have to enclose the top and bottom flexural reinforcement. For this reason, the installation of these stirrups in situ is a time-consuming job and in thin slabs with 6–8 in. (150–200 mm) thickness it is virtually impossible.

In view of the aforementioned difficulties, another type of shear reinforcement was developed in the late sixties: The so-called shear head which resulted from the research of Corley and Hawkins (4) and is not part of the design codes in North America. In Europe, a closely related development is the Geilinger collar, shown in Fig. 4. It consists of steel channel sections forming a rectangle somewhat larger than the column size and the load is transferred from the

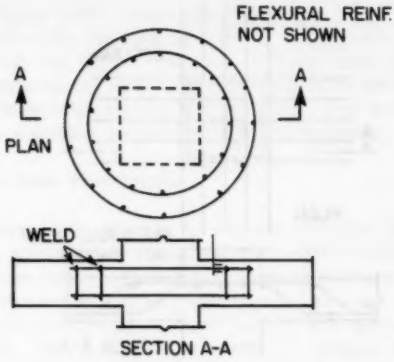

FIG. 3.—Vertical Bars Welded to Horizontal Rings

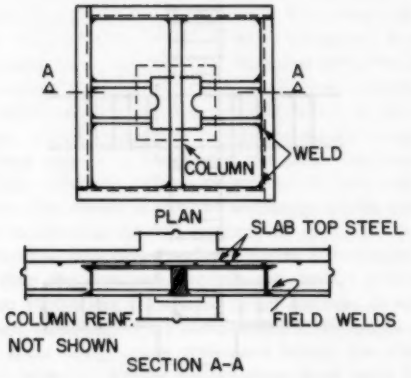

FIG. 4.—Geilinger Collar

slab to the collar and from there to the column by heavy steel plates welded to the channels. Because the bearing stress under these plates would be excessive an additional horizontal steel plate is required underneath.

The shear head and the Geilinger collar have drawbacks: First, they are rather expensive. Second, they may interfere with the reinforcement of the column and may be difficult to place. Third, the depth of the structural steel sections

must be substantially smaller than the slab thickness as there are usually two layers of reinforcing bars to be placed above and below the structural steel sections. When the concrete cover is 3/4 in. (19 mm) and the reinforcing bar diameter is 5/8 in. (16 mm), the height available to accommodate the structural steel sections is equal to $t - 4$ in. ($= t - 102$ mm), in which t = the slab thickness. In relatively thin slabs, the available height is not sufficient for the required structural steel section and shear heads cannot be used. This difficulty may be avoided in the case of the Geilinger collar by making its depth approximately

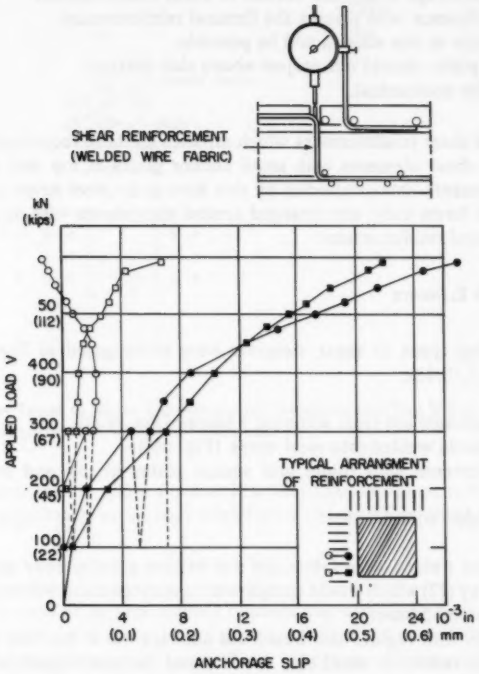

FIG. 5.—Anchorage Slip Versus Applied Load at Top Bent of Shear Reinforcement [Welded Wire Fabric (13)]

equal to the slab thickness and butt-welding to it the flexural reinforcement interrupted by the collar.

Another technique to increase the shear strength of reinforced concrete flat plates is by prestressing the zone around the column by means of high-tensile bolts passing through vertical holes in the slab tightened manually and anchored to steel plates at the top and bottom faces of the slab. This method was used in practice to strengthen existing slabs which showed some sign of shear distress. Ghali, et al. (7) demonstrated experimentally that substantial increase in punching

shear strength can be achieved by this technique. However, in a normal case, it may not be architecturally acceptable to have the anchor plates and nuts protruding outside the slab thickness. Also, application of the prestress adds to the labor cost.

The difficulties considered in context with the different types of shear reinforcements lead to the following requirements for shear reinforcement in flat plates:

1. Good anchorage at top and bottom of shear reinforcement.
2. No interference with placing the flexural reinforcement.
3. Installation in thin slab should be possible.
4. Anchor plates should not project above slab surface.
5. It must be economical.

The type of shear reinforcement which satisfies all these requirements consists of individual shear elements with small anchor plates at top and bottom. The individual elements, interconnected by thin bars or by steel strips to make their placing in the forms easy, are arranged around the column with no interference with the flexural reinforcement.

Types of Shear Elements

The following types of shear elements were investigated at The University of Calgary (1,5,10,12):

1. Short segments cut from standard I beams [Fig. 6(*a*)].
2. Nelson studs welded into steel strips [Fig. 6(*b*)].
3. Shear elements with round and square plates at top and bottom [Fig. 6(*c*)].
4. Bent welded wire fabric.

Of these, the welded wire fabric did not behave satisfactorily unless placed in a specific way (12) which would complicate construction and will not, therefore, be further examined here.

Nelson studs with regular size heads did not turn out to be fully satisfactory because of the relatively small size heads (head diameter equal twice the bar diameter). Anchorage slip was observed and only a fraction of the yield strength of the studs would develop. This result was not surprising considering the extremely high bearing stresses that develop underneath the anchor heads under these conditions.

Excellent results were obtained with shear elements (experiments are presently underway at the University of Calgary to determine the minimum required size of the anchor head) for which the anchor head had a bearing area 9 or 10 times the stem area, for yield strength of the stem = 43 ksi (450 MPa) and concrete strength = 5,600 ksi (39 MPa).

The segments cut from standard I-beams are also well suited for the purpose because the thickness of the flange increases towards the stem. However, from a production point of view there seems to be no inexpensive way to cut relatively

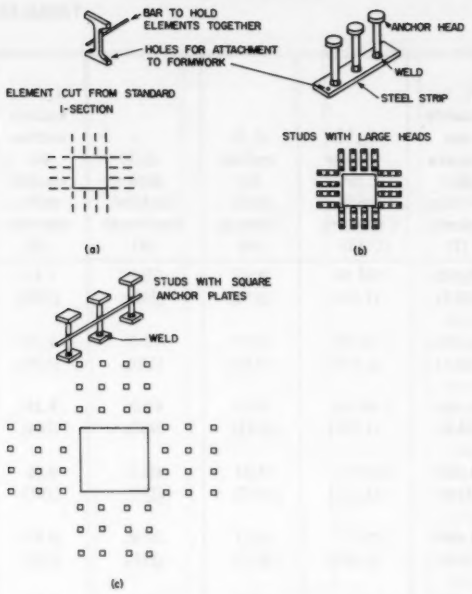

FIG. 6.—New Types of Shear Reinforcement Elements and Top Views Showing their Possible Arrangement in Vicinity of Columns

small segments from a rolled I-beam. Practical solutions seem to be Nelson-type studs with large heads or vertical steel bars with square or round anchor plates.

Tests

To date, a total of 40 slab column connections with new shear reinforcement have been tested. Of these tests, six were subjected to unbalanced bending and axial forces; these size tests will not be reviewed here as the results are not fully conclusive. All other test specimens were subjected to axial force only. The flexural reinforcement ratio was approx 1.1% and the design concrete strength was 4,000 psi (28 MPa).

Most of the test specimens had a 6-ft (1.83-m) square slab, 6 in. (153 mm) thick, and a 12-in. (305-mm) square column. Four slabs had rectangular columns 8×24 in.^{2} (203×610 mm^2) and 11 slabs had a 9.8-in. (250-mm) square column; the latter size was chosen in order to reach higher shear stresses.

Perhaps the most important conclusions of these tests are that, with the good anchorage provided by the anchor plates, the full yield strength of the new types of shear reinforcement can be reached, and that only the shear in excess of $4\sqrt{f'_c}$ (psi) ($\simeq 0.33\sqrt{f'_c}$ (MPa)) needs to be resisted by shear reinforcement. To back up these conclusions, a few characteristic results are listed in Table

TABLE 1.—Summary of

Test (1)	f'_c, in pounds per square inch (in mega-pascals) (2)	b_o,[a] in inches (in milli-meters) (3)	d, in inches (in milli-meters) (4)	V_c,[b] kips (in kilo-newtons) (5)	A_v,[c] in square inches (in square milli-meters) (6)	f_y, in kips per square inch (in mega-pascals) (7)
SC3 (1)	4,400 (30.3)	65.96 (1,676)	4.49 (114)	78.9 (351)	1.11 (719)	42.5 (293)
SC3 (1)	4,510 (31.1)	65.96 (1,676)	4.49 (114)	79.8 (355)	1.30 (838)	42.5 (293)
SC7 (12)	5,110 (35.2)	67.00 (1,702)	4.75 (121)	91.0 (405)	1.15 (744)	50.4 (345)
MV6 (14)	4,210 (29.0)	57.2 (1,452)	4.45 (113)	66.1 (294)	0.46 (298)	47.2 (325)
PSI	4,680 (32.3)	57.5 (1,460)	4.53 (115)	70.8 (315)	0.92 (594)	50.8 (350)
PS2	4,900 (33.8)	57.5 (1,400)	4.53 (115)	72.4 (322)	0.92 (594)	43.5 (300)

[a] b_o = perimeter of a critical section at $d/2$ from column face.
[b] $V_c = b_o d\, 0.33 \sqrt{f'_c\,(\text{MPa})} = [b_o d\, 4 \sqrt{f'_c\,(\text{psi})}]$.
[c] A_v = cross section area of shear reinforcement elements on the first row at $d/2$

1. In this table the yield capacity of the shear elements located within a distance d from the face of the column is added to the shear capacity of concrete, $V_c = 4\sqrt{f'_c}\,(\text{psi})\, b_o d \simeq 0.33 \sqrt{f'_c}\,(\text{MPa})\, b_o d$ and compared with the experimental ultimate load $V_{u\,\text{test}}$ (d = the effective depth, b_o = the perimeter of a critical section at a distance $d/2$ from column faces). Only those tests in which the shear elements within a distance d have reached yield are listed. The American Concrete Institute (ACI) Code 318-1977 (2) and the Canadian Code CAN A23.3-M77 (3), require that the shear reinforcement carries the shear stress in excess of $2\sqrt{f'_c}\,(\text{psi})$ $(0.17\sqrt{f'_c}\,(\text{MPa}))$ and that the total ultimate nominal shear stress by the concrete and steel does not exceed $6\sqrt{f'_c}\,(\text{psi})$ $(0.5\sqrt{f'_c}\,(\text{MPa}))$.

In the graphs Fig. 7(*a*) and (*b*), the applied load V is partitioned into $V_{s\,\text{test}}$ and $V_{c\,\text{test}}$ resisted by shear reinforcement and concrete, respectively. The part $V_{s\,\text{test}}$ (ordinate below the curve) is the tensile force measured in the shear reinforcement located within distance d from the face of the column. The part of shear resisted by concrete is equal to $V_{c\,\text{test}} = V - V_{s\,\text{test}}$. The fact that the concrete maintains its capacity to resist a shear stress of $v_c = 4\sqrt{f'_c}\,(\text{psi})$

Test Data and Results

$V_s = A_v f_y$, in kips (in kilonewtons) (8)	$v_s + v_c$, in kips (in kilonewtons) (9)	v_u test, in kips (in kilonewtons) (10)	$\frac{v_{u\,\text{test}}}{b_o d \sqrt{f'_c}}$ (11)	$\frac{V_{u\,\text{test}}}{V_s + V_c}$ (12)	Description of shear reinforcement (13)
47.2 (210)	126.1 (561)	142.1 (632)	7.2 (0.59)	1.13	I-segments cut from standard I-beam [Fig. 6(*b*)]
55.2 (245)	135.0 (600)	141.6 (630)	7.1 (0.59)	1.05	I-segments cut from standard I-beams [Fig. 6(*b*)]
57.9 (257)	148.9 (662)	140.0 (623)	6.2 (0.51)	0.94	I-segments cut from standard I-beam [Fig. 6(*b*)]
21.8 (97)	87.9 (391)	112.9 (502)	6.8 (0.56)	1.28	Bars with square anchor plates [Fig. 6(*c*)]
46.7 (208)	117.5 (522)	130.4 (580)	7.4 (0.61)	1.11	Bars with square anchor plates [Fig. 6(*c*)]
40.0 (178)	112.4 (500)	127.0 (565)	7.0 (0.58)	1.13	Bars with square anchor plates [Fig. 6(*c*)]

from column face (spacing between rows = $s = d$).

$= 0.33 \sqrt{f'_c\,(\text{MPa})}$ in combination with effectively anchored shear reinforced is here evident by noting that at ultimate, the ordinate $V_{s\,\text{test}}$ is smaller than the value ($V - 4\sqrt{f'_c\,(\text{psi})}\, b_o d$), represented by line AB in Fig. 7(*a*) and (*b*).

The current codes (2,3) assume for calculation of the cross section area of shear reinforcement that the concrete can resist shear $V_c = 2\sqrt{f'_c\,(\text{psi})}\, b_o d$ ($0.17\sqrt{f'_c\,(\text{MPa})}\, b_o d$). Although the test results represented in Fig. 7(*a*) and (*b*) indicate that at ultimate the concrete resists shear stress equal to or larger than $4\sqrt{f'_c\,(\text{psi})}$, in the sections to follow a more conservative value is suggested for the design of shear reinforcement (Eq. 3 or Eq. 4).

Of the tests listed in Table 1, MV6 is particularly interesting in that all three rows of shear elements have yielded before the ultimate load is reached. The stress in the shear elements is indicated in Fig. 8 at three stages of loading for the slab reinforced by shear elements with square anchor plates. It should be emphasized, however, that this test is perhaps somewhat extreme with regard to its rather fine distribution of shear elements, but nonetheless it demonstrated that well distributed and well anchored shear elements generate a ductile type

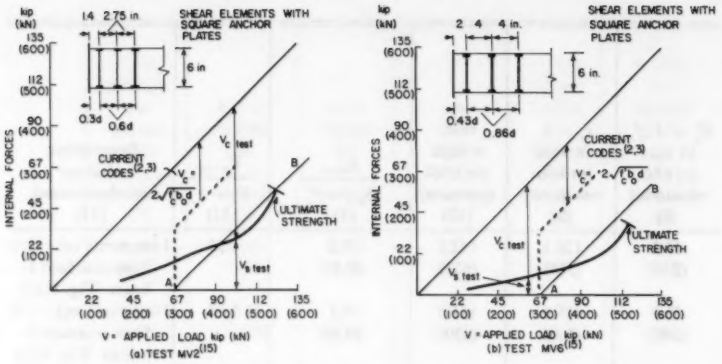

FIG. 7.—Partitioning of External Applied Force V into Internal Forces $V_{s\,test}$ and $V_{c\,test}$ Resisted by Shear Reinforcement and Concrete

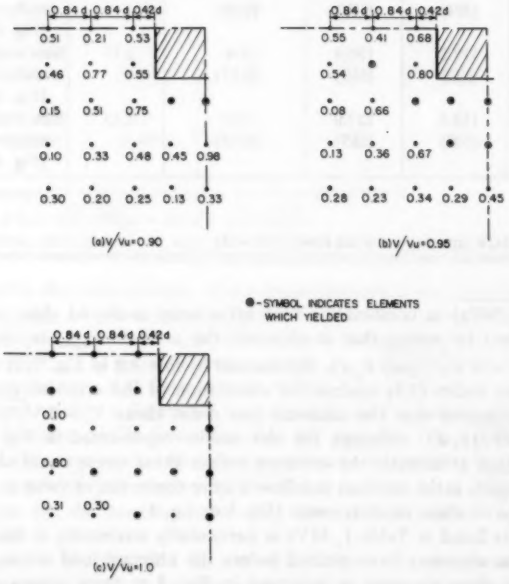

FIG. 8.—Quarter Top Views of Test Slab Indicating Stresses in Shear Reinforcement Elements as Fractions of Yield Stress at Load Levels: 90%, 95% and 100% of Ultimate [Test MV-6 (15)]

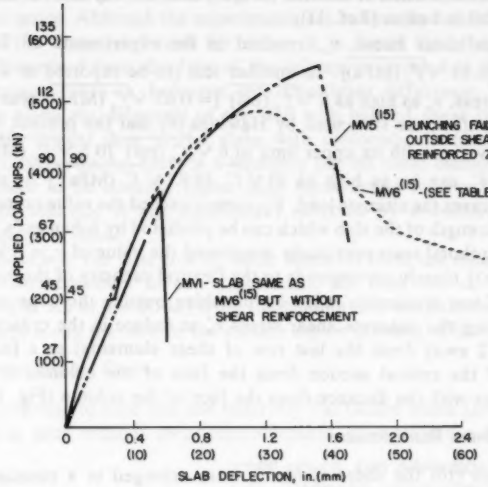

FIG. 9.—Load Versus Deflection

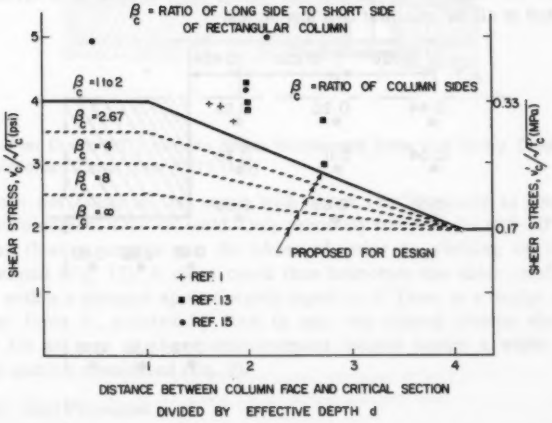
β_c = RATIO OF LONG SIDE TO SHORT SIDE OF RECTANGULAR COLUMN
β_c = RATIO OF COLUMN SIDES
β_c = 1 to 2
β_c = 2.67
β_c = 4
β_c = 8
β_c = ∞
0.33
0.17
PROPOSED FOR DESIGN
+ REF. 1
■ REF. 13
• REF. 15
SHEAR STRESS, $v_c/\sqrt{f'_c}$ (psi)
SHEAR STRESS, $v_c/\sqrt{f'_c}$ (MPa)
DISTANCE BETWEEN COLUMN FACE AND CRITICAL SECTION DIVIDED BY EFFECTIVE DEPTH d

FIG. 10.—Experimental and Proposed Design Values for Nominal Shear Stress that can be Resisted by Concrete at Critical Section outside Shear Reinforced Zone

of shear failure. Fig. 9 indicates that even after exceeding the ultimate load, the connection is still capable of transferring load. This experiment also indicates that there is a redistribution of internal forces which corresponds to the variable angle truss model in beams (Ref. 11).

The maximum shear stress, v_n, reached in the experiments of Table 1 is $7.2\sqrt{f'_c}$ (psi) [$0.59\sqrt{f'_c}$ (MPa)]. In another test (to be reported in a separate paper), shear stress, v_n as high as $8\sqrt{f'_c}$ (psi) [$\simeq 0.67\sqrt{f'_c}$ (MPa)] was reached. These results confirm the statement by Hawkins (6) that the present ACI code is rather conservative with its upper limit of $6\sqrt{f'_c}$ (psi) [$0.5\sqrt{f'_c}$ (MPa)] and he shows that V_n can be as high as $10\sqrt{f'_c}$ [$0.83\sqrt{f'_c}$ (MPa)]. It should be noted that in all cases the ultimate load, V_n, cannot exceed the value corresponding to the flexural strength of the slab which can be predicted by Johansen's yield-line theory. In the authors' tests previously mentioned the value of $v_n = 8\sqrt{f'_c}$ (psi) [$0.67\sqrt{f'_c}$ (MPa)] closely corresponds to the flexural capacity of the specimens.

A number of test specimens failed by punching outside the zone reinforced for shear. Plotting the concrete shear stress v'_c at failure in the critical section (at distance $d/2$ away from the last row of shear elements) as a function of the distance of the critical section from the face of the column, it is found that v'_c decreases with the distance from the face of the column (Fig. 10).

Distribution of Shear Reinforcement

In earlier tests (10) the shear elements were arranged in a circular pattern around the column. It is found, however, that this is not the ideal arrangement because of some interference with the flexural steel. Placing the shear element parallel to the faces of the column is more practical, and such arrangements are adopted in all but our first two test series.

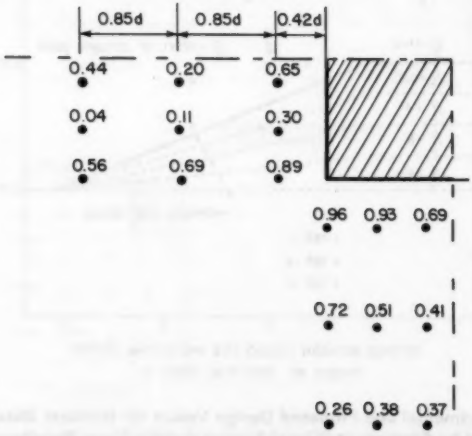

FIG. 11.—Quarter Top View of Test Slab Indicating Stresses in Shear Reinforcing Elements as Fractions of Yield Stress. Shear Reinforcement Arranged in Bands Facing Column. Load Level: 96% of Ultimate

The question, whether a concentration of the shear reinforcement in bands facing the column sides (Fig. 6) or uniform distribution in rows covering the entire area around the column (Fig. 8) is more effective, is dealt with in a recent test series. Although the experiments are not totally conclusive the failure is outside the zone reinforced for shear, it is found that the reinforcement within a distance d from the face of the column is stressed to the same extent in both cases. There is, however, one significant difference: The transverse expansion along the diagonals of the slab with banded shear reinforcement is substantially higher than in the slabs with uniformly distributed shear reinforcement. Accordingly, there is a tendency for the shear elements at the edges of each band to be stressed higher than those inside the band (Fig. 11). But the overall behavior is not significantly affected by concentrating the shear reinforcement in bands.

The distance of the first row of shear elements from the face of the column must not be excessive. In one experiment, the first row of shear elements was placed at 3.2 in. ($\simeq 0.70d$) from the column and this resulted in a punching shear failure along the face of the column *before* yielding of the shear elements.

Inclination of Failure Crack

It is interesting to note that the relatively flat failure crack (20°–30°) normally observed in tests without shear reinforcement, or outside the shear-reinforced

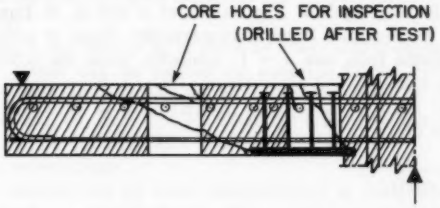

FIG. 12.—Flat Crack (25°) outside Shear Reinforced Zone and Steep Crack (50°) in Shear Reinforced Zone [Test SC12 (13)]

zone, does not occur in the zones with shear reinforcement as long as the shear reinforcement does not yield. Only relatively steep cracks (40°–50°), mostly bent-over flexural cracks can be observed prior to yielding of the shear reinforcement (Fig. 12). A shear crack thus intercepts the shear reinforcement situated within a distance approximately equal to d. Thus, in a design equation, the shear force V_s resisted by steel in any one critical section should only account for an area of shear reinforcement located within a width $= \pm d/2$ from the section considered (Eq. 9).

Suggested Code Provisions

Shear reinforcement for flat plates must be securely anchored to the concrete as close as possible to the top and bottom slab surfaces. The following are suggested rules for the design of such reinforcement. The symbols used and the equations adopted comply as much as possible with current ACI and Canadian Codes (2,3).

1. With shear reinforcement, the design of the critical section perpendicular to the plane of the slab—and located so that its perimeter is at $d/2$ from the face of the column—should be based

$$v_u \leq \phi\, v_n \quad \ldots\ldots\ldots\

elements as the first row; otherwise, the area may be reduced at a section farther away from the column face in which v_u is smaller, but the requirement of Eq. 6 shall be satisfied at all sections.

5. The first row of shear reinforcement shall not be closer than $d/4$ from the column face when $4\sqrt{f'_c}$ (psi) $< v_u/\phi \le 6\sqrt{f'_c}$ (psi) [$0.33\sqrt{f'_c}$ (MPa) $< v_u/\phi \le 0.50\sqrt{f'_c}$ (MPa)] in which v_u is calculated at a section $d/2$ away from the column face, the first row shall not be farther than $d/2$ from the column face and s shall not exceed $3d/4$. When $6\sqrt{f'_c}$ (psi) $< v_u/\phi \le 8\sqrt{f'_c}$ (psi) [$0.50\sqrt{f'_c}$ (MPa) $< v_u/\phi \le 0.67\sqrt{f'_c}$ (MPa)], the first row shall not be farther than $0.35d$ from the column face and s shall not exceed $d/2$. With rectangular columns (or with a square equivalent in area to a circular column), the shear reinforcement may be arranged in bands of widths equal to the column sides.

Comparison with Present Codes

The design rules suggested in the previous section differ from the current ACI and Canadian Codes (2,3) in the following:

1. Higher nominal shear stress, v_u, is allowed when well anchored shear reinforcement is used: ($8\sqrt{f'_c}$ (psi) instead of $6\sqrt{f'_c}$ (psi) $0.67\sqrt{f'_c}$ (MPa) instead of $0.5\sqrt{f'_c}$ (MPa).
2. In determining the zone to be covered by shear reinforcement, the nominal shear stress, v'_c, that can be carried by concrete in the absence of shear reinforcement is reduced gradually as the critical section is moved away from the column face (Fig. 10, Eqs. 3 or 4). When the critical section is at a distance d or closer from the column face, the value of v'_c given by Fig. 10 is the same as in the current codes.
3. The cross section area of shear reinforcement is designed to resist shear in excess of a value v_c higher than in the current codes (2,3). For example, for a square column at a critical section $d/2$ away from the column, Eqs. 4 or 5 gives $v_c = 3\sqrt{f'_c}$ (psi) (= $0.25\sqrt{f'_c}$ (MPa)) instead of $2\sqrt{f'_c}$ (psi) [$0.17\sqrt{f'_c}$ (MPa)] in the current codes (2,3). This increase is justified by the results of the aforementioned tests which in fact indicate that larger values of stress can be assumed to be carried by concrete.

It is to be noted that Eq. 6 gives the area of shear reinforcement per unit length of the perimeter of the critical section rather than the total area required for the whole section as in the current codes (2,3). The writers prefer to use Eq. 6 in the form presented here because its application can be extended to the case when moment is transferred between the slab and the column. In this case, the nominal shear stress v_u to be used in Eq. 6 is that caused by the combined effect of the factored vertical shearing force and the "unbalanced" moment transferred by eccentricity of shear in accordance with the current codes (Section 11.12.2.2 of Ref. 2 or Section 9.14.2 of Ref. 3).

When no moment is transferred between the slab and the column, the foregoing design equations can be put in similar form to the equations of the codes (2,3)

as shown in the following equations: The design of any critical section of periphery b_o shall be based on

$$V_u \leq \phi V_n \quad \ldots \ldots \ldots

5. Dilger, W. H., Ghali, A., and El-Masri, M. Z., "Flat Plates with Special Shear Reinforcement Subjected to Static and Dynamic Moment Transfer," *Proceedings, Journal of the American Concrete Institute*, Vol. 75, No. 10, Oct., 1978, p. 543–549.
6. Feld, J., "Lessons from Failures of Concrete Structures," Monograph Series, *Monograph No. 1*, American Concrete Institute, 1964, pp. 30–32.
7. Ghali, A., Sargious, M., and Huizer, A., "Vertical Prestressing of Flat Plates Around Columns," *Shear in Reinforced Concrete, SP 42–38*, American Concrete Institute, 1974, pp. 905–920.
8. Hawkins, N. M., "Shear Strength of Slabs with Shear Reinforcement," *Shear in Reinforced Concrete, SP-42*, American Concrete Institute Special Publication 1974, pp. 785–816.
9. "The Shear Strength of Reinforced Concrete Members-Slabs," by the Joint ASCE-ACI Task Committee 426 on Shear and Diagonal Tension of the Committee on Masonry and Reinforced Concrete," *Journal of the Structural Division*, ASCE, Vol. 100, ST8, Proc. Paper 10733, Aug., 1974, pp. 1543–1591.
10. Langohr, H., Ghali, A., and Dilger, W. H., "Special Shear Reinforcement for Concrete Flat Plates," *Proceedings, Journal of the American Concrete Institute*, Vol. 73, No. 3, Mar., 1976, pp. 141–146.
11. Leonhardt, F., and Moennig, E., *Lectures on Reinforced Concrete*, Vol. 3, New York, N.Y., 1974, pp. 241.
12. Seible, F., Ghali, A., and Dilger, W. H., "Shear Reinforcing Units for Flat Plates," *American Concrete Institute Journal*, Vol. 77, No. 1, Jan.–Feb., 1980, pp. 28–35.
13. Thurlimann, B., "Plastic Analysis of Reinforced Concrete Beams," *International Association for Bridge and Structural Engineers Colloquium*, Introductory Report, Copenhagen, Denmark, 1979, pp. 71–90.
14. Van der Voet, F., "The Shear Strength of Slabs with Mechanically Anchored Shear Reinforcement," thesis presented to the University of Calgary, at Calgary, Canada, in 1980, in partial fulfillment of the requirements for the degree of Master of Science.

Appendix II.—Notation

The following symbols are used in this paper:

A_v = area of shear reinforcement elements in one row parallel to column periphery;
b_o = perimeter of critical section;
d = distance from extreme compression fibre to centroid of flexural reinforcement (effective depth of slab);
f'_c = specified compressive strength of concrete, in megapascals (pounds per square inch);
f_y = specified yield strength of reinforcement;
s = spacing between rows of shear reinforcement elements measured perpendicular to column face;
V = applied shear force in test;
V_c = nominal shear strength provided by concrete;
V_n = nominal shear strength (force);
V_s = nominal shear strength provided by shear reinforcement;
V_u = ultimate shear strength in test, or shear force due to factored load in design;
v_c = assumed nominal shear stress resisted by concrete at ultimate to be used in design for calculation of required shear reinforcement;
v'_c = nominal shear stress that can be resisted by concrete at critical section outside shear reinforced zone;
v_n = nominal shear stress at ultimate;

v_u = nominal shear stress produced by factored load;
α = ratio of distance between column face and critical section to slab effective depth d;
β_c = ratio of long side to shorter side of rectangular column; and
ϕ = strength reduction factor.

POINT LOADS ON COMPOSITE DECK-REINFORCED SLABS

By Charles W. Roeder,[1] M. ASCE

INTRODUCTION

Composite form-reinforced floors, of the type shown in Fig. 1, are commonly used in modern construction. Moreover, this construction is economical. These decks are typically designed for distributed loads. Various studies (1,2,5,6,7) have investigated the behavior of floors under this loading. However, they are frequently loaded with concentrated loads such as wheels of forklifts, or machinery. The behavior of these elements under this loading is not well understood.

This paper describes an experimental study of the behavior of the subject floor system under concentrated loads. The study was motivated by observed damage in an existing building on a U.S. Government facility. The building was inspected and a series of nondestructive load tests were performed. Test specimens were designed to simulate this floor system and they were tested to failure in a laboratory. The results of these tests indicate that the continuity of the floor system restrains and limits deflections. This results in a greater capacity for resisting concentrated loads. This capacity may be several times larger than that predicted by existing design procedures.

BACKGROUND

The behavior of individual components of composite form-reinforced decks are generally well understood (1,2). Composite beams are known to be influenced by the size and geometry of the ribs, and special design provisions have been proposed for these beams. Other studies (5,6,7) have considered the behavior of slabs when they are isolated from the beam. Shear bond failure (7) is recognized as the most common mode of failure, but flexural failures and punching shear failures are also known to occur.

These existing results are valuable but they do not consider the full complexity of the composite floor system. Complex states of stress are developed in the

[1]Assoc. Prof., Dept. of Civ. Engrg., Univ. of Washington, Seattle, Wash. 98195.

Note.—Discussion open until May 1, 1982. To extend the closing date one month, a written request must be filed with the Manager of Technical and Professional Publications, ASCE. Manuscript was submitted for review for possible publication on October 31, 1980. This paper is part of the Journal of the Structural Division, Proceedings of the American Society of Civil Engineers, ©ASCE, Vol. 107, No. ST12, December, 1981. ISSN 0044-8001/81/0012-2421/$01.00.

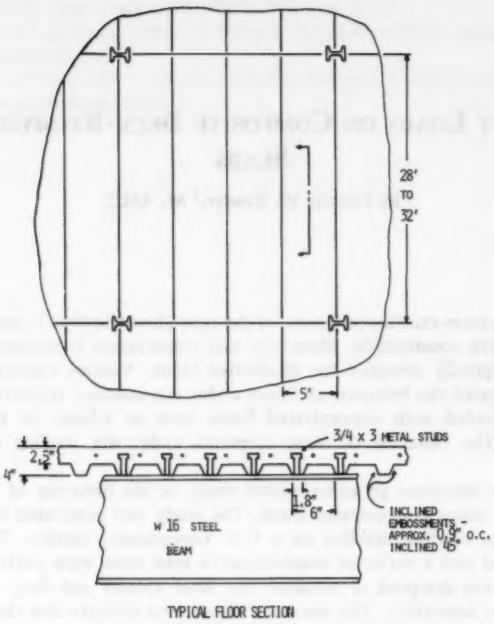

FIG. 1.—Sketch of Floor System

slab. Compressive, bending, and shear stresses are developed in the slab due to bending of the slab and the composite beams. Local stresses and punching shear stress may also develop in the vicinity of the applied load. Compatibility and relatively complex boundary conditions, which are introduced by the continuity of the floor system, must also be maintained. These problems combine to form a more complex structural system than has been studied in previous research. This study considers this more complex behavior.

Experimental Program

The damaged floor was constructed, as shown in Fig. 1. W16 wide flange beams were spaced 5 ft (1.525 m) on center, and they spanned between steel frames which were 28–32 ft (8.54–9.76 m) apart. The beams were composite beams with 3/4 × 3 in. (19 × 76 mm) metal studs and simple Type 2 (3) end connections. The slab was 4 in. (102 mm) thick (maximum thickness), with 6 × 6 in. welded wire mesh with #10 wire. The metal deck was 20 gage steel in 36 in. (0.915 m) widths, and it was continuous over 4 span lengths. The ribs were 1.5 in. (38 mm) deep with inclined embossments, as indicated in Fig. 1. The concrete strength varied between 2,500–4,000 psi (17,250–27,600 kPa).

Three groups of test specimens were designed to simulate the above floor system (Fig. 2). The same metal deck, wire mesh, and headed metal studs were used. The studs were welded through the metal deck into the flange of a W 8 × 48 beam. This beam size was chosen to satisfy similitude requirements. The normal weight concrete was mixed in a single batch and was designed to have a 2,500–3,000 psi (17,200–20,700 kPa) seven day strength.

Groups A and B used single panel widths, four span sections of metal deck. They were identical except that the metal deck and wire mesh were continuous for four spans in Group B, and spliced over each beam in Group A. Each span was tested independently by a procedure analogous to a shear bond test (5). However, the specimens were different from typical shear bond specimens

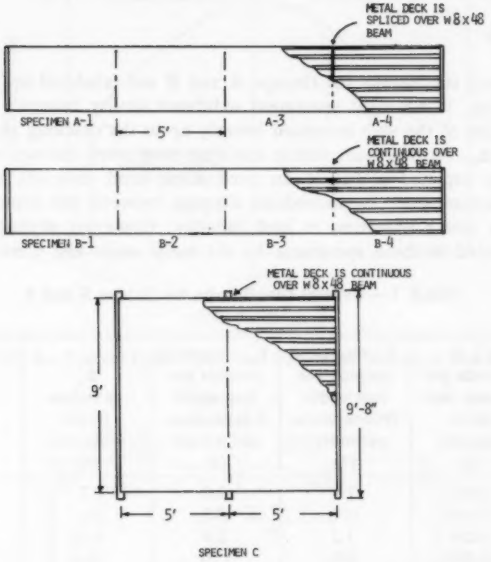

FIG. 2.—Sketch of Test Specimens

because of the metal studs and the continuity of the slab. The fourth specimen of both groups (A-4 and B-4) had an 8 in. (203 mm) diam core cut through the slab and metal deck after the concrete had set. Specimen C was designed to simulate a large continuous section of the floor and to determine the effect of this continuity on the behavior of the structure. The slab was designed to be a full scale model of the prototype structure, but the beams were 0.5–0.33 scale because of space limitations.

All loads were applied with a 2,500 kip (11,125 kN) Baldwin Hydraulic Testing Machine. Groups A and B were loaded with a uniform line load which was applied at midspan through a steel wide flange. Six dial gages were attached to these specimens to measure slab deflection. The loads were applied monotoni-

cally, except that a cyclic loading was used for Specimens A-3 and B-3. The cyclic loading was used to reproduce the effect of repeated loadings on a slab which had sustained previous damage. It was applied by first loading the specimen to a load just above the load of visible cracking in the slab. The specimen was then unloaded, and the load was repeated until failure. Specimen *C* was loaded with concentrated loads which were applied to the slab at various locations through steel plates of various sizes (3 × 3, 5 × 5, 10 × 10, and 15 × 15 in.) (76 × 76, 127 × 127, 254 × 254, and 381 × 381 mm, respectively). The thickness of the steel plates were chosen to minimize deformation of the plate and to provide a uniform distribution of load over the applied area. Strain gages and dial gages were attached to the flanges of the beams, and at 1 ft (0.305 m) intervals on the midspan of the slab of Specimen C.

Test Results

The general test results for Groups A and B are tabulated in Table 1, and shown in Fig. 3. All eight specimens exhibited similar behavior. The center line deflection of the slab increased linearly up to the cracking shear, V_s, and deflection, Δ_s. At this load, visible cracking progressed through the depth of the slab, as depicted in Fig. 4. In most shear bond tests (7), this cracking would be accompanied by immediate slippage between the concrete and the metal deck, and a reduction in load capacity. However, slippage and uplift were prevented in these specimens by the metal studs and continuity of the

TABLE 1.—General Test Results for Groups A and B

Specimen (1)	f'_c, in pounds per square inch (kilopascals) (2)	V_s, thousand pounds per foot width (kilonewtons per meter) (3)	V_u, thousand pounds per foot width (kilonewtons per meter) (4)	Δ_s, in inches (millimeters) (5)	Δ_u, in inches (millimeters) (6)
A-1	3,050 (21,000)	1.3 (19)	2.6 (38)	0.2 (5)	1.2 (30)
A-2	3,050 (21,000)	1.2 (18)	2.4 (35)	0.15 (3.8)	1.3 (33)
A-3	3,980 (27,500)	0.8 (12)	1.8 (26)	0.08 (2.7)	1.0 (25.4)
A-4	4,050 (28,000)	1.7 (25)	2.2 (32)	0.15 (3.8)	1.2 (30)
B-1	3,180 (22,000)	1.8 (26)	2.6 (38)	0.15 (3.8)	1.5 (38)
B-2	3,250 (22,500)	1.7 (25)	3.5 (51)	0.15 (3.8)	1.1 (28)
B-3	3,950 (27,000)	1.7 (25)	3.8 (55)	0.23 (5.8)	1.6 (41)
B-4	4,050 (28,000)	1.6 (23)	3.0 (44)	0.17 (4.3)	1.3 (33)
C	4,200 (29,000)	—	—	—	—

slab. Thus, a trussing action developed, as in Fig. 4. This action produced a significant increase in shear capacity at reduced stiffness until the ultimate shear and deflection, V_u and Δ_u, were attained. At the ultimate load, the concrete began to crack around the metal studs and slippage and uplift occurred. A reduction in load occurred after the slip.

A comparison of the results for Groups A and B provides a measure of the influence of the continuity of wire mesh and metal deck on the shear bond capacity. The comparison shows that the continuous metal deck caused an

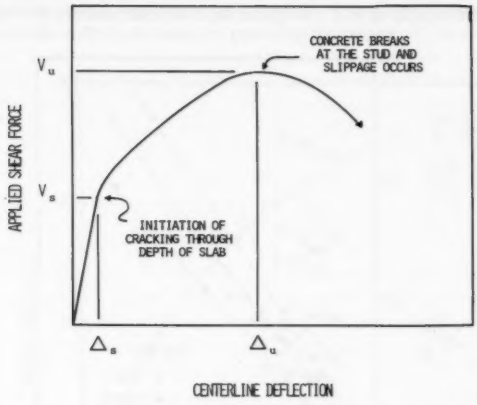

FIG. 3.—Typical Force-Deflection Curves for Groups A and B

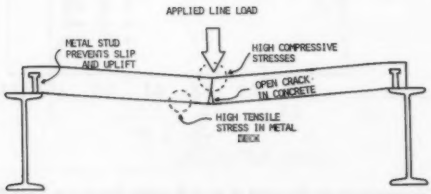
APPLIED LINE LOAD
METAL STUD PREVENTS SLIP AND UPLIFT
HIGH COMPRESSIVE STRESSES
OPEN CRACK IN CONCRETE
HIGH TENSILE STRESS IN METAL DECK

FIG. 4.—Trussing Action of Slab

approximate average 40–50% increase in shear bond capacity over the spliced deck specimens of Group A. However, there was considerable scatter in the data. This increase is somewhat surprising, because continuity does not reduce maximum shear forces. However, a visual inspection of the specimens at the ultimate load provides a hypothesis for explaining this phenomenon. Considerable negative curvature was noted in the metal deck over the beams. The metal studs connected the metal deck to the beam flange and the flanges added considerable rotational stiffness to the metal deck. The increased stiffness caused the metal deck to carry a larger portion of the shear force, as is predicted by sandwich beam theory (4). Thus, it is believed that this stiffening effect

was largely a function of the metal studs and the beam flange width and thickness.

Specimen A-3 was tested under cyclic loading. However, the concrete was broken at one corner prior to testing. The initial break extended down to the metal studs and prevented the slip restraint and trussing action which was noted in the other specimens. This led to a significant reduction in V_s and V_u, and provides further evidence of the importance of the slip restraint provided by the studs and the blocking action of adjacent spans. Specimen B-3 was also tested under cyclic loading. The cyclic loading produced some deterioration in the strength and stiffness of both A-3 and B-3. However, the deterioration progressed more rapidly in A-3. The more rapid deterioration in A-3 was attributed

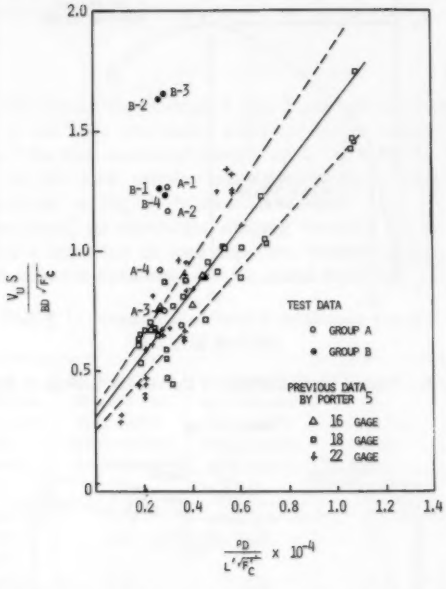

FIG. 5.—Comparison of Groups A and B with Previous Test Results (5)

to the initial damage noted for Specimen A-3. With specimens A-4 and B-4, a hole was cut through the floor in the zone of high shear stress. The holes were cut because it was suggested that this operation could cause premature separation and loss of shear bond capacity. Both specimens had lower strength relative to other members of their group (Fig. 5). However, further testing is needed to properly assess the degree of this reduction.

The results of these tests on specimen groups A and B were also compared to previously reported shear bond tests without stud shear connectors (7). The comparison is shown in Fig. 5. The previous tests were on the same type metal deck as used in this study, but the deck was inverted. It is recognized that the results for the inverted deck may not be directly comparable to the results

of this study. However, the comparison of Fig. 5 is believed to be a conservative measure of the beneficial effect of stud restraint and blockage of adjacent spans. The inverted deck has a larger shear area with more steel at the extreme fiber than a normal slab of the same thickness. The shear embossments and bond characteristics are similar. Thus, the inverted deck is expected to have lower bending and shear stresses, and higher strength, if the end restraint conditions are identical. This comparison shows that the continuity and restraint, which was provided by the studs and the continuous floor, significantly increased the capacity over those in previous tests (7). Increases of 50–100% were obtained with simple span metal deck and stud restraint, and adjacent span blockage. Continuous decks with stud restraint provided increases of 100–150%.

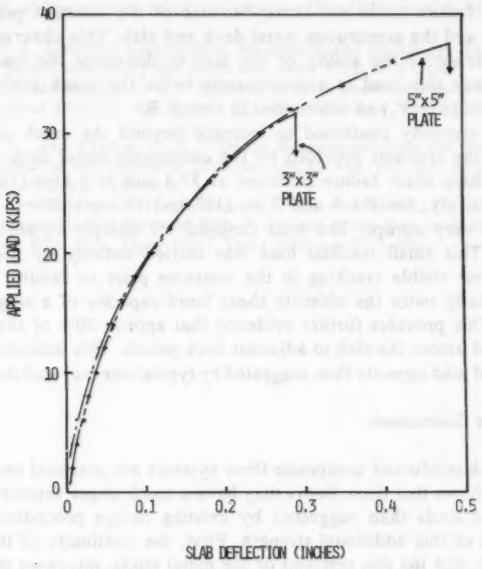

FIG. 6.—Load-Deflection Curves for Specimen C

Specimen C was loaded with a series of point loads at different locations. Most of these tests were nondestructive. General conclusions which can be drawn from these tests are as follows. Maximum slab deflections occur near the applied load, but they are smoothly distributed over a considerable distance. A study of these deformations indicated that a significant portion of the applied load was transmitted across the weak direction of the slab. Only approx 50% of the applied load was directly supported by the loaded deck panel. The remainder was distributed to adjacent panels. It should be noted that the deflections of Specimen C were compared to those obtained in a load test of the prototype structure, and the maximum deflections and distribution of deflection were similar.

Two locations of Specimen C were loaded to failure and these results are

examined in greater detail. Both tests were performed with the load at the center of the beam span, and at the center of a deck panel. The deformation of the slab (deflection of the beam is removed) under the concentrated load is shown in Fig. 6. No concrete cracks were visible prior to these tests. The first load was applied through a 5 × 5 in. (127 × 127 mm) steel plate, and the second load used a 3 × 3 in. (76 × 76 mm) plate. Both tests exhibited similar behavior. The force-deformation curve increased without incident up to the 20–24 kips (89–107 kN) load range. In this load range, the specimen emitted numerous cracking sounds, and the strains in the metal deck immediately below the applied load showed a sharp increase. However, there was no visible cracking on the slab surface. This was believed to mark the initiation of the shear bond cracking in the panel immediately under the load, but complete shear bond failure could not occur because of the restraint provided by the metal studs and the continuous metal deck and slab. This observation provides further evidence of the ability of the slab to distribute the load in its weak direction since this load is approximately twice the crack initiation load for a single panel ($6 \times V_s$) as determined in Group B.

The load capacity continued to increase beyond the crack initiation range because of the restraint provided by the continuous metal deck and the metal studs. Punching shear failure occurred at 37.4 and 31.5 kips (166.4 and 140.2 kN), respectively, for the 5 and 3 in. (127 and 76 mm) plates. This mode of failure was very abrupt. The load dropped off sharply to about 20% of its maximum. This small residual load was carried entirely by the metal deck. There was no visible cracking in the concrete prior to failure. The 37.4 kip load was nearly twice the ultimate shear bond capacity of a single deck panel ($6 \times V_u$). This provides further evidence that approx 50% of the applied load is distributed across the slab to adjacent deck panels. This indicates much larger concentrated load capacity than suggested by typical one way slab design methods.

Summary and Conclusions

Metal deck reinforced composite floor systems are practical and economical. This study shows that these floors may have a much larger capacity for resisting concentrated loads than suggested by existing design procedures. There are two sources of this additional strength. First, the continuity of the metal deck and the slab, and the slip restraint of the metal studs, increases the shear bond capacity. Second, the continuity of the slab restricts the deformation of the floor system. This tends to distribute the deflections, bending stress, and shear stress across the weak direction of the floor to adjacent deck panels.

While these tests clearly indicate that slabs can resist large concentrated loads, the results are not readily usable by the design profession. These tests were performed with a single metal deck type, stud size, span length, and concrete depth. Further study is needed to evaluate the effect of these parameters and to develop strength predictions which can be readily used by the engineering profession.

Acknowledgments

Most of the experimental work, which is described in this paper, was funded

by the U.S. Navy through Centrac Engineering Associates in Lynnwood, Wash. N. Bass and A. K. Batra served as contacts with these agencies and provided numerous suggestions. The writer also thanks N. M. Hawkins for his continuous advice throughout this study.

APPENDIX.—REFERENCES

1. "Composite Steel-Concrete Construction," by Subcommittee on the State-of-the-Art Survey of the Task Committee on Composite Construction of the Committee on Metals, Structural Division, ASCE, *Journal of the Structural Division*, Vol. 100, No. ST5, May, 1974.
2. Iyengar, H. S., *Composite and Mixed Steel-Concrete Construction for Buildings*, ASCE, New York, N.Y., 1977.
3. *Manual of Steel Construction*, American Institute of Steel Construction, 8th ed., Chicago, Ill., 1980.
4. Plantema, F. J., *Sandwich Construction, the Bending and Buckling of Sandwich Beams, Plates and Shells*, John Wiley and Sons, Inc., New York, N.Y., 1966.
5. Porter, M. L., and Ekberg, C. E., "Behavior of Steel-Deck-Reinforced Slabs," *Journal of the Structural Division*, ASCE, Vol. 103, No. ST3, Proc. Paper 12826, Mar., 1977, pp. 663–677.
6. Porter, M. L., and Ekberg, C. E., "Design Recommendations for Steel Deck Floor Slabs," *Journal of the Structural Division*, ASCE, Vol. 102, No. ST11, Proc. Paper 12528, Nov., 1976, pp. 2121–2136.
7. Porter, M. L., Ekberg, C. E., Greimann, L. F., and Elleby, H. A., "Shear-Bond Analysis of Steel-Deck-Reinforced Slabs," *Journal of the Structural Division*, ASCE, Vol. 102, No. ST2, Proc. Paper 12611, Dec., 1976, pp. 2255–2268.

TECHNICAL NOTES

Note.—Discussion open until May 1, 1982. To extend the closing date one month, a written request must be filed with the Manager of Technical and Professional Publications, ASCE. This paper is part of the Journal of the Structural Division, Proceedings of the American Society of Civil Engineers, ©ASCE, Vol. 107, No. ST12, December, 1981.

Technical Notes

To provide a place within ASCE for publication of technical ideas that have not advanced, as yet, to the point where they warrant publication as a Proceedings paper in a *Journal*, the publication of Technical Notes was authorized by the Board of Direction on October 16–18, 1967, under the following guidelines:

1. An original manuscript and two copies are to be submitted to the Manager of Technical and Professional Publications, ASCE, 345 East 47th Street, New York, N.Y., 10017, along with a request by the author that it be considered as a Technical Note.
2. The two copies will be sent to an appropriate Technical Division or Council for review.
3. If the Division or Council approves the contribution for publication, it shall be returned to Society Headquarters with appropriate comments.
4. The technical publications staff will prepare the material for use in the earliest possible issue of the *Journal*, after proper coordination with the author.
5. Each Technical Note is not to exceed 4 pages in the *Journal*. As an approximation, each full manuscript page of text, tables, or figures is the equivalent of one-half a *Journal* page.
6. The Technical Notes will be grouped in a special section of each *Journal*.
7. Information retrieval abstracts and key words will be unnecessary for Technical Notes.
8. The final date on which a Discussion should reach the Society is given as a footnote with each Technical Note.
9. Technical Notes will not be included in *Transactions*.
10. Technical Notes will be included in ASCE's annual and cumulative subject and author indexes.

The manuscripts for Technical Notes must meet the following requirements:

1. Titles must have a length not exceeding 50 characters and spaces.
2. The author's full name, Society membership grade, and a footnote reference stating present employment must appear on the first page of the manuscript. Authors need not be Society members.
3. The manuscript is to be submitted as an original copy (with two duplicates) that is typed double-spaced on one side of 8-1/2-in. (220-mm) by 11-in. (280-mm) white bond paper.
4. All mathematics must be typewritten and special symbols must be properly identified. The letter symbols used must be defined where they first appear, in figures or text, and arranged alphabetically in an Appendix.—Notation.
5. Standard definitions and symbols must be used. Reference must be made to the lists published by the American National Standards Institute and to the *Authors' Guide to the Publications of ASCE*.
6. Tables must be typed double-spaced (an original ribbon copy and two duplicate copies) on one side of 8-1/2-in. (220-mm) by 11-in. (280-mm) paper. An explanation of each table must appear in the text.
7. Figures must be drawn in black ink on one side of 8-1/2-in. (220-mm) by 11-in. (280-mm) paper. Because figures will be reproduced with a width of between 3 in. (76 mm) to 4-1/2 in. (110 mm), the lettering must be large enough to be legible at this width. Photographs must be submitted as glossy prints. Explanations and descriptions must be made within the text for each figure.
8. References cited in text must be typed at the end of the Technical Note in alphabetical order in an Appendix.—References.
9. Dual units, i.e., U.S. Customary followed by SI (International System) units in parentheses, should be used throughout the paper.

Optimum Design of Three-Span I-Beams

By Abul K. Azad,[1] M. ASCE

Introduction

In designing three-span I-beams or girders, designers may encounter situations where the locations of the interior supports are not prefixed and can be varied, if advantageous. A common example is design of three-span highway overpasses where the location of piers can sometimes be adjusted to produce an economical design. In order to find the most economical design from the viewpoint of minimum weight, the optimum locations of the interior supports must be determined. The search becomes difficult even for a constant height web, if the flange plates are varied to save material. Considerable research has been done in the area of optimization of I-shapes using various assumptions and approaches. Refs. 1–4, 6, 8, 10 are a representative of such work based on elastic design methods. Various cases of optimum plastic design of I-beams (5,7,9) are covered in Ref. 7 which also provides a comprehensive list of references of such work.

This paper presents a plastic design method to determine the minimum-weight design that is of a symmetrical three-span I-beam of given length and is subjected to uniformly distributed load. The beam is symmetrical in cross section, and has an unchanged web of constant height. Flange areas are varied considering only the maximum positive and negative moments, thus, introducing only one cutoff point in each span and two cutoff points in the center span. Such a restricted number of cutoff points for relatively short span beams is not uncommon since too many cutoff points would increase the cost of welding.

Method

For a typical I-section, shown in Fig. 1, the total area, A, and the approximate plastic section modulus, Z_x, can be written

$$A = 2A_f + ht \quad \ldots\ldots (1)$$

$$Z_x = A_f h + \frac{h^2 t}{4} \quad \ldots\ldots (2)$$

[1]Assoc. Prof. of Civ. Engrg., Univ. of Petroleum and Minerals, Dhahran, Saudi Arabia.

Note.—Discussion open until May 1, 1982. To extend the closing date one month, a written request must be filed with the Manager of Technical and Professional Publications, ASCE. Manuscript was submitted for review for possible publication on January 21, 1981. This paper is part of the Journal of the Structural Division, Proceedings of the American Society of Civil Engineers, ©ASCE, Vol. 107, No. ST12, December, 1981. ISSN 0044-8001/81/0012-2433/$01.00.

The value of Z_x required of a beam section to resist a design moment, M_p, must at least equal

$$Z_x = \frac{M_p}{F_y} \quad \ldots\ldots\ldots\ldots\ldots\ldots\ldots\ldots\ldots\ldots\ldots\ldots\ldots\ldots\ldots\ldots\ldots\ldots\ldots\ldots\ldots\ldots (3)$$

in which F_y = the yield stress of steel. Using Eqs. 1–3, the total weight, $\bar{W}$, of a beam can be expressed

$$\bar{W} = \rho \sum_n \sum_i \left(\frac{2M_{pi}\ell_i}{hF_y} + \frac{ht\ell_i}{2} \right) \quad \ldots\ldots\ldots\ldots\ldots\ldots\ldots\ldots\ldots\ldots\ldots\ldots\ldots\ldots (4)$$

in which ρ = the unit weight of steel; M_{pi} = the design moment for the segment length, ℓ_i; and n = the number of spans, $n = 3$. Eq. 4 shows that, for a chosen web, the weight is minimum when the summed value of $\Sigma M_{pi}\ell_i$ for all spans is minimum.

Referring to the symmetrical I-beam of length, L, in Fig. 2, the following equations can be written:

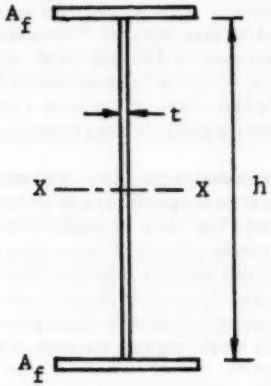

FIG. 1.—Typical I-Section

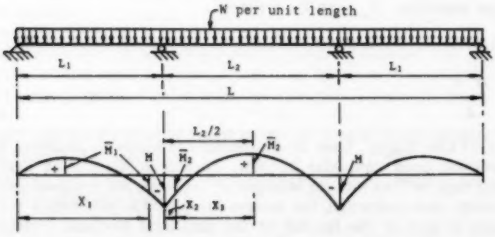

FIG. 2.—Symmetrical Three-Span Beam

$$L_1 = \frac{L}{2+\beta} \quad \ldots\ldots (5)$$

$$M = \gamma W L_1^2 \quad \ldots\ldots (6)$$

$$\bar{M}_1 = \frac{w L_1^2 (0.5-\gamma)^2}{2} \quad \ldots\ldots (7)$$

$$\bar{M}_2 = w L_1^2 \left(\frac{\beta^2}{8} - \gamma\right) \quad \ldots\ldots (8)$$

$$X_1 = 2.4142(0.5-\gamma) L_1 \quad \ldots\ldots (9)$$

$$X_2 = L_1 (0.5\beta - \sqrt{0.5\beta^2 - 4\gamma}) \quad \ldots\ldots (10)$$

$$X_3 = L_1 \sqrt{0.5\beta^2 - 4\gamma} \quad \ldots\ldots (11)$$

in which $\beta = \frac{L_2}{L_1}$ $\ldots\ldots (12)$

and γ, as defined by Eq. 6, is a value to be determined.

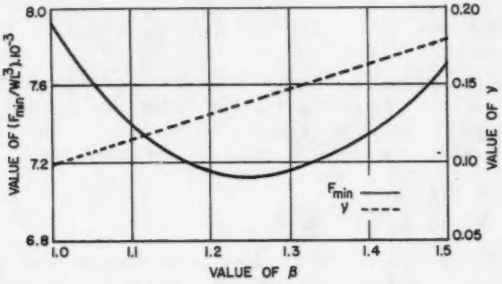

FIG. 3.—Values of F_{min} and γ Versus Values of β

Using Eqs. 5–11, the objective function, $F = \Sigma M_{Pi} \ell_i$ for all spans, becomes

$$F = 2wL_1^3 \left\{ 1.2071\,[(0.5-\gamma)^3 - 2\gamma(0.5-\gamma)] + \gamma + \frac{\gamma\beta}{2} - \left(2\gamma - \frac{\beta^2}{8}\right)\sqrt{0.5\beta^2 - 4\gamma} \right\} \quad \ldots\ldots (13)$$

For a given value of β, setting $\partial F/\partial\gamma = 0$, the condition for F_{min} is

$$0.5\beta - 1.1124 + 8.4497\gamma - 3.6213\gamma^2 = \frac{1.25\beta^2 - 12\gamma}{\sqrt{0.5\beta^2 - 4\gamma}} \quad \ldots\ldots (14)$$

For an assumed value of β, the value of γ to produce F_{min} can be obtained from Eq. 14 by trial. The values of γ and F_{min} for various values of β are shown in Fig. 3. While the optimum value of $\beta = 1.25$, and the corresponding

$F_{min} = 0.007124wL^3$ and $\gamma = 0.1384$, Fig. 3 shows that an economical design can be obtained within the range of $\beta = 1.2$–1.3. While the exact relationship between β and γ is described by Eq. 14, Fig. 3 shows that the value of γ varies almost linearly with β. Thus, the weight of the beam depends upon the support locations and the corresponding support moment, and each span weight is dependent upon its span length. The optimum segment lengths for the end span agree with the results presented in Ref. 9.

Optimum Web.—Once the optimum design moments and the corresponding segment lengths are known, the next step is to find the optimum web for the minimum weight design. The flange areas required for various segments to provide the bending strength can be determined from Eqs. 2–3 because h and t are known.

Since the web thickness must correspond to commercially available plate thickness, and it must provide the shear resistance of the beam, the minimum acceptable web thickness is selected which would be capable of carrying the shear force within the guidelines of the code practice. The procedure for such a selection of web thickness would be similar to the method in Ref. 1. For a selected web thickness t, the optimum web height is obtained by setting $\partial \bar{W}/\partial h = 0$, and

$$h = 0.1688L\sqrt{\frac{w}{tF_y}} \quad \ldots \quad (15)$$

This height is acceptable if it satisfies the design restrictions on h from the practical view point and on the ratio h/t. In the case in which there is no practical height limitation, the optimum height to satisfy the ratio $h/t = k$, a constant, is obtained by replacing t with h/k and setting $\delta \bar{W}/\delta h = 0$, and

$$h = 0.3848\sqrt[3]{\frac{wkL^2}{F_y}} \quad \ldots \quad (16)$$

The value of h from Eq. 16 may have to be modified in design since the value of t from $t = h/k$ may not yield a plate thickness commercially available. Knowing h, t, M, and optimum segment lengths, the proportioning of the beam can be finalized.

Conclusions

A plastic design method to find the minimum-weight design of a symmetrical three-span continuous I-beam of given length is presented. The beam is subjected to uniformly distributed load, and has an unchanged web of constant height. Based on one cutoff point in each end span and two cutoff points in the center span, the optimum ratio of the center span to the end span is determined as 1.25. The method provides the optimum segment lengths, the corresponding moment distribution, and the optimum web height for the beam.

Acknowledgment

This paper is part of the research work sponsored by the University of Petroleum and Minerals under the grant CE/STRUCTURE/32.

Appendix.—References

1. Azad, A. K., "Economic Design of Homogeneous I-Beams," *Journal of the Structural Division*, ASCE, Vol. 104, No. ST4, Proc. Paper 13701, Apr., 1978, pp. 637–648.
2. Azad, A. K., "Continuous Steel I-Girders: Optimum Proportioning," *Journal of the Structural Division*, ASCE, Vol. 106, No. ST7, Proc. Paper 15575, July, 1980, pp. 1543–1555.
3. Chong, K. P., "Optimization of Unstiffened Hybrid Beams," *Journal of the Structural Division*, ASCE, Vol. 102, No. ST2, Proc. Paper 11907, Feb., 1976, pp. 401–409.
4. Holf, E. C., and Heithecker, G. C., "Minimum Weight Proportions for Steel Girders," *Journal of the Structural Division*, ASCE, Vol. 95, No. ST10, Proc. Paper 6838, Oct., 1969, pp. 2205–2217.
5. Prager, W., and Rozvany, G. I. N., "Plastic Design of Beams: Optional Locations of Supports and Steps in Yield Moment," *International Journal of Mechanical Sciences*, Vol. 17, No. 12, Cambridge, England, Dec., 1975, pp. 627–631.
6. Razani, R., and Goble, G. G., "Optimum Design of Constant-Depth Plate Girders," *Journal of the Structural Division*, ASCE, Vol. 92, No. ST2, Proc. Paper 4787, Apr., 1966.
7. Rozvany, G. I. N., "Optimal Flexural Systems," Pergamon Press Ltd., Oxford, England, 1976.
8. Schilling, C. S., "Optimum Properties of I-Shaped Beams," *Journal of the Structural Division*, ASCE, Vol. 100, No. ST12, Proc. Paper 11007, Dec., 1974, pp. 2385–2401.
9. Smith, E. A., "Minimum-Weight Design of Nonuniform Beams," *Journal of the Structural Division*, ASCE, Vol. 105, No. ST7, July, 1979, pp. 1559–1564.
10. Vachajitpan, P., and Rockey, K. C., "Design Method for Optimum Unstiffened Girders," *Journal of the Structural Division*, ASCE, Vol. 104, No. ST1, Proc. Paper 13459, Jan., 1978, pp. 141–155.

Aeroelastic Stability of Suspension Bridges

By Augustin Petre[1] and Ramiro Sofronie[2]

Introduction

The aim of this note is to develop a theory on the aeroelastic stability of suspension bridges that takes into account the drag effects of aerodynamically shaped decks (1,2,3). The theory is applied both to classical suspension bridge systems, and to recently developed prestressed suspension bridge systems (4)

[1]Head, Dept. of Aeronautic Engrg., Polytechnic Inst. of Bucharest, Bucharest, Romania.
[2]Assoc. Prof. of Civ. Engrg., Dept. of Civ. Engrg., Polytechnic Inst. of Bucharest, Bucharest, Romania.

Note.—Discussion open until May 1, 1982. To extend the closing date one month, a written request must be filed with the Manager of Technical and Professional Publications, ASCE. Manuscript was submitted for review for possible publication on March 12, 1981. This paper is part of the Journal of the Structural Division, Proceedings of the American Society of Civil Engineers, ©ASCE, Vol. 107, No. ST12, December, 1981. ISSN 0044-8001/81/0012-2437/$01.00.

(Fig. 1). Practical methods to solve reliability the stability problems of suspension bridges are offered.

Basic Assumptions.—The only two deformations considered significant in problems of the type treated herein are bending and torsion (5).

The elastic forces corresponding to the previously defined deformations will be expressed by differential operators. Since the elastic lines are reference axes, the expressions of elastic forces are independent of one another, i.e. elastic coupling terms do not appear.

The structural damping forces are considered according to Voigt's model (3). They will be written with the aid of a complex modulus of elasticity and are included in the expressions of elastic forces. The imaginary component of these expressions shows the loss by friction.

The inertia forces are generated by the mass of decks, cables, and hangers assumed to be uniformly distributed spanwise. Due to the vertical symmetry of bridge cross-sections, the mass centers coincide with the elastic centers.

The aerodynamic forces are considered according to the unsteady incompressible flow theory, and the classic aerodynamic operators of strip type. The

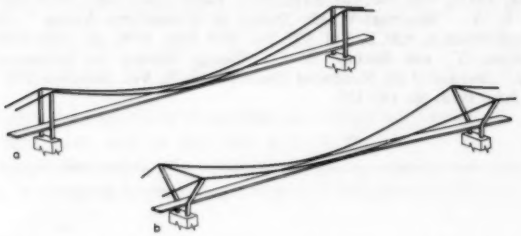

FIG. 1.—Classical (*a*) and Prestressed (*b*) Suspension Bridge System

assumption that these operators are applicable is justified by the increasing use of streamlined suspension bridge decks, the aerodynamic characteristics of which are similar to those of airfoils (6).

To calculate the equilibrium stability between the previously described forces, it is assumed that the bridge deck is subjected to an arbitrary but small perturbation consisting of a vertical displacement, ω or a transverse rotation, ϕ, or both. Consequently, under the wind action, aerodynamic forces of lift and drag develop. From the interaction between these aerodynamic forces and the elastic restoring forces there results a motion or a deformation, according to whether the influence of inertia forces is significant or not. However, if the components of the initial perturbation decrease and vanish, the resulting aeroelastic phenomenon is stable. On the contrary, if the initial perturbation increases, the phenomenon is unstable. Between the two equilibrium states there is a limit state in which the aerodynamic forces are perfectly balanced by the elastic forces. In this state, any additional perturbation, however small, does not encounter any opposition from the suspension bridge structure. It is this limit state of neutral equilibrium that defines the onset of the aeroelastic phenomena of flutter or divergence (7).

Governing Equations.—In the most general case, to the initial perturbation

of bending and torsion previously assumed, there corresponds the motion

$$\frac{\partial^2}{\partial x^2}\left[(1+ig_w)\,EI\frac{\partial^2 w}{\partial x^2}\right]+m\frac{\partial^2 w}{\partial t^2}-L_a(w,\phi)+\frac{\partial^2}{\partial x^2}(M_z\phi)=0 \quad \ldots\ldots (1a)$$

$$\frac{\partial}{\partial x}\left[(1+ig_\phi)\,GI_d\frac{\partial\phi}{\partial x}\right]-J\frac{\partial^2\phi}{\partial t^2}+M_a(w,\phi)-M_z\frac{\partial^2 w}{\partial x^2}=0 \quad \ldots\ldots\ldots (1b)$$

in which in each equation the first three terms represent elastic forces with structural damping, inertia forces, and lifting airloads. The last terms introduce the drag effects and, for a simply supported deck, the bending moment M_z associated with the uniform running drag has the expression

$$M_z=\frac{\zeta b V^2 C_D}{2}x(\ell-x) \quad \ldots\ldots\ldots\ldots\ldots\ldots\ldots\ldots\ldots (2)$$

in which V, ζ, b, ℓ, and C_D are airspeed, density, deck semichord, bridge span, and drag coefficient, respectively. For simple harmonic motion of circular frequency ω, Eqs. 1*a* and 1*b* become

$$W_o\frac{d^2}{dx^2}\left[(1+ig_w)\,EI\frac{d^2 w}{dx^2}\right]-\omega^2 mW_o w(x)-L_a(w,\phi)\frac{d^2}{dx^2}(M_z\phi)=0 \quad (3a)$$

$$\emptyset_o\frac{d}{dx}\left[(1+ig_\phi)\,GI_d\frac{d\phi}{dx}\right]+\omega^2 J\emptyset_o\phi(x)+M_a(w,\phi)-M_z\frac{d^2 w}{dx^2}=0 \quad \ldots (3b)$$

If, in Eq. 1, the inertia forces are neglected, initial perturbation reduces to a bending-torsional deformation (7).

Note that the two components of the motion (1) are always aerodynamically coupled. But as Eqs. 3*a* and 3*b*, associated with the boundary conditions $w(o) = w(\ell) = o$ and $\phi(o) = \phi(\ell) = 0$ form Sturm-Liouville systems, they can be put to the periodical motion (2), become

$$w(x)=\int_o^x G_w(x,\xi)\left\{\omega^2 mw(\xi)+\frac{1}{W_o}L_a(w,\phi)-\frac{1}{W_o}\frac{d^2}{d\xi^2}[M_z(\xi)\,\phi(\xi)]\right\}d\xi$$

$$+\int_x^\ell G_w(x,\xi)\left\{\omega^2 mw(\xi)+\frac{1}{W_o}L_a(w,\phi)-\frac{1}{W_o}\frac{d^2}{d\xi^2}[M_z(\xi)\phi(\xi)]\right\}d\xi \quad (4a)$$

$$\phi(x)=\int_o^x G_\phi(x,\xi)\left[\omega^2 J\phi(\xi)+\frac{1}{\emptyset_o}M_a(w,\phi)-\frac{1}{\emptyset_o}M_z(\xi)\frac{d^2 w(\xi)}{d\xi^2}\right]d\xi$$

$$+\int_x^\ell G_\phi(x,\xi)\left[\omega^2 J\phi(\xi)+\frac{1}{\emptyset_o}M_a(w,\phi)-\frac{1}{\emptyset_o}M_z(\xi)\frac{d^2 w(\xi)}{d\xi^2}\right]d\xi \quad \ldots\ldots (4b)$$

In these integral equations $G_w(x,\xi)$ and $G_\phi(x,\xi)$ are Green's influence functions for bending and torsion, respectively, of the considered suspension bridge systems.

The canonical expressions of aerodynamic force and its moment, with respect to the elastic axis in the adopted strip-theory, are given in Ref. 7. The analysis technique does not change when other expressions are preferred.

In order to calculate the stability boundaries, integral equations (4) are to be first nondimensionalized. The unknown parameters are

$$X = \frac{V}{b\omega} \quad \text{and} \quad Z = (1 + ig)\frac{GI_d}{\omega^2 J\ell^2}, \quad \text{where} \quad g = g_w = g_\phi, \ldots\ldots\ldots (5)$$

for dynamic stability, and

$$V_D = \frac{\pi\zeta V^2\ell^2}{EI} \ldots\ldots\ldots (6)$$

for the static stability. They are to be determined as functions of the following four dimensionless quantities:

$$p = \frac{EIb^2}{GI_d\ell^2}; \quad r^2 = \frac{J}{mb^2}; \quad m_o = \frac{m}{\pi\zeta b^2}; \quad C = \frac{C_D}{2\pi} \ldots\ldots\ldots (7)$$

combined in the ten symbols $A_1, A_2, \ldots A_{10}$ (7).

Classical Suspension Bridge System.—The special features of this structure, as treated herein, are the following: (1) The cables hang freely in vertical planes following the funicular lines of the loads applied on the deck; and (2) the cross-sections of the bridge system (which includes the cables) are open (Fig. 1*a*). For this type of bridge with a deck of constant cross-section, Green's influence functions, $G_w(x,\xi)$ and $G_\phi(x,\xi)$, and integral Eqs. 4*a* and 4*b* of dynamic stability, as well as those of static stability, are given in Ref. 7.

Prestressed Suspension Bridge System.—The special features of this structure, as treated herein, are the following: (1) The cables follow the geodetic lines of the funicular surface of vertical loads applied on the deck; and (2) the cross-sections of the bridge system (which includes the cables) are closed (10) (Fig. 1*b*). For this type of bridge, with a deck of constant cross-section, Green's influence functions and the integral Eqs. 4 of dynamic stability, 4*a* and 4*b*, as well as those of static stability, are given in Ref. 7.

Solution Methods.—The two static and dynamic problems of aeroelastic stability previously described are, in fact, eigenvalue problems. Since by using Green's influence functions the governing equations were put into integral form, it is more practical to transform them into algebraic equations. The operation can be done, for example, by punctual collocation, with the aid of the tangent method. Thus, integral equations 4*a* and 4*b*, for aeroelastic flutter, take the form

$$[w] = \frac{1}{Z}\left((A_1 + iA_2)[G_w][w] + \frac{\emptyset_o}{W_o}(A_3 + iA_4)[G_w][\phi] + \frac{\emptyset_o}{W_o}A_9[D_w][\phi]\right) \ldots\ldots\ldots (8a)$$

$$[\phi] = \frac{1}{Z}\left(\frac{W_o}{\emptyset_o}(A_5 + iA_6)[G_\phi][w] + (A_7 + iA_8)[G_\phi][\phi] + \frac{W_o}{\emptyset_o}A_{10}[D_\phi][w]\right) \ldots\ldots\ldots (8b)$$

in which the effects of drag were introduced by the operators D_w and D_ϕ; the ratio $W_o/\emptyset_o$ contains the phase difference between the two components of motion; and, obviously, the normalized vectors, $[w]$ and $[\phi]$, replace the complex mode shapes, $w(x)$ and $\phi(x)$. Such algebraic systems also could be directly obtained by a finite element technique. However, for aeroelastic stability problems, the previously described method is much simpler and reliable.

In order to solve this linear system, two methods can be used, the direct method and the iterative one. The well-known method of assumed modes is not so adequate in the case of suspension bridges because it is difficult to predict the common deformations of the cables and decks. In the direct method, the matrix of a linear system is transformed into the Hessenberg matrix and the eigenvectors and eigenvalues of this matrix are then determined (3). The method is useful when the explored field is completely unknown, although it requires more computing time, and, for plotting the V-g curves, each eigenvalue has to be pursued. The iterative method is, in fact, the inverse power method. It is a much faster method but not always convergent enough, especially when the critical velocities of divergence and flutter, affected by drag, assume close values.

Both methods were used by the writers to investigate the aeroelastic stability of suspension bridges. For example, by assuming for dimensionless quantities (7) the values $p = 0.001$, $r^2 = 0.25$, $m_o = 1$, $C = 0$ (hence without drag), $\bar{\mu} = 1$, and $\bar{\lambda} = 10$, according to Eq. 5, the dimensionless critical velocity of flutter

$$V_F = \frac{X}{\sqrt{\mathbf{Re}(Z)}}; \quad \text{or} \quad V_F = \frac{V\ell}{b}\sqrt{\frac{J}{GI_d}} \qquad \ldots\ldots\ldots\ldots\ldots\ldots (9)$$

takes for the classical funicular bridge, the value $V_F = 4.3447$, and for the prestressed geodetic bridge, $V_F = 13.673$, i.e. 3.147 times larger. If, for the same parameters, $\bar{\mu}$ increases from 1 to 10, the critical velocity of the funicular bridge becomes $V_F = 13.937$, i.e. 3.208 times higher. But as a consequence of aerodynamic drag, the critical velocity of the same funicular bridge decreases to $V_F = 7.244$ for $C = 0.02$, and to $V_F = 1.7552$ for $C = 0.04$, i.e. it becomes 1.924 and 7.940 times lower, respectively.

Conclusions

1. The aeroelastic stability of suspension bridges is strongly influenced by the aerodynamic drag of span decks. By taking into account the effects of drag in stability analyses, the two components of deformation or motion are always coupled. A consequence of drag is the reduction of the absolute values of divergence and flutter critical velocities with respect to the values calculated only for lifting forces. In addition, the ratio between the two critical velocities also can be modified. Thus, if without drag the critical velocity of divergence is higher than the corresponding critical velocity of flutter, as a consequence of the drag effect, the inequality sign can be reversed.

2. The governing equations, determined as presented herein, allow a comparison between the two structural systems of suspension bridges dealt with in this note. Thus, while their bending components are formally identical, the torsional components are essentially different. Classical suspension bridges are

more sensitive to torsion than prestressed suspension bridges. For this reason, the effect of drag is greater on the former than on the latter. Also, while funicular bridges behave quite differently in bending and torsion, geodetic bridges have a similar behavior in both degrees of freedom.

3. The analysis technique based on Green's influence functions used herein is an efficient tool for the study of aeroelastic stability of the two types of suspension bridges considered herein. In addition, it allows one to discover the aerodynamic and structural parameters responsible for any forms of static or dynamic instability and to modify them conveniently. The same analysis technique can be used for the aeroelastic optimization of suspension bridge systems.

Appendix.—References

1. Petre, A., *Teoria aeroelasticitatii, Statica, Ed. Academiei R.S.R.*, Bucureşti, Romania, 1966.
2. Petre, A., *Teoria aeroelasticitatii, Fenomene dinamice periodice, Editura Academiei R.S.R.*, Bucureşti, Romania, 1973.
3. Petre, A., Ashley, H., "Drag Effects on Wing Flutter," *Journal of Aircraft*, Vol. 13, No. 10, Oct., 1976, pp. 755–763.
4. Sofronie, R., "Suspension Bridge," *United States Patent* No. 3,857,130.
5. Petre, A., "On the deformation of one-dimensional structures," *Rev. Roum. Sci. Techn.-Méc. Appl.* Vol. 25, No. 1, pp. 85–98, Bucharest, Romania, 1980.
6. Scanlan, R. H., Tomko, J. J., Airfoil and Bridge Deck Flutter Derivatives, *Journal of the Engineering Mechanics Division*, ASCE, Vol. 97, No. EM6, Dec., 1971, pp. 1717–1737.
7. Petre, A., Sofronie, R., "Aeroelastic Stability of Suspension Bridges," *Wind Engineering, Proceedings of the Fifth International Conference*, Fort Collins, Colorado, U.S.A., July, 1979, J. E. Cermak, Ed., Pergamon Press, Oxford, U.K., 1980.
8. Sofronie, R., "Vertical Deflection of Suspension Bridges," *Rev. Roum. Sci. Techn.-Méc. Appl.*, Vol. 24, No. 3, pp. 485–505, Bucarest, Romania, 1979.
9. Sofronie, R., "Torsional Deflection of Suspension Bridges," *Rev. Roum. Sci. Techn.-Méc. Appl.*, Vol. 24, No. 4, pp. 647–664, Bucarest, Romania, 1979.
10. Sofronie, R., "Optimum Shape of Prestressed Suspension Bridges," *Rev. Roum. Sci. Techn.-Méc. Appl.*, Vol. 24, No. 6, pp. 933–951, Bucarest, Romania, 1979.

Reinforced Concrete Beams in Pure Torsion

By Himat T. Solanki,[1] M. ASCE

Introduction

Design provisions for torsion are now available in various codes (2,4,5), but the approaches differ considerably. Out of these approaches, space truss theory

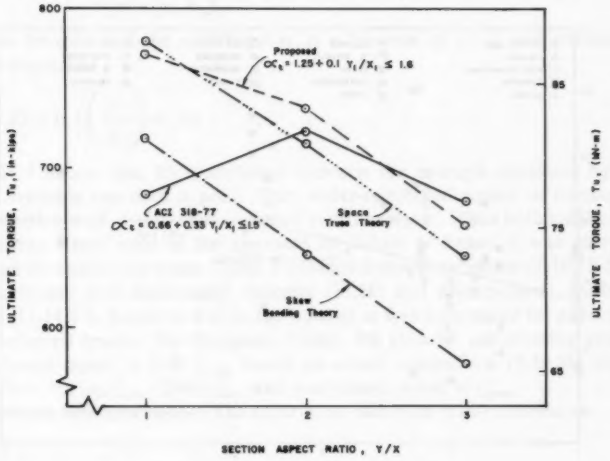

FIG. 1.—Effect of y/x on Ultimate Torque

and skew bending theory predict the true behavior of the reinforced concrete beams. Past research (16) shows the comparison of torsional strength of reinforced concrete beams with different theories (Fig. 1). By considering only the under-reinforced beams with stirrup spacing, $s \leq (x_1 + y_1)/4$, the American Concrete Institute (ACI) method has been studied in this paper and then modified. The

[1]Engr., United Engrs. and Contractors, 30 S. 17th St., 15M3, Philadelphia, Pa. 19101; Formerly Chf. Design Engr., Transportation Dept., Engrg. Div., Sarasota, Fla.

Note.—Discussion open until May 1, 1982. To extend the closing date one month, a written request must be filed with the Manager of Technical and Professional Publications, ASCE. Manuscript was submitted for review for possible publication on October 18, 1979. This paper is part of the Journal of the Structural Division, Proceedings of the American Society of Civil Engineers, ©ASCE, Vol. 107, No. ST12, December, 1981. ISSN 0044-8001/81/0012-2443/$01.00.

under-reinforced beams were determined by the Mitchell and Collins approach (18).

Theory.—The ultimate torque of a rectangular beam can be expressed as (2)

$$T_u = T_c + T_s \quad \ldots \quad (1)$$

in which T_u = ultimate torque; T_c = torque resisted by the concrete at ultimate; and T_s = torque resisted by the reinforcement at ultimate.

By using a "full" elastic stress distribution as proposed by Kuyt (11), the torque resisted by concrete can be expressed as

$$T_c = \frac{1}{3} x^2 \left(y - \frac{1}{4} x \right) 2.4 \sqrt{f'_c} \quad \ldots \quad (2)$$

in which f'_c = cylinder compressive strength of concrete; x = smaller overall

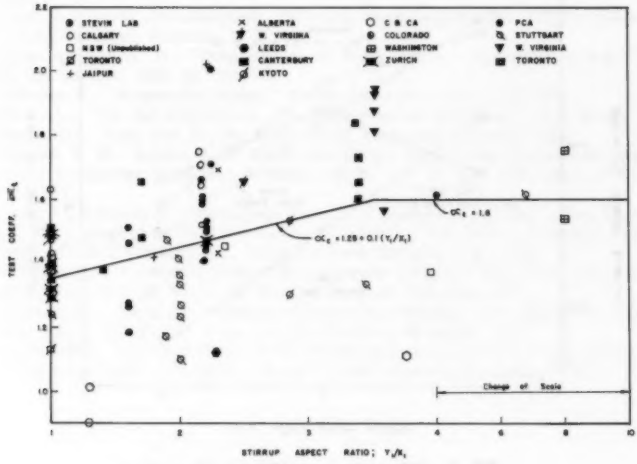

FIG. 2.—Experimental α_t as Function of y_1/x_1

dimension of rectangular section; and y = larger overall dimension of rectangular section.

According to the philosophy of ACI 318–77, the torque resisted by the reinforcement can be expressed as follows (2):

$$T_s = \alpha_t A_t x_1 y_1 \frac{f_{sy}}{s} \quad \ldots \quad (3)$$

in which A_t = area of one leg of a closed stirrup; f_{sy} = yield strength of stirrup; x_1 = smaller center to center dimension of a closed rectangular stirrup; y_1 = larger center to center dimension of a closed rectangular stirrup; s = spacing of stirrups; and α_t = a coefficient.

For beams having an unequal volume of longitudinal and stirrup steels, Eq. 3 may be multiplied by $\sqrt{m}$, in which $m = \rho_l f_{ly} / \rho_s f_{sy}$ = ratio of yield force of longitudinal reinforcement to yield force of closed stirrups per unit volume. Substituting the value of T_c and T_s into Eq. 1, the ultimate torque of a rectangular reinforced concrete section having unequal volume of longitudinal and stirrup steels can be expressed

$$T_u = \frac{1}{3} x^2 \left(y - \frac{1}{4} x \right) (2.4) \sqrt{f'_c} + \alpha_t \sqrt{m}\, A_t x_1 y_1 \frac{f_{sy}}{s} \quad \ldots\ldots\ldots\ldots (4)$$

According to the ACI 318–77, the coefficient α_t is a function of y_1/x_1. Therefore, all the computed values of α_t were plotted as a function of y_1/x_1 in Fig. 2 by using T_u, test and Eq. 5:

$$\alpha_t = \frac{[T_{u,\text{test}} - (0.8)\, x^2 (y - 0.25x) \sqrt{f'_c}\,]\, s}{\sqrt{m}\, x_1 y_1 A_t f_{sy}} \quad \ldots\ldots\ldots\ldots\ldots\ldots (5)$$

It can be seen that the coefficient α_t is a function of y_1/x_1 and statistically can be expressed

$$\alpha_t = 1.25 + 0.1 \left(\frac{y_1}{x_1} \right) \leq 1.6 \quad \ldots\ldots\ldots\ldots\ldots\ldots\ldots\ldots (6)$$

Table 1 shows that the correlation between the strength predicted by Eq. 4 and available test data is good. Only under-reinforced square or rectangular beams with $s \leq (x_1 + y_1)/4$ are included in this analysis. When both longitudinal and stirrup steels yield at the approach of failure of beam, it was classified as an under-reinforced beam. Table 1 includes hollow box beams (7,10,13,14,15, 18,19), beams with lightweight concrete (21,26) and asymmetrical reinforced beams (13,14,17). Based on Ref. 6, the value of m was determined for asymmetrical reinforced beams. For European beams, the cylinder compressive strength was chosen equal to $0.85\, f_{\text{cube}}$ based on actual comparison (9,24,25) instead of $(0.76 + 0.2 \log f_{\text{cube}}/2840) f_{\text{cube}}$ and was chosen equal to f_{prism}.

Minimum Reinforcement.—The criteria for minimum reinforcement is

$$T_u \geq T_{cr} \quad \ldots\ldots\ldots\ldots\ldots\ldots\ldots\ldots\ldots\ldots\ldots\ldots\ldots\ldots (7)$$

Taking $T_{cr} = 1/3 x^2 (y - 0.25x)\, 6\sqrt{f'_c}$ and using Eq. 4

$$\frac{1}{3} x^2 (y - 0.25x)\, 2.4 \sqrt{f'_c} + \alpha_t \sqrt{m}\, A_t x_1 y_1 \frac{f_{sy}}{s}$$

$$\geq \frac{1}{3} x^2 (y - 0.25x)\, 6\sqrt{f'_c} \quad \ldots\ldots\ldots\ldots\ldots\ldots\ldots\ldots\ldots (8)$$

Substituting for m in Eq. 8; assuming $f_{ly} = f_{sy} = f_y$ and rearranging

$$A_l \geq \frac{2(x_1 + y_1)\, s}{A_t} \left[\frac{1.2\, x^2 (y - 0.25x) \sqrt{f'_c}}{\alpha_t x_1 y_1 f_y} \right]^2 \quad \ldots\ldots\ldots\ldots\ldots (9)$$

Maximum Reinforcement.—The criteria for maximum reinforcement are

$$T_u \leq T_{u(\text{limit})} \quad \ldots\ldots\ldots\ldots\ldots\ldots\ldots\ldots\ldots\ldots\ldots\ldots\ldots (10)$$

TABLE 1.—Correlation of Results Under-Reinforced Beams

Source (1)	Beam (2)	$T_{u,test}$, in kip-inches (3)	$T_{u,calc}$, in kip-inches (4)	$T_{u,test} / T_{u,calc}$ (5)
Portland Cement Association	B3	332	363.2	0.91
	D3[b]	346	375.9	0.92
	D4[b]	424	494.6	0.86
	M2	359	339.4	1.06
	I2	319	311.2	1.02
	I3	404	392.7	1.03
	I4	514	499.7	1.03
	G2	357	350.0	1.02
	G3	439	444.2	0.99
	G4	574	566.5	1.01
	G6	346	349.9	0.99
	G7	466	466.5	1.00
	G8	650	625.0	1.04
	N1	80.5	75.1	1.07
	N1a	79.6	75.3	1.06
	N2	128	119.5	1.07
	N3	108	112.3	0.96
	K2	210	203.5	1.03
West Virginia	G6	123	111.6	1.10
	G9	156	133.7	1.17
	G12	181	155.5	1.16
	T15	197	200.9	0.98
	G15	220.5	192.0	1.15
West Virginia	TT6	79.92	74.0	1.08
West Virginia	G4[c]	79.0	78.4	1.01
West Virginia	G4[c]	80.34	75.4	1.06
University of Washington	D4	221.0	204.6	1.08
	D5	293.0	303.4	0.97
University of Colorado	A3	94.6	93.6	1.01
University of Toronto	PT4[b]	620	608.4	1.02
	PT5[b]	577	557.1	1.04
	PT6[b]	573	643.5	0.89
University of Toronto	C2[b]	644	623.2	1.03
	C3[b]	613	620.3	0.99
University of Calgary	A1	116	111.8	1.04
	A1R	111	110.2	1.01
	A2	200	172.7	1.16
	A3	246	228.9	1.07
	B1	114	102.6	1.11
	B1R	109	101.0	1.08
	B2	184	159.9	1.15
	B3	224	218.4	1.03

TABLE 1.—*Continued*

(1)	(2)	(3)	(4)	(5)
University of Alberta	1-1[d]	122	109.7	1.11
	2-1	181	186.6	0.97
Leeds University	HB13[b]	51.3	60.6	0.85
Cement & Concrete Association	12	108.9	137.4	0.80
	16	52.2	64.6	0.81
	52	81.4	109.6	0.75
Delft University of Technology	54	71.2	64.2	1.11
	55	83.3	66.4	1.25
Eidgenössische Technische Hochschule	T1[b]	1,270	1,173.8	1.08
	T2[b]	1,266	1,185.2	1.07
	T3[d]	907	935.1	0.97
	T4[b]	1,288	1,187.5	1.08
Eidgenössische Technische Hochschule	T5[b]	1,414	1,413.0	1.00
	T8[d]	1,075	1,089.0	0.99
University of Stuttgart	VS2	177	213.1	0.83
	VS3	258	286.6	0.90
	VQ1	191	203.2	0.94
	VQ2	177	213.1	0.83
	VQ3	181	208.3	0.87
	VQ9	198	197.0	1.00
	VB2	373	426.0	0.86
	VB3	420	450.6	0.93
	VB4[b]	439	462.0	0.95
	VH1	193	198.4	0.97
	VM2	354	360.5	0.98
	VM3	844	879.0	1.02
	VM4	2,474	2,891.0	0.86
Malaviya Regional Engineering College	2	79	78.8	1.00
	G4	115	88.1	1.30
Kyoto University	RaI	27	30.9	0.87
	RaII	38	38.1	1.00
University of New South Wales	7&7A	105	100.6	1.04
	8&8A	98	99.8	0.98
	9&9A	92	104.5	0.90
University of Canterbury	T1A	192	190.1	1.01
	T1B	203	190.6	1.06
	T1C	196	189.6	1.03
	634	219	195.1	1.12
	644	285	265.0	1.07
	1,034	426	380.4	1.12
	1,044	538	479.3	1.13
	1,055	686	663.5	1.03
	1,244	529	531.1	1.00

TABLE 1.—*Continued*

(1)	(2)	(3)	(4)	(5)
	1,644	853	781.7	1.09
	1,655	1,058	1,042.6	1.01
				1.01[e]
				0.10[f]

[a]1 kip-in. = 0.113 kN·m.
[b]Hollow beams.
[c]Lightweight concrete beams.
[d]Asymmetrical reinforced concrete beams (m for beams 1–1, T-3 and T-8 are 0.99, 0.47, and 1.02, respectively).
[e]Mean.
[f]Standard deviation.

Taking $T_{u(\text{limit})} = 1/3\, x^2(y - 0.25x)\, 12\sqrt{f'_c}$ and using Eq. 4

$$\frac{1}{3} x^2(y - 0.25x)\, 2.4\sqrt{f'_c} + \alpha_t \sqrt{m}\, A_t x_1 y_1 \frac{f_{sy}}{s}$$

$$\leq \frac{1}{3} x^2(y - 0.25x)\, 12\sqrt{f'_c} \quad \ldots \ldots \ldots \ldots \ldots \ldots \ldots \ldots \quad (11)$$

Substituting for m in Eq. 11, assuming $f_{ly} = f_{sy} = f_y$ and rearranging

$$A_t \leq \frac{2(x_1 + y_1)\, s}{A_t} \left[\frac{3.2\, x^2(y - 0.25x)\sqrt{f'_c}}{\alpha_t x_1 y_1 f_y} \right]^2 \quad \ldots \ldots \ldots \ldots \quad (12)$$

Conclusions

1. If the other parameters are held constant, the torsional strength of a reinforced concrete beam decreases with an increase in aspect ratio, y/x.
2. The coefficient α_t varies with y_1/x_1 and can be calculated by using Eq. 6.
3. Eq. 4 satisfactorily predicts torsional moments of under-reinforced square or rectangular beams having $s \leq (x_1 + y_1)/4$.
4. Eq. 9 is a simple expression for minimum reinforcement while Eq. 12 is for maximum reinforcement.
5. Because the beams with stirrup spacing $s \leq (x_1 + y_1)/4$ are considered in Table 1, it is necessary to increase the value of α_t compared to the ACI Code.

Acknowledgment

The writer sincerely thanks the reviewers for their comments. The writer also thanks Charles L. Goode for his constant encouragement and appreciates the assistance of Tina Brahim and Irene Peart, Cement & Concrete Association, Slough, England.

Appendix.—References

1. Bruggeling, A. S. G., and Bueren, R. V., "Onderzoek naar het gedrag van gewapend-

betonbalken, belast op zuivere wringing," *Cement*, Vol. XXIII, No. 12, Dec., 1971, pp. 617–619.

2. "Building Code Requirements for Reinforced Concrete," ACI Committee 318, American Concrete Institute, Detroit, Mich., 1977, 102 pp.
3. Cameron, R. S., "A Study of Reinforced Concrete Subjected to Pure Torsion," *Master of Engineering Report*, University of Canterbury, Christchurch, New Zealand, 1971, 70 pp.
4. "Code for the Design of Concrete Structures for Buildings," Canadian Standards Association, (CSA A23.3–1973), Rexdale, Canada, 1973, 123 pp.
5. "Concrete Structures Code," Standards Association of Australia, (AS 1480–1974), Sydney, Australia, 101 pp.
6. Elfgren, L., "Reinforced Concrete Beams Loaded in Combined Torsion, Bending, and Shear—A Study of the Ultimate Load-Carrying Capacity," *Rapport 71:3*, Institutionen for Konstruktionsteknik Betongbyggnad, CTH, Goteborg, Sweden, Nov., 1971, 201 pp.
7. Evans, R. H., and Sarkar, S., "A Method of Ultimate Strength Design of Reinforced Concrete Beams in Combined Bending and Torsion," *The Structural Engineer*, Vol. 43, No. 10, Oct., 1965, pp. 327–334.
8. Fretheim, I. B., "Flexure-Torsion Interaction Behavior of Reinforced Concrete Beams," *Master of Science Engineering Report*, University of Colorado, Boulder, Colo., 1971, 83 pp.
9. Gausel, E., "Ultimate Strength of Prestressed I-Beams Under Combined Torsion, Bending, and Shear," *ACI Journal*, Proceedings, Vol. 67, No. 9, Sept., 1970, pp. 675–678.
10. Hsu, T. T. C., "Torsion of Structural Concrete—Behavior of Reinforced Concrete Rectangular Members," *Torsion of Structural Concrete*, American Concrete Institute, SP-18, Detroit, Mich., 1968, pp. 261–306.
11. Kuyt, B., "A Study of the Torsional Section Modulus for Rectangular Concrete Beams," *De Ingenier*, No. 22, June, 1972, pp. Bt 19–22.
12. Kemp, E. L., "Behavior of Concrete Members Subjected to Torsion and to Combined Torsion, Bending, and Shear," *Torsion of Structural Concrete*, SP-18, American Concrete Institute, Detroit, Mich., 1968, pp. 179–201.
13. Lampert, P., Luchinger, P., and Thurlimann, B., "Torsionsversuche an Stahl—und Spannbetonbalken," *Bericht Nr. 6506-4*, Institut fur Baustatik, ETH, Zurich, Switzerland, Feb., 1971, 99 pp.
14. Lampert, P., and Thurlimann, B., "Torsionsversuche an Stahlbetonbalken," *Bericht Nr.* 6506-2, Institut fur Baustatik, ETH, Zurich, Switzerland, June, 1968, 101 pp.
15. Leonhardt, F., and Schelling, G., "Torsionversuche an Stahlbetonbalken," *Heft 239*, Deutscher Ausschuss fur Stahlbeton, Berlin, Germany, 1974, 122 pp.
16. McMullen, A. E., and Rangan, V. B., "Pure-Torsion in Rectangular Sections—A Re-examination," *Journal of the American Concrete Institute*, Proceedings, Vol. 75, No. 10, Oct., 1978, pp. 511–519.
17. McMullen, A. E., and Warwaruk, J., "The Torsional Strength of Rectangular Reinforced Concrete Beams Subjected to Combined Loading," *Report No. 2*, Department of Civil Engineering, University of Alberta, Edmonton, Canada, 1967, 234 pp.
18. Mitchell, D., and Collins, M. P., "The Behavior of Structural Concrete Beams in Pure Torsion," *Publication No. 74-06*, Department of Civil Engineering, University of Toronto, Toronto, Canada, 1974, 88 pp.
19. Mitchell, D., and Collins, M. P., "The Effects of Stirrup Spacing and Longitudinal Restraint on the Behavior of Reinforced Concrete Beams Subjected to Pure Torsion," *Publication No. 71-22*, Department of Civil Engineering, University of Toronto, Toronto, Canada, 1971, 49 pp.
20. Mukherji, P. R., and Kemp, E. L., "Ultimate Torsional Strength of Plain, Prestressed, and Reinforced Concrete Member of Rectangular Cross Section," Civil Engineering Studies, *Report No. 2003*, West Virginia University, Morgantown, W.Va., 1967, 100 pp.
21. Mukherji, S. K., Wilhelm, W. J., and Kemp, E. L., "Torsional Strength and Stiffness of Rectangular Plain and Reinforced Lightweight Aggregate Concrete Members," *Report No. 2014*, Department of Civil Engineering, West Virginia University, Morgantown, W.Va., 1972, 75 pp.

22. Okada, K., Nishibayashi, S., and Abe, T., "Experimental Studies on the Strength of Rectangular Reinforced and Prestressed Concrete Beams Under Combined Flexure and Torsion," *Transactions*, Japan Society of Civil Engineers, No. 131, July, 1966, pp. 39–51.
23. Pandt, G. S., "Ultimate Torque of Rectangular Reinforced Concrete Beams," *Journal of the Structural Division*, ASCE, Vol. 96, No. ST9, Proc. Paper 7503, Sept., 1970, pp. 1987–1995.
24. Petersson, T., "Shear and Torsion in Reinforced Concrete Beams," Statens Institut for Byggnadsforskning, *Document D 10:*, KTH, Stockholm, Sweden, 1972, 276 pp.
25. Sandegren, D. S., and Yu, C. W., "An Equilibrium-Compability Approach to the Determination of Strength of Reinforced Concrete Beams Under Combined Bending and Torsion," *Magazine of Concrete Research*, Vol. 30, No. 102, Mar., 1978, pp. 3–10.
26. Souza, J. C. L., and Wilhelm, W. J., "Torsional Strength and Stiffness of Rectangular Plain and Reinforced All-Light-Weight Aggregate Concrete Members," *Report No. 2021*, Department of Civil Engineering, West Virginia University, Morgantown, W.Va., 1973, 58 pp.
27. Swann, R. A., "Experimental Basis for a Design Method for Rectangular Reinforced Concrete Beams in Torsion," *Technical Report 42.452*, Cement and Concrete Association, London, England, 1970, 38 pp.
28. Wyss, A. N., Garland, J. B., and Mattock, A. H., "A Study of the Behavior of I-Section Prestressed Concrete Girders Subjected to Torsion," *Structures and Mechanics Report No. SM69–1*, University of Washington, Seattle, Wash., 1969, 46 pp.

DISCUSSION

Note.—This paper is part of the Journal of the Structural Division, Proceedings of the American Society of Civil Engineers, ©ASCE, Vol. 107, No. ST12, December, 1981. ISSN 0044-8001/81/0012-2453/$01.00.

Discussions

Discussions may be submitted on any Proceedings paper or technical note published in any *Journal* or on any paper presented at any Specialty Conference or other meeting, the *Proceedings* of which have been published by ASCE. Discussion of a paper/technical note is open to anyone who has significant comments or questions regarding the content of the paper/technical note. Discussions are accepted for a period of 4 months following the date of publication of a paper/technical note and they should be sent to the Manager of Technical and Professional Publications, ASCE, 345 East 47th Street, New York, N.Y. 10017. The discussion period may be extended by a written request from a discusser.

The original and three copies of the Discussion should be submitted on 8-1/2-in. (220-mm) by 11-in. (280-mm) white bond paper, typed double-spaced with wide margins. The length of a Discussion is restricted to two *Journal* pages (about four typewritten double-spaced pages of manuscript including figures and tables); the editors will delete matter extraneous to the subject under discussion. If a Discussion is over two pages long it will be returned for shortening. All Discussions will be reviewed by the editors and the Division's or Council's Publications Committees. In some cases, Discussions will be returned to discussers for rewriting, or they may be encouraged to submit a paper or technical note rather than a Discussion.

Standards for Discussions are the same as those for Proceedings Papers. A Discussion is subject to rejection if it contains matter readily found elsewhere, advocates special interests, is carelessly prepared, controverts established fact, is purely speculative, introduces personalities, or is foreign to the purposes of the Society. All Discussions should be written in the third person, and the discusser should use the term "the writer" when referring to himself. The author of the original paper/technical note is referred to as "the author."

Discussions have a specific format. The title of the original paper/technical note appears at the top of the first page with a superscript that corresponds to a footnote indicating the month, year, author(s), and number of the original paper/technical note. The discusser's full name should be indicated below the title (see Discussions herein as an example) together with his ASCE membership grade (if applicable).

The discusser's title, company affiliation, and business address should appear on the first page of the manuscript, along with the *Proceedings* paper number of the original paper/technical note, the date and name of the *Journal* in which it appeared, and the original author's name.

Note that the discusser's identification footnote should follow consecutively from the original paper/technical note. If the paper/technical note under discussion contained footnote numbers 1 and 2, the first Discussion would begin with footnote 3, and subsequent Discussions would continue in sequence.

Figures supplied by the discusser should be designated by letters, starting with A. This also applies separately to tables and references. In referring to a figure, table, or reference that appeared in the original paper/technical note use the same number used in the original.

It is suggested that potential discussers request a copy of the *ASCE Authors' Guide to the Publications of ASCE* for more detailed information on preparation and submission of manuscripts.

Seismic Design Input for Secondary Systems[a]

Closure by Mahendra P. Singh,[5] M. ASCE

The writer would like to thank Murga and O'Connor for their interest in the paper, and for their thoughtful and interesting comments. Indeed, if design ground motions were defined as random processes and characterized in some appropriate form, the need for direct generation of floor spectra approaches would not arise. However, the definition of design earthquakes by some characteristics of a random process is not a straightforward and easy task. The definition in terms of a (design) power spectral density function (PSDP) is rather very tempting, and has in fact been used by many investigators including the writer to study dynamic behavior of structures under earthquake type of excitation. This form of characterization is preferred because analytical manipulations are relatively simple and manageable. Mathematically speaking, however, the earthquake motions cannot be characterized by a PSDF as they are not stochastically stationary in character. Then, does it mean that many important developments in earthquake engineering made on the basis of the assumption that a PSDF exists are all wrong? Probably not entirely, and at least not qualitatively. Quantitatively, however, there is room for further improvements.

A realistic earthquake motion model must, of course, be nonstationary. But what is the exact cause or form of nonstationarity is a sensitive point and difficult to answer. Stationary models modulated by deterministic time functions (also called envelope functions) have often been used as nonstationary models for earthquakes. These modulation functions are generally assumed to start with a motion buildup phase followed by a strong motion (stationary) phase and then by a decaying phase. Other forms of modulation functions have also been used. However, to prescribe models for designs, a more precise definition of the modulation function parameters and PSDF will be required. To obtain these parameters directly by a statistical analysis of available ground records is at best a delicate task. Whereas to obtain these parameters from a given spectrum and then use them as input in the analysis is quite unnecessary especially when a spectrum can be directly used in a so-called single-step direct approach. The discussers refer to the topic of composite damping and modelling uncertainties. In a direct approach, these problems also don't seem insurmountable (15,16).

The writer, however, fully supports the views of the discussers that the research must continue to define a realistic stochastic model for earthquake ground motions.

[a]February, 1980, by Mahendra P. Singh (Proc. Paper 15207)

[5]Assoc. Prof., Dept. of Engrg. Sci. and Mechanics, Virginia Polytechnic Institute and State Univ., Blacksburg, Va. 24061.

APPENDIX.—REFERENCES

15. Singh, M. P., "Seismic Response by SRSS for Nonproportional Damping," *Journal of the Engineering Mechanics Division*, ASCE, Vol. 106, No. EM6, Proc. Paper 15948, Dec., 1980, pp. 1405–1419.
16. Singh, M. P., "Seismic Response of Structures with Random Parameters," presented at the Sept. 8–13, 1980, 7th World Conference on Earthquake Engineering, held at Istanbul, Turkey.

DESIGN OF COUNTERSTRESSED CABLE STRUCTURES[a]

Errata

The following corrections should be made to the original paper:

Page 2259, line 5: Should read "relief" instead of "refief"
Page 2262, first line, third paragraph: Should read "H^H" instead of "h^H"

RESEARCH NEEDS IN STABILITY OF METAL STRUCTURES[b]

Discussion by Peter F. Adams[c]

The paper by Bjorhovde provides a comprehensive summary of the next set of critical problems that must be closely defined and solved in order to improve the present state of understanding of the stability of metal members and frames. Task Group 4, "Frame Stability and Columns as Frame Members," of the Structural Stability Research Council has attempted, over the past several years, to collect, discuss, and critically examine the research related to the stability of steel building frames and the writer has been requested to communicate, on behalf of Task Group 4, to discuss the progress and future directions in this particular area.

As outlined by Bjorhovde, the general thrust of the Task Group's effort has been to encourage studies and assess results that will be useful in moving

[a] November, 1980, by Dennis Clark (Proc. Paper 15794).
[b] December, 1980, by Reidar Bjorhovde (Proc. Paper 15926).
[c] Prof. of Civ. Engrg., Univ. of Alberta, Edmonton, Canada.

the profession eventually from the "K factor" approach to design to the "P Delta" approach, in recognition of the fact that this latter approach can be used to more readily reflect those factors and influences that have a significant effect on the behavior of the building frame. In fact, the design standard adopted by the Canadian Standards Association has been written to encourage the use of the P-Delta approach, with encouraging results. (Canadian Standards Association, "Steel Structures for Buildings—Limit States Design," CAN 3—S16.1—M78, Rexdale, Ontario.)

The Task Group recognizes, however, that while the supporting evidence for the "P-Delta" approach is at least as well developed as that used to introduce the "K-Factor" approach, additional information is required relating to the behavior of actual structures, since this behavior is directly reflected in the P-Delta method. Specifically, since an elastic analysis is used to predict the story sway deflections at the factored load level (implied values of these deflections are used even in an allowable stress design) it is important to know the extent of the underestimation of these deflections and the corresponding stability effects. Thus, the parametric studies referred to by Bjorhovde are of primary importance.

Secondly, it is important to be able to extend the "P-Delta" approach to different structual systems. This implies the ability to predict the story sway deflections of such systems. Bjorhovde has mentioned studies of semirigid systems and infilled frames. In addition, the stiffening influence of standard connections, the member width effect, etc., provide other areas where research information can be used directly in the design method.

And finally, it is essential to come to an understanding of how secondary effects other than P-Delta influence the behavior of the structure. How important is the influence of axial load on member stiffnesses? Are there practical systems where these member effects are significant? At the present time it appears that these cases will be rare indeed but as a part of the continuing study of the behavior of steel frames this important question should be addressed.

Efforts to improve the understanding of the behavior of steel structures will never be completed. In the present period the Task Group has also attempted to encourage studies that will assist in the application of the P-Delta approach to particular classes of structures. One such study is sponsored by the American Institute of Steel Construction and has consisted of an extensive literature review and computer study. The study will recommend the adoption of the P-Delta approach for inclusion in design specifications and will focus on the factors required for a conservative application of the approach to both the combined loading case and the gravity load only case.

By Joachim Lindner[9] and Narayanan Subramanian[10]

The writers would like to commend the author for bringing out an extensive report on the research needs in stability of metal structures. The lateral torsional

[9]Full Prof., Fachgebiet Stahlbau, Technical Univ. of Berlin, Berlin, West Germany.
[10]Alexander von Humboldt Fellow, Fachgebiet Stahlbau, Technical Univ. of Berlin, Berlin, West Germany.

buckling of beams are not only important in the construction phase, but also during the life of the structure (69).

The author has listed: (1) Residual stresses on beams; (2) effect of residual stress on inelastic lateral torsional buckling strength of beams; (3) parametric studies on effect of residual stress and initial out-of-straightness; (4) laterally supported continuous beams; (5) effect of cross-sectional distorsions; and (6) effect of coped ends as research needs for laterally unsupported beams. The writers are of the opinion that the following should also be included as research needs for the case of beams.

1. *Effect of shape of beams*: Most of the research that has been done is either on symmetrical or unsymmetrical I-Beams. Therefore research is warranted in channel and Z Sections, which are quite often used as purlins.
2. *Effect of sheeting on lateral torsional buckling*: It has been shown that the diaphragm bracing, if properly utilized, can eliminate the need of other types of bracing (59). The lateral torsional restraint by the roof or floor decking depends on a number of factors. Much research has to be done to include the restraint provided by the sheeting, which will provide economical solutions (62,68).
3. *Intermediate restraints*: The intermediate restraints substantially increase the critical moments on beams. The effect of these intermediate restraints are equally important as that of the effect of end restraints (66).
4. *The effect of bottom flange restraint*: Very little is known about the effect of bottom flange restraints (57), though certain amount of literature is available on the effect of mixed end restraints (67).
5. *Effect of openings on lateral buckling of beams*: For aesthetic appearance and to save material, castellated beams are being increasingly used. Practically very little work has been reported on the influence of openings on the overall lateral stability of a slender castellated beam (58,61).

The design formula recommended by European Convention for Constructional steel work (ECCS) for laterally unsupported beams is given (64) by

$$\frac{M_u}{M_p} = (1 + \lambda^{2n})^{-1/n} \quad \ldots\ldots\ldots\

APPENDIX.—REFERENCES

57. Bartels, D., and Bos, C. A. M., "Investigations of the Effect of the Boundary Condition on the Lateral Buckling Phenomenon, Taking Account of Cross-Sectional Deformation," *Heron*, Vol. 19, No. 1, Delft, The Netherlands, 1973, pp. 1–26.
58. Coull, A., and Alvarez, M., "Effect of Opening on Lateral Buckling of Beams," *Journal of the Structural Division*, ASCE, Vol. 106, No. ST12, Proc. Paper 15874, Dec., 1980, pp. 2553–2560.
59. Errera, S. J., and Apparao, T. V. S. R., "Design of I-Shaped Beams with Diaphragm Bracing," *Journal of the Structural Division*, ASCE, Vol. 102, No. ST4, Proc. Paper 12051, Apr., 1976, pp. 769–781.
60. Fukumoto, Y., Itoh, and Kubo, M., "Strength Variation of Laterally Unsupported Beams," *Journal of the Structural Division*, ASCE, Vol. 106, No. ST1, Proc. Paper 15142, Jan., 1980, pp. 165–181.
61. Kerdal, D., and Nethercot, D. A., "Lateral Torsional Buckling of Castellated Steel Beams—A State-of-the-Art Review," *Report No. 4043/43/CB/01*, Department of Civil and Structural Engineering, University of Sheffield, Sept., 1979.
62. Lindner, J., "Anschlußmomente von Trägern, die zur Kippanssteifung herangezogen werden," *Die Bautechnik*, No. 10, 1973, pp. 342–344.
63. Lindner, J., and Gietzelt, R., "Biege drillknicken—Eraläuterungen, Versuche, Beispiele," *Stahlbau-Verlag*, Köln, W. Germany, No. 10, 1980, pp. 38.
64. Lindner, J., et al., "Laterally Supported and Unsupported Beams," European Convention for Constructional Steelwork, Introductory Report," *Second International Colloquium on Stability of Steel Structures*, Liege, Belgium, Apr., 1977, pp. 127–143.
65. Massonnet, C., ed., *Second International Colloquim on Stability of Steel Structures*, Liege, Preliminary Report, E.C.C.S. and I.A.B.S.E., Apr. 13–15, 1977, pp. 191–196, and pp. 233–240.
66. Nethercot, D. A., and Rockey, K. C., "The Lateral Buckling of Beams Having Discrete Intermediate Restraints," *The Structural Engineer*, Vol. 50, No. 10, Oct., 1972, pp. 391–403.
67. Nethercot, D. A., and Rockey, K. C., "Lateral Buckling of Beams with Mixed End Conditions," *The Structural Engineer*, Vol. 51, No. 4, Apr., 1973, pp. 133–138.
68. Oxford, J., "Zur Kippstabilisierung Stählerner I-Dachplatten mit Imperfektionen in geneigten Dächern bis zum Erreichen der Plastischen Grenzlast durch die Biege—und Schubsteifigkeit der Dacheindeckung," *Der Stahlbau*, Berlin, West Germany, 1976, No. 10, pp. 301–311 and No. 12, pp. 365–371.
69. Zamecnik, F. J., "Errors in Utilization of Cold-Formed Steel Members," *Journal of the Structural Division*, ASCE, Vol. 106, No. ST12, Proc. Paper 15941, Dec., 1980, pp. 2493–2508.

PROPOSED SPECIFICATIONS FOR STEEL BOX GIRDER BRIDGES[a]

Discussion by Charles Seim,[4] F. ASCE and Steve Thoman[5]

The Author's proposed specification advances the art of bridge engineering and fills in a gap in the design of long span steel box girder bridges. In the

[a]December, 1980, by Roman Wolchuck (Proc. Paper 15942).

[4]Senior Vice-Pres., T. Y. Lin International, San Francisco, Calif.
[5]Staff Engr., T. Y. Lin International, San Francisco, Calif.

writers' opinion, at the present time, steel box girders are not competitive for spans shorter than about 500 ft with a concrete deck and possibly 750 ft (229 m) with a steel orthotropic deck. Whereas a prestressed concrete bridge of these span lengths requires a box girder configuration. Many times engineers or owners compare the cost of steel box girders with concrete box girders because of their similarity in appearance. However, if the comparison is made on the type of bridge considering only its economic span range, the steel plate girder or steel truss type may be more competitive with the concrete box. The point is that more economy may be obtained by cost comparison of bridge types rather than by refinement of stiffener arrangement for a steel box girder bridge.

The writers consulted on the designers of a composite steel box girder bridge having five continuous spans of 310 ft, 400 ft, 450 ft, 400 ft, and 310 ft. The trapezoidal box section consisted of three webs having a maximum depth of 21.4 ft and a minimum depth of 10.4 ft. The report "Design Specifications for Steel Box Girders" submitted to the FHWA by the firm of Wolchuck and Mayrbaurl was utilized as the basis of the design criteria for the webs and flanges. It became apparent that in the hands of a designer not familiar with buckling design or behavior that the proposed specification required effort considerable beyond the techniques employed for the design of other elements of the bridge. A shortened version of the proposed specification was abstracted to simplify and ensure a more manageable design.

Perhaps the final version of the specification could be divided into a shorter simplified section and a section in the more complex form as the proposed specification now exists. Thus, the designer could choose the degree of refinement he wishes to apply to his design. For example, the proposed specification determines the total strength of a web panel as sum of the beam shear strength and the tension field strength. The rigidity required of the girder flanges to adequately anchor the tension field forces has not been extensively test proven. Therefore the proposed specification makes the assumption of neglecting the flange rigidity, corresponding to a lower limit of the tension field strength. A simplification can be made by ignoring the tension field strength which greatly reduces the design complexity without greatly increasing costs.

Since the proposed specification has not had the test of application by skilled designers to a variety of span lengths and box sizes, the specifications should be used with discretion until these parametor studies are completed and the profession has accepted the specification as a new design tool. The author has made an excellent start and the writers hope that some form of the proposed specification will ultimately be approved.

Edge Stiffeners for Thin-Walled Members[a]

Discussion by Srinivasan Sridharan[4]

The authors are to be congratulated for a very interesting and valuable paper on the subject. There appear, however, some questions on their postbuckling analysis. The computer approach (8) they have adopted does not appear to have taken into account the nonlinear contribution of in-plane displacement of plate elements in the strain displacement relations, very vital in modelling the type of buckling and postbuckling behavior considered. This comment is of particular significance regarding the lip of the channel which does suffer large scale in-plane displacements. This difficulty is reflected in Fig. 6, which indicates very nearly the same buckling stresses for a spectrum of d/t ratios (d/t = 18.2, 15, 9.9, and 8.0), a trend clearly contradicted by Fig. 4.

The authors do not mention the boundary conditions and the mode of application of load employed in the analysis. Was the load applied by prescribing uniform end shortening to simulate the experimental set up?

Finally, what was the nature of failure? For the proportions of lipped channels tested (w/t = 45.6, Fig. 11), one would expect failure by an interaction of initial imperfections and plastic yielding. If so, would they comment on the value of a purely elastic postbuckling analysis?

---

[a]February, 1981, by Thomas P. Desmond, Teoman Pekoz, and George Winter (Proc. Paper 16056).

[4]Asst. Prof., Dept. of Civ. Engrg., Washington Univ. in St. Louis, St. Louis, Mo. 63130.

Technical Papers

Original papers should be submitted in triplicate to the Manager of Technical and Professional Publications, ASCE, 345 East 47th Street, New York, N.Y. 10017. Authors must indicate the Technical Division or Council, Technical Committee, Subcommittee, and Task Committee (if any) to which the paper should be referred. Those who are planning to submit material will expedite the review and publication procedures by complying with the following basic requirements:

1. Titles must have a length not exceeding 50 characters and spaces.

2. The manuscript (an original ribbon copy and two duplicate copies) should be double-spaced on one side of 8-1/2-in. (220-mm) by 11-in. (280-mm) paper. Three copies of all figures and tables must be included.

3. Generally, the maximum length of a paper is 10,000 word-equivalents. As an *approximation*, each full manuscript page of text, tables or figures is the equivalent of 300 words. If a particular subject cannot be adequately presented within the 10,000-word limit, the paper should be accompanied by a rationale for the overlength. This will permit rapid review and approval by the Division or Council Publications and Executive Committees and the Society's Committee on Publications. Valuable contributions to the Society's publications are not intended to be discouraged by this procedure.

4. The author's full name, Society membership grade, and a footnote stating present employment must appear on the first page of the paper. Authors need not be Society members.

5. All mathematics must be typewritten and special symbols must be identified properly. The letter symbols used should be defined where they first appear, in figures, tables, or text, and arranged alphabetically in an appendix at the end of the paper titled Appendix.--Notation.

6. Standard definitions and symbols should be used. Reference should be made to the lists published by the American National Standards Institute and to the *Authors' Guide to the Publications of ASCE*.

7. Figures should be drawn in black ink, at a size that, with a 50% reduction, would have a published width in the *Journals* of from 3 in. (76 mm) to 4-1/2 in. (110 mm). The lettering must be legible at the reduced size. Photographs should be submitted as glossy prints. Explanations and descriptions must be placed in text rather than within the figure.

8. Tables should be typed (an original ribbon copy and two duplicates) on one side of 8-1/2-in. (220-mm) by 11-in. (280-mm) paper. An explanation of each table must appear in the text.

9. References cited in text should be arranged in alphabetical order in an appendix at the end of the paper, or preceding the Appendix.—Notation, as an Appendix.—References.

10. A list of key words and an information retrieval abstract of 175 words should be provided with each paper.

11. A summary of approximately 40 words must accompany the paper.

12. A set of conclusions must end the paper.

13. Dual units, i.e., U.S. Customary followed by SI (International System) units in parentheses, should be used throughout the paper.

14. A practical applications section should be included also, if appropriate.